ADVANCED MATERIALS
www.advmat.de

Recent Advances in 4D Printing of Advanced Materials and Structures for Functional Applications

Xue Wan, Zhongmin Xiao, Yujia Tian, Mei Chen, Feng Liu, Dong Wang, Yong Liu, Paulo Jorge Da Silva Bartolo, Chunze Yan, Yusheng Shi, Ruike Renee Zhao, Hang Jerry Qi, and Kun Zhou**

4D printing has attracted tremendous worldwide attention during the past decade. This technology enables the shape, property, or functionality of printed structures to change with time in response to diverse external stimuli, making the original static structures alive. The revolutionary 4D-printing technology offers remarkable benefits in controlling geometric and functional reconfiguration, thereby showcasing immense potential across diverse fields, including biomedical engineering, electronics, robotics, and photonics. Here, a comprehensive review of the latest achievements in 4D printing using various types of materials and different additive manufacturing techniques is presented. The state-of-the-art strategies implemented in harnessing various 4D-printed structures are highlighted, which involve materials design, stimuli, functionalities, and applications. The machine learning approach explored for 4D printing is also discussed. Finally, the perspectives on the current challenges and future trends toward further development in 4D printing are summarized.

1. Introduction

3D printing, also known as additive manufacturing (AM), is a versatile technology that allows the direct fabrication of 3D objects with complicated geometries by accumulating materials layer by layer with the guidance of digital models.[1] Evolving from 3D printing, 4D printing introduces a fourth dimension of time, garnering significant interest since its conceptualization in 2013.[2–4] It involves dynamic changes in the shape, property, or functionality of printed parts in response to external stimuli, such as heat,[5] light,[6] electric fields,[7] magnetic fields,[8] solvents,[9] and even multi-stimuli.[10] 4D printing can also involve printing of 2D objects which can respond to stimuli over time.[9,11] As an innovative technology, 4D printing facilitates the fabrication of functional intelligent devices and microstructures across diverse applications, including biomedical engineering, electronics, photonics, robotics, and actuators.

4D printing simplifies the design and manufacturing of complex parts by converting intricate 3D geometries into simplified structures capable of self-transformation, thereby streamlining part assembly. Moreover, 4D-printed parts boast short production time and minimal use of supporting material, particularly for complex morphology.[12] The self-transformation, self-assembly, and self-repair capabilities inherent in 4D-printed structures

X. Wan, Z. Xiao, Y. Tian, M. Chen, P. J. D. S. Bartolo, K. Zhou
Singapore Centre for 3D Printing
School of Mechanical and Aerospace Engineering
Nanyang Technological University
Singapore 639798, Singapore
E-mail: kzhou@ntu.edu.sg

M. Chen, K. Zhou
HP–NTU Digital Manufacturing Corporate Lab
School of Mechanical and Aerospace Engineering
Nanyang Technological University
Singapore 639798, Singapore

F. Liu, Y. Liu
State Key Laboratory of Powder Metallurgy
Central South University
Changsha 410083, China

D. Wang
School of Mechanical Engineering
Shanghai Jiao Tong University
Shanghai 200240, China

C. Yan, Y. Shi
State Key Laboratory of Materials Processing and Die & Mould Technology
Huazhong University of Science and Technology
Wuhan 430074, China

R. R. Zhao
Department of Mechanical Engineering
Stanford University
Stanford, CA 94305, USA

H. J. Qi
School of Mechanical Engineering
Georgia Institute of Technology
Atlanta, GA 30332, USA
E-mail: qih@me.gatech.edu

The ORCID identification number(s) for the author(s) of this article can be found under https://doi.org/10.1002/adma.202312263

DOI: 10.1002/adma.202312263

enable their autonomous reconfiguration to adapt to the environment without external intervention. McKinsey predicts that by 2030, 10% of the manufacturing processes will be replaced by AM.[13] As an exciting branch of AM, 4D printing has attracted enormous interest from both academia and industry of different disciplines. Therefore, a comprehensive understanding of the latest achievement in 4D printing is highly demanded.

According to ISO/ASTM 52900:2021, the AM technology is divided into seven major techniques: vat photopolymerization (VPP), material extrusion (MEX), powder bed fusion (PBF), binder jetting (BJT), material jetting (MJT), directed energy deposition (DED), and sheet lamination (SHL). Each printing technique differs from another in the printer apparatus, curing principle, and characteristics of the materials. Up to date, these printing techniques (except SHL) have been employed in 4D printing, either individually or combined into hybrid printing. Among these techniques, VPP and MEX are the most frequently employed ones as they are low-cost, adapt to diversified materials, and facilitate efficient multi-material printing.

Various types of materials such as polymers, metals, ceramics, and their combinations have been employed in a wide range of printing methods. Stimuli-responsive materials are the most commonly used materials in 4D printing. Typical stimuli-responsive materials or smart materials include shape memory polymers (SMPs), liquid crystal elastomers (LCEs), and hydrogels, with inherent responses to external stimuli.

SMPs exhibit the shape memory effect (SME) that allows them to revert from temporary shapes to their original shapes.[14–16] Conventional SMPs could be regarded as a combination of reversible switching segments and a network structure.[17] The former responds to external stimuli, enabling SMPs to undergo shape changes. The latter provides mechanical integrity and determines the permanent shape. Taking thermo-responsive one-way SMPs as an example, the reversible switching segments rely on a transition temperature T_{trans}, which can be the glass transition temperature T_g for amorphous SMPs or the melting temperature T_m for semi-crystalline SMPs. During the programming process, strain energy is stored in the material, allowing it to maintain its temporary shape. Upon the heat stimulus, this stored energy is released, triggering the shape recovery to the permanent shape. LCEs are a class of stimuli-responsive materials that integrate both the elastic behavior of slightly crosslinked polymer networks and the anisotropic properties of liquid crystals (LCs).[18–20] LCEs undergo reversible and anisotropic shape changes in response to stimuli such as heat, light, and electric and magnetic fields.[21–24] Hydrogels are composed of crosslinked polymer chains that create a porous structure, allowing them to absorb and retain water within their networks.[25–27]

In addition to the inherent properties, stimuli-responsive properties could also be realized by incorporating functional additives to endow specific responses. Recently, metals and ceramics with higher strength than that of polymers have gained increasing attention in 4D printing. The intrinsic SME based on phase transitions of metal alloys and the compositional and structural transformations during ceramics sintering endows the corresponding 4D-printed parts with unique properties and functionalities. The integration of various materials into multi-material objects creates new possibilities in 4D-printed structures as they possess enhanced functionalities, gradient properties, and intricate geometries.

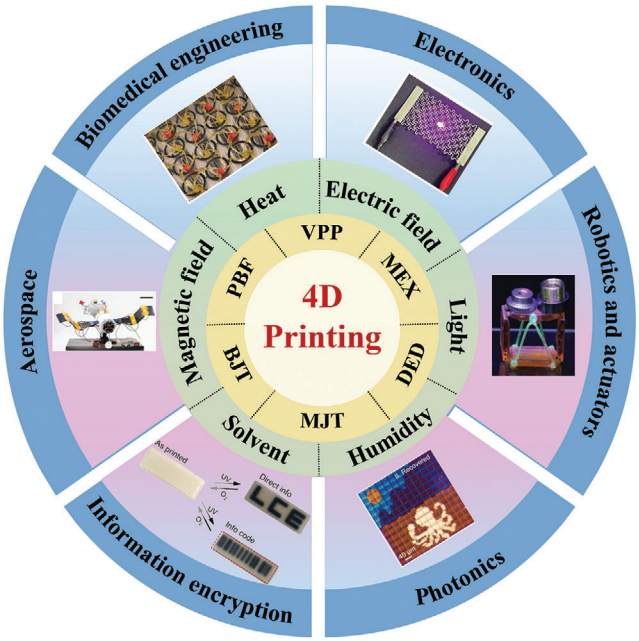

Figure 1. Overview of 4D-printed materials and structures with regard to printing techniques, stimuli, and applications. Printing techniques: VPP, MEX, PBF, BJT, MJT, and DED. Representative stimuli: heat, light, electric field, magnetic field, solvent, and humidity. Primary applications: biomedical engineering (reproduced with permission.[49] Copyright 2020, Wiley-VCH Verlag GmbH), electronics (reproduced with permission.[50] Copyright 2022, Wiley-VCH Verlag GmbH), robotics and actuators (reproduced with permission.[51] Copyright 2022, Wiley-VCH Verlag GmbH), photonics (reproduced with permission.[5] Copyright 2021, Springer Nature), aerospace (reproduced with permission.[52] Copyright 2021, Wiley-VCH Verlag GmbH), and information encryption (reproduced with permission.[53] Copyright 2023, Wiley-VCH Verlag GmbH).

There are many review articles available that discuss the research progress on 4D printing from different perspectives. For example, some focus primarily on printing materials, including SMPs,[28] LCEs,[29,30] hydrogels,[31,32] and multi-materials.[33] Some emphasize a specific stimulus method, such as humidity.[34] Some place particular emphasis on printing techniques or methods, including VPP,[35] direct ink writing (DIW),[36] and fused filament fabrication (FFF).[37] Microscale structures have received priority attention in one of these reviews.[38] There are also reviews focusing on specific application domains, such as biomedical engineering,[39–41] orthopedics,[42] robotics,[43] and textiles.[44] Several reviews have provided thorough overviews of research advancements in 4D printing from a broader perspective.[45–48] As the interest in 4D printing continues increasing with its rapid advancements, the demand for up-to-date reviews has become more pressing than ever to provide a comprehensive understanding that encompasses the latest research developments.

In this paper, we review the burgeoning development of 4D printing with a primary focus on progress made in the recent three years from the aspects of printing techniques, stimuli, and applications (**Figure 1**). The printing strategies adopted in each

Table 1. Overview of various printing techniques for 4D printing.

Printing technique	Printing method	Printing material	Advantage–Disadvantage	Typical resolution	Refs.
Vat photopolymerization (VPP)	Stereolithography (SLA)	Photocurable polymers	✓ Large printing size ✓ High accuracy ✓ Good surface finish ☒ Relatively low printing speed ☒ Limited to photopolymers	10–150 μm	[54]
	Digital light processing (DLP)	Photocurable polymers	✓ High accuracy ✓ Relatively high printing speed ☒ Limited to photopolymers	15–100 μm	[55]
	Two-photon polymerization (TPP)	Photocurable polymers	✓ High resolution ✓ High printing speed ☒ Limited volume ☒ High cost	<100 nm	[56]
Material extrusion (MEX)	Fused filament fabrication (FFF)	Thermoplastic polymers Polymer–Metal	✓ Low-cost printers ✓ Ease of use ✓ Large-scale fabrication ☒ Out-of-plane anisotropy ☒ Limited resolution	100–400 μm	[57]
	Direct ink writing (DIW)	Thermoplastic polymers Thermoset polymers Metals Ceramics	✓ Material versatility ✓ Ease of multi-material printing ☒ Relatively low printing speed ☒ Relatively low resolution ☒ Limited geometry	100–1200 μm	[1]
Powder bed fusion (PBF)	Selective laser sintering (SLS)	Thermoplastic polymers Metals Alloys Ceramics	✓ Material versatility ✓ No need for support structures ✓ High mechanical strength ☒ High-cost printers ☒ Poor surface finish	20–150 μm	[58]
	Selective laser melting (SLM)	Metals Alloys	✓ High mechanical strength and density ✓ Material versatility ✓ Reduced waste ☒ High-cost printers ☒ Poor surface finish	70–100 μm	[59]
Binder jetting (BJT)	BJT	Metals	✓ High printing speed ☒ Poor surface finish ☒ Poor mechanical properties	100–380 μm	[1]
Material jetting (MJT)	PolyJet™	Photocurable polymers	✓ High accuracy ✓ Good surface finish ☒ Limited to photopolymers	16–85 μm	[1]
Directed energy deposition (DED)	Laser DED	Metals Alloys	✓ Large-scale printing ✓ High mechanical strength	250 μm	[60]
	Electron beam DED	Metals Alloys	✓ High density ☒ High-cost printers ☒ Poor surface finish		

technique are discussed regarding the materials categories of SMPs, LCEs, hydrogels, metals, ceramics, active materials integrated with functional additives, and multi-materials. The advantages and limitations of each printing technique in realizing functional structures are considered, and their applications are highlighted. **Table 1** presents an overview of these techniques together with their applicable materials for 4D printing and summarizes their respective advantages and limitations. Finally, the current challenges, future directions, and prospects regarding 4D printing are systematically discussed. This review not only serves as a comprehensive guide for the fabrication of functional materials and structures with different stimulus responses but also offers insights and inspiration for future advancements toward novel 4D printing.

2. Printing Techniques

Among various AM techniques, VPP, MEX, PBF, BJT, MJT, and DED have been used in 4D printing, either individually or combined into hybrid printing. In this section, printing techniques employed in 4D printing are presented in detail, with a particular focus on their applicable printing materials. Beyond the individual printing techniques, this section delves into the realm of hybrid printing, an innovative paradigm that integrates multiple

techniques. The integration of diverse printing methods unlocks design freedom and engineering possibilities, allowing for the fabrication of complex 4D-printed constructs with enhanced performance and functionality.

2.1. Vat Photopolymerization

VPP is a technique in which a liquid photopolymer stored in a vat is selectively cured by visible or ultraviolet (UV) light. Photopolymer resins usually comprise three components: monomers (or oligomers or a mixture), photoinitiators, and photoabsorbers. Upon exposure to light, photoinitiators emit reactive species that act as catalysts, promoting the formation of chains between monomers and oligomers, ultimately resulting in a crosslinked solid. Based on the different curing methods, VPP is usually classified into stereolithography (SLA), digital light processing (DLP), two-photon polymerization (TPP), and volumetric printing.[61] Among these methods, DLP and TPP are the most used ones for 4D printing. **Table 2** summarizes the applicable materials for various VPP methods and their physical properties.

2.1.1. Digital Light Processing

DLP uses a digital light device to selectively project UV light onto a liquid photopolymer resin to form a solid object layer by layer, offering low cost and high precision.[62,63] Since the entire pattern of each layer can be dynamically generated using the digital mirror device (DMD) or dynamic masks such as liquid crystal display (LCD), a fast printing speed can be achieved.[64] DLP has been widely adopted to fabricate SMPs, LCEs, and hydrogels.

There are versatile UV-curable SMP formulations suitable for DLP. For example, an SMP, consisting of a monofunctional acrylate as the chain builder and a soft and a hard diacrylate as the dual crosslinkers, exhibited distinct geometrical complexity such as infinity rings.[65] Zhang et al. fabricated a mechanically robust SMP that exhibited a large stretchability of 1240% at a temperature 30 °C higher than T_g, along with superior fatigue resistance properties over 10000 repetitive cycles.[52] The large deformation mechanism was attributed to the existence of hydrogen bonds and a high molecular aliphatic urethane diacrylate (AUD) crosslinker content (**Figure 2a**). Halogen bond (XB) interaction was incorporated to fabricate supramolecular SMPs for the first time, which exhibited lower hydrophilicity than hydrogen-bonded SMPs, enabling their applications in aqueous environments.[66]

To improve the toughness of DLP-printed epoxy SMPs, an aliphatic urethane acrylate was added into an epoxy vinyl ester resin, and various structures at the micro- to macro-scale with high deformability were built.[67] Wang et al. proposed a simple method for fabricating tough SMP gels by polymerizing an acrylate monomer in a solvent mixture, leading to in situ phase separation with micrometer-sized stiff polymer-rich and soft solvent-rich domains.[68]

Multi-material SMPs could be realized by modulating the light intensity via the DMD during DLP printing, or the so-called grayscale DLP printing,[69,70] to control the spatial distribution. For example, different levels of light intensity result in different crosslinking densities so that multi-material SMPs consisting of different T_g and mechanical properties could be obtained.[71] Recently, Yue et al. used grayscale DLP to fabricate multi-material SMPs with cold-programming capabilities, where a temporary shape could be programmed at low temperatures without the traditional heating–cooling cycle.[72] This unique SME was based on the mechanism that the relaxation time was significantly reduced at high stress, allowing the programmed plastic deformation of the SMP to recover upon heating. As demonstrated in Figure 2b, a heterogenous hinge module with glassy fibers embedded in a rubbery matrix could achieve a bending configuration after cold programming and recover to the original shape upon heating.

Reversible SMPs have garnered significant attention because of their distinctive deformation mechanisms and reversible actuation between two different shapes. Shi et al. proposed a strategy to fabricate reversible SMPs with two crystalline phases possessing two different T_m values based on a thiol–acrylate click reaction.[73] Figure 2c demonstrates the mechanism and the monomers involved in the construction of reversible crystalline SMPs. This two-way SME was attributed to the crystallization-induced elongation (CIE) and melting-induced contraction (MIC) in the semi-crystalline polymer network.[74] Similar 4D-printed SMP structures comprising two switching segments also demonstrated a two-way SME.[75]

To achieve biocompatibility, a shape memory poly(glycerol sebacate) acrylate-co-hydroxyethyl methacrylate was synthesized with T_{trans} close to human body temperature.[76] An elastomeric and soft aliphatic poly(carbonate urethane) (PCU) was synthesized via the radical thiol–ene addition, exhibiting good biocompatibility and cytocompatibility as it degraded into non-acidic products through a surface erosion profile.[77]

Since a pure DLP-printed SMP has relatively low strength for practical use, polymer composites are highly required. It was found that the addition of carbon fibers (CFs) decreased the curing rate and crosslinking density of an epoxy-based shape memory polymer composite (SMPC) but increased its tensile strength and shape recovery rate.[78] The incorporation of silica improved the mechanical strength by an order of magnitude, served as a "superior catalyst" that altered the light scattering, and significantly increased the printing speed while maintaining good optical transparency.[79] Figure 2d demonstrates the rapid curing mechanism of the silica nanoparticles, which reduced the layer curing time from 4 to 0.7 s.

Dynamic covalent bonds are usually introduced to realize reprocessability and self-healing properties such as in the case of vitrimer epoxy.[80] To extend this concept toward 4D printing, Chen et al. employed the two-stage curing method that incorporated dynamic reactions into an acrylate–epoxy hybrid resin, achieving recyclable DLP 4D printing of high-performance thermoset SMPs.[81] Cui et al. incorporated dynamic thiocarbamate bonds into a photocurable methacrylate to prepare a polythiourethane (PTU)-based SMP.[82] As shown in Figure 2e, the crack could be easily repaired when damaged.

The typical shape recovery of SMPs follows a single recovery manner. By taking references of how living organisms achieve it, Peng et al. designed a supramolecular SMP with sufficient ureidopyrimidinone (UPy) hydrogen bond, which endowed the SMP with a unique spatio–temporal shape-morphing programmability.[83] As demonstrated in Figure 2f, when an

Table 2. Overview of representative VPP-based 4D-printed materials with regard to the composition, stimulus, and physical properties.

Printing method	Material type	Material composition	Stimulus	Physical property	Refs.
DLP	SMP	Isobornyl acrylate (IBOA), poly(ethylene glycol) diacrylate (PEGDA), tricyclo[5.2.1.02,6] decanedimethanol diacrylate (TcddA), hexyl acrylate, Irgacure 819, Sudan I	Heat	T_g: 70 °C	[65]
		Poly(glycerol sebacate) acrylate-co-hydroxyethyl methacrylate, Irgacure 819	Heat	T_g: 37.8 °C	[76]
		Epoxy vinyl ester resin, aliphatic urethane acrylate, (5-ethyl-1,3-dioxan-5-yl) methyl acrylate, trimethylolpropane triacrylate (TMPTA)	Heat	T_g: 67–86 °C	[67]
		Tert-butyl acrylate (tBA), aliphatic urethane diacrylate (AUD), IBOA, diphenyl(2,4,6-trimethylbenzoly) phosphine oxide (TPO)	Heat	T_g: 46–54 °C	[52]
		Poly(carbonate urethane), pentaerythritol tetra (3-mercaptopropionate) (PETMP), Irgacure 819, paprika extract, isophorone di(allyl urethane)	Heat	T_g: ≈0–88 °C	[77]
		Bisphenol A diglycidyl ether (DGEBA), acrylate acid, polyethylene glycol dimethacrylate, TPO, triethylamine (TEA), toluhydroquinone, carbon fibers (CFs)/carbon nanotubes (CNTs)	Heat	T_g: ≈67 °C	[78]
		Diethylene glycol diacrylate, tBA, phenylbis (2,4,6-trimethylbenzoyl) phosphine oxide, silica dispersion	Heat	T_g: 37–63 °C	[79]
		Polycaprolactone-diacrylate, polypentadecalactone-diacrylate, PETMP, Irgacure 819	Heat	T_{m1}: 65 °C T_{m2}: 120 °C	[73]
		2,2′-(ethylenedioxy) diethanethiol (EDDET), 2-isocyanatoethyl methacrylate, *N*,*N*-Diisopropylethylamin, methyl methacrylate, Irgacure 819	Heat	*E*: 1.2 GPa σ_c: 61.9 MPa R_f: 97% R_r: 98%	[82]
		PETMP, ureidopyrimidinone (UPy) acrylate, bisphenol A ethoxylate diacrylate (BPAEDA), Irgacure 819	Time	T_g: 6 °C	[83]
		N-(3-(3,6-bis-(5-iodo-1-mesityl-1H-1,2,3-triazol-4-yl)-9H-carbazol-9-yl)propyl)methacrylamide, methacrylic acid, butyl methacrylate, triethylene glycole dimethacrylate, Irgacure 819	Heat	T_g: 69–96 °C R_f: >95% R_r: 99%	[66]
		PEGDA, bisphenol A ethoxylate dimethacrylate (BPA), Iragure 819, Sudan I	Heat	T_g: 60 °C	[49]
		Polylactic acid (PLA)	Heat	T_g: 70.6 °C	[99,100]
		BPAEDA, poly-*N*,*N*′-(m-phenylene)isophthalamide, *N*,*N*-dimethylacrylamide, Irgacure 819	Heat	T_g: 148 °C	[101]
	SMP gel	Hydroxyethyl methacrylate (HEMA), poly(ethyleneglycol) (PEG), poly(propylene glycol), 2-hydroxy-2-methylpropiophenone	Heat	T_g: 75 °C	[68]
	Multi-material SMP	2,5-bis(5-tert-butyl-benzoxazol-2-yl)thiophene	Heat, pressure	T_{g1}: 60 °C T_{g2}: 83 °C	[71]
		2-hydroxyethyl acrylate, IBOA, AUD, Irgacure 819, Sudan I	Heat	T_{g1}: 87 °C T_{g2}: 66 °C T_{g3}: −14 °C	[72]
	LCN	RM257, (4′-pentyl-4-biphenylcarbonitrile), SiC, Omnirad 2100	Solvent	N/A	[88]
	Multi-material hydrogel	Polyurethane (PU), 2-isopropylthioxanthone, acrylic acid (AAC), HEMA, PEGDA	Solvent	N/A	[92]
	Photopolymer	Urethane dimethacrylate, methacrylate, photoinitiator	Solvent	N/A	[93]
		TMPTA, AUD, n-butyl acrylate (BA), Irgacure 819, Sudan I	Heat	N/A	[94]
	Living polymer	EDDET, 2,2-dimethoxy-2-phenylacetophenone (DMPA), trimethylolpropane diallyl ether, Tetraallyloxyethane, diethylene glycol divinyl ether, Irgacure 819, Sudan II	Heat, chemical	*E*: 0.6 MPa	[84]
TPP	SMP	IBOA, PEGDA, TcddA, Irgacure 819	Heat	T_g: 25 °C	[65]
		Vero, 2-hydroxy-3-phenoxypropyl acrylate, TPO, BPA	Heat	T_g: ≈40 °C	[5]
	LCN	RM82, RM257, 2-methyl-1,4-phenylene bis(4-(((4-(acryloyloxy) butoxy)carbonyl)oxy)benzoate), 2-tertbutylbenzene-1,4-diol, 4-(4-(6-acryloyloxyhexyloxy)benzoyloxy)benzonitrile, bis(2,4,6-trimethylbenzoyl)phenylphosphine oxide	Heat	T_{NI}: 100 °C T_g: 69 °C	[109]
	Hydrogel	Poly(N-isopropylacrylamide) (PNIPAM), gold nanorods (AuNRs)	Light	LCST: ≈32 °C	[112]
		AAC, NIPAM, polyvinylpyrrolidone, dipentaerythritol hexaacrylate, 4,4'-bis(diethylamino)benzophenone	pH	N/A	[113]
	Multi-material hydrogel	IP-S, NIPAM	Heat, pH	N/A	[114]
	Photoresist	IP-S	Solvent	N/A	[115]

T_g: glass transition temperature; T_m: melting point; *E*: elastic modulus; $T_{N/SmC}$: temperature at nematic-to-smectic-C phase transition; δ_s: yield strength; MFIS: magnetic field–induced strain; σ_c: tensile strength; R_f: shape fixity ratio; R_r: shape recovery ratio; LCST: lower critical solution temperature; T_{NI}: temperature at nematic-to-isotropic phase transition.

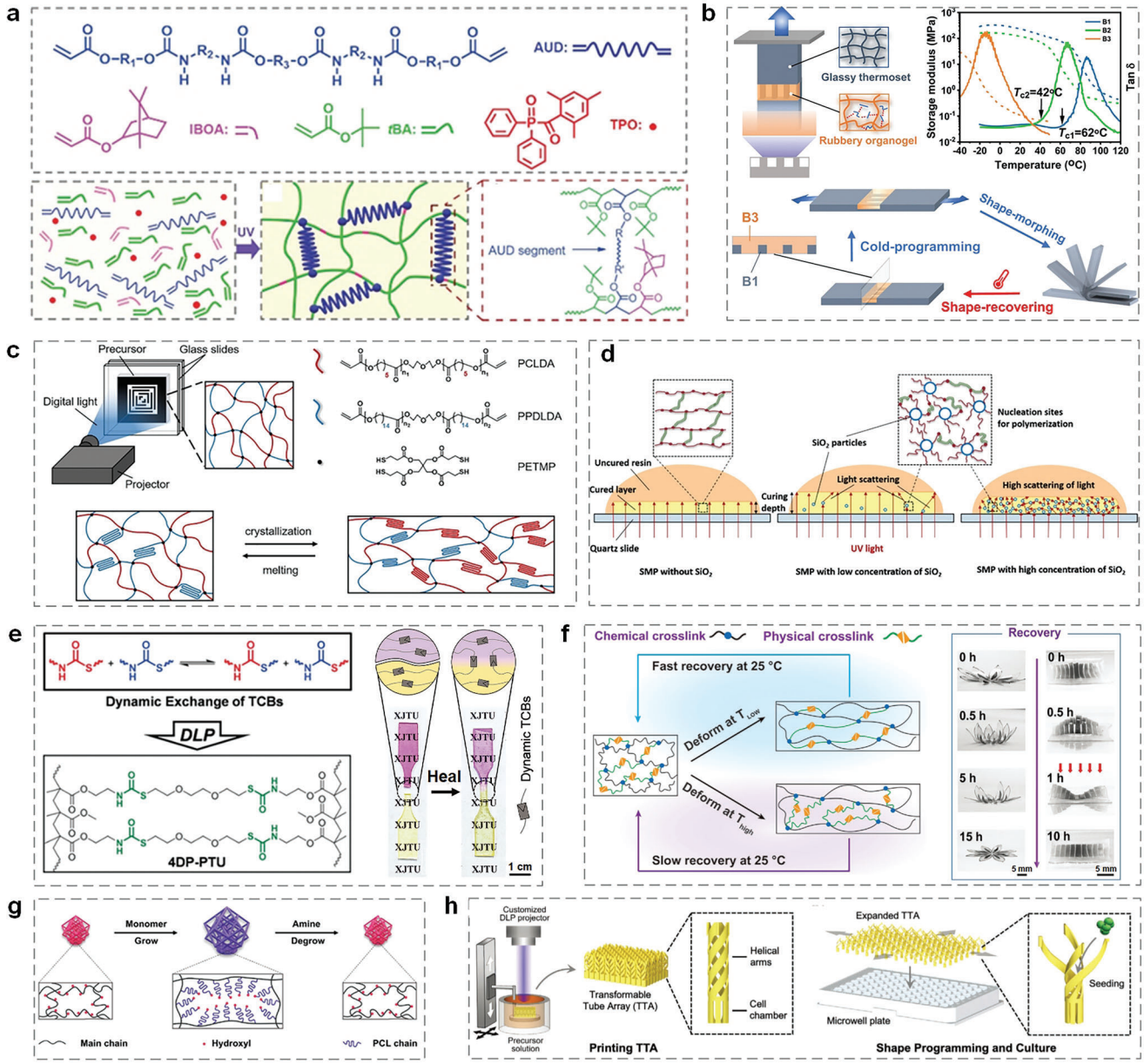

Figure 2. DLP-based 4D printing of SMPs. a) Schematic diagram of the large deformation mechanism of an SMP with ample hydrogen bonds and AUD segments. Reproduced with permission.[52] Copyright 2021, Wiley-VCH Verlag GmbH. b) Schematic diagram of the grayscale DLP setup for a multi-material SMP, thermomechanical properties, and design of a heterogenous hinge module. Reproduced with permission.[72] Copyright 2023, Springer Nature. c) Schematic diagram of the mechanism and monomers employed for the construction of reversible crystalline SMPs. Reproduced with permission.[73] Copyright 2021, Elsevier. d) Schematic diagram of the mechanism of silica particles as nucleation sites for fast curing. Reproduced with permission.[79] Copyright 2020, Elsevier. e) Dynamic exchange reaction and chemical structure in PTU. Reproduced with permission.[82] Copyright 2022, Wiley-VCH Verlag GmbH. f) Mechanism of programming pathways and complex autonomous shape deformation. Reproduced with permission.[83] Copyright 2021, Wiley-VCH Verlag GmbH. g) Chain network change during growth and degrowth of polymers. Reproduced with permission.[84] Copyright 2023, Wiley-VCH Verlag GmbH. h) Structural design of a transformable tube array made of SMPs. Reproduced with permission.[49] Copyright 2020, Wiley-VCH Verlag GmbH.

external force was applied at different temperatures, the faster hydrogen bond exchange rate during deformation at a lower temperature resulted in a faster recovery speed. This strong time-temperature dependency of UPy units was explored as the mechanism for unique autonomous shape changes. Inspired by the cyclic regeneration of turritopsis nutricula, a polymer was designed where the pendent hydroxyl group initiated living polymerization of ε-caprolactone so that the printed polymer grew in an ambient air environment.[84] A subsequent organic amine enabled the cleavage of the polymerized poly ε-caprolactone (PCL) chain into original hydroxyl groups for degrowth, as depicted in Figure 2g.

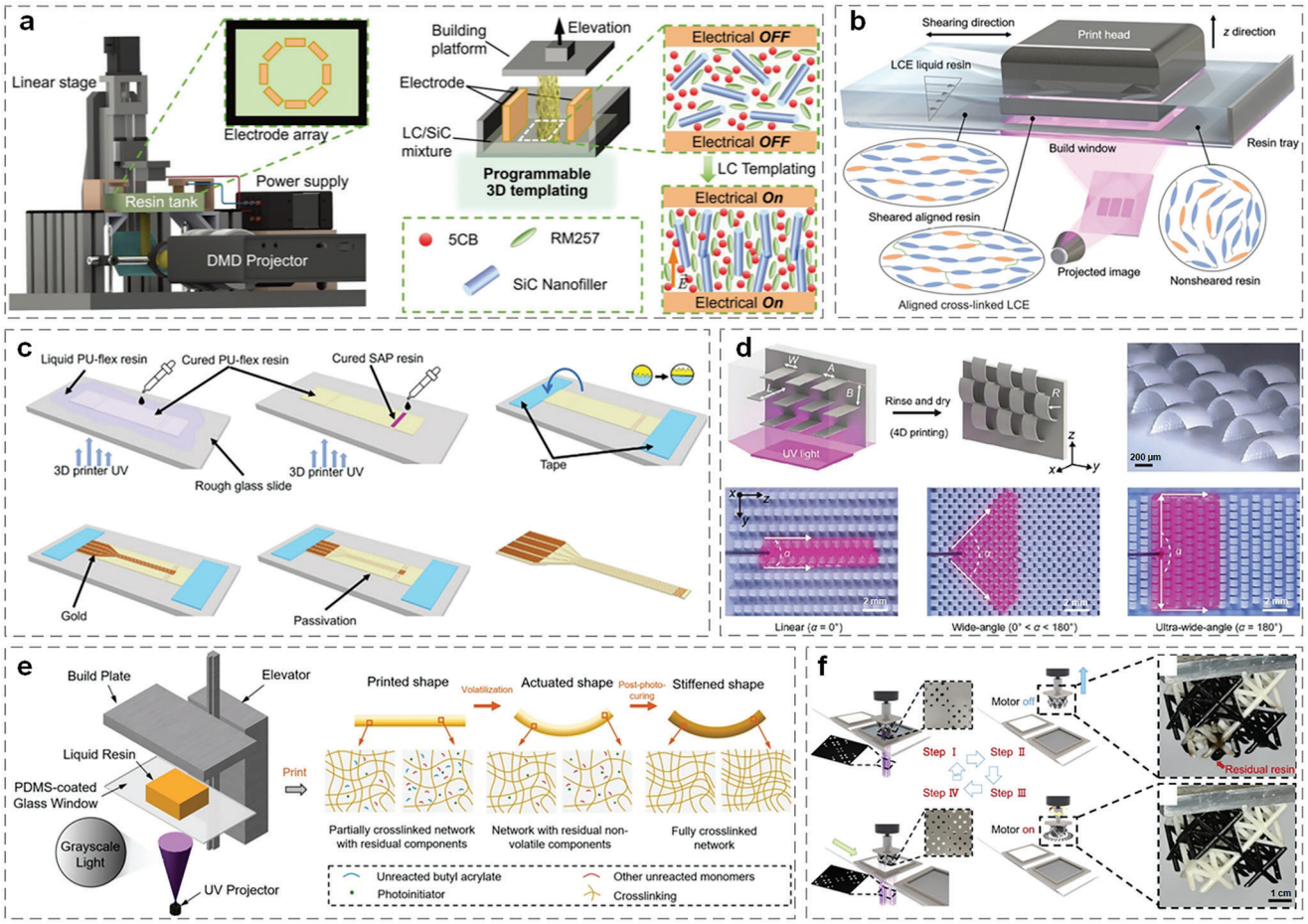

Figure 3. DLP-based 4D printing of LCEs, hydrogels, and other materials. a) Schematic setup of the LC templating-assisted VPP process. Reproduced with permission.[88] Copyright 2022, Wiley-VCH Verlag GmbH. b) Schematic diagram of the printing process of an LCE with shear alignment through the cyclic rotation of the resin tray. Reproduced with permission.[89] Copyright 2021, American Association for the Advancement of Science. c) Schematic diagram of the fabrication process of a 4D-printed hydrogel-based electrode. Reproduced with permission.[92] Copyright 2023, Wiley-VCH Verlag GmbH. d) Illustration of 4D-printed re-entrant structures and the unidirectional liquid transport with different angles. Reproduced with permission.[93] Copyright 2023, Wiley-VCH Verlag GmbH. e) Illustration of grayscale DLP printing and the shape transformation mechanism based on volatilization upon heating. Reproduced with permission.[94] Copyright 2020, American Chemical Society. f) Working principle of centrifugal multi-material printing. Reproduced with permission.[97] Copyright 2022, Springer Nature.

In addition to using DLP-printed SMPs individually, complex structures can be designed to demonstrate compatibility with other materials, such as cell lines. Figure 2h demonstrates a 4D-printed transformable tube array made of an SMP, consisting of lower chambers where cells were seeded and upper helical arms for shape transformation with a 3.6-time size change.[49]

DLP has been used for both polydomain and monodomain LCE structures. Various complex porous lattice structures were fabricated based on polydomain LCEs with high resolution.[85,86] Different from SMPs, which depend more on the shape programming step after printing, the LC alignment of monodomain LCEs contributes to the anisotropic mechanical and actuation properties. Several LC alignment methods have been developed and incorporated into the DLP printing process, including exertion of external fields,[87,88] shear forces,[89] the shape memory mechanism,[90] and the solvent-assisted entropic method.[91]

A reorientable magnetic field has been proved to successfully induce the molecular orientations of LCs voxel by voxel.[87] Another strategy was based on leveraging photopolymerization-induced phase separation (PIPS) and an electric field, as depicted in **Figure 3a**.[88] The long-range alignment of LCs in turn aligned the non-electro-responsive silicon carbide (SiC) nanofillers to enhance the physical properties. Shear flow during the DLP process can also align LCs. Through the cyclic rotation of the resin tray and built-in shear separation, an LCE structure with spatial mesogen alignment and a well-orientated order was realized layer by layer, as shown in Figure 3b.[89]

Although the mesogen alignment of an LCE is usually fixed during the chemical synthesis, there are some methods to reprogram the LC alignment post-synthesis, such as the shape memory mechanism. Chen et al. introduced a crystalline phase into a DLP-printed LCE network with crystalline melting transition above the nematic-to-isotropic phase transition temperature T_{NI}, thereby enabling the programmability of the mesogen alignment.[90] When the printed part was heated above T_m, the alignment could be erased so that repeated reprogrammability

was achieved. The solvent-assisted entropic approach is another efficient method to reprogram the LC alignment. Jin et al. developed an entropic approach for programming the mesogen alignment by employing directed solvent evaporation from an isotropic LCE organogel under stress.[91] Meanwhile, the alignment of the DLP-printed LCE could be erased and reprogrammed via reswelling and deswelling under stress, respectively. These methods decoupled the LCE synthesis and molecular alignment, thereby enabling the creation of diverse shape-morphing structures with unprecedented spatial and temporal control.

Hiendlmeier et al. 4D-printed an electrode of a bilayer substrate consisting of a flexible polyurethane (PU) and a superabsorbent sodium acrylate hydrogel by DLP, followed by sputtering microcracked gold as conductive layers as shown in Figure 3c.[92] This 4D-printed electrode exhibited a stretchability of above 20% and could be bent easily to facilitate the implantation during surgery.

Besides utilizing intrinsic smart materials, there are other routes to realize autonomous shape transformation. For example, butterfly wing–inspired 4D-printed re-entrant structures enabled unidirectional liquid transportation at different angles controlled by Laplace pressure, as shown in Figure 3d.[93] Exploiting the heterogeneity in grayscale DLP printing is another method. Unreacted volatile monomers could escape upon heating, which led to a mismatch in the shrinkage strain that enabled autonomous shape transformation.[94] Figure 3e demonstrates the experimental setup of grayscale DLP printing together with the shape change mechanism where the reaction of monomers varied along the thickness direction. Similarly, the heterogeneous crosslinking density along the thickness direction triggered the bending actuation because of the removal of unreacted monomers in ethanol.[95] Thus, it led to a shape change of the printed microneedle barb from a flat shape to a backward-facing curved shape.

A DLP-based multi-material printer was built to construct hybrid structures consisting of highly stretchable hydrogel covalently bonded with various UV-curable polymers, including hydrogel–SMP multi-materials.[96] This multi-material printer was later modified with a centrifugal setup to construct large heterogeneous structures with programmable composition, properties, and functions at the voxel level, as shown in Figure 3f.[97] Various heterogeneous structures were fabricated by integrating SMP with hard polymer or hydrogel with digital polymer containing hard and soft voxels.

In addition to using the DMD, the LCD screen is also employed in DLP.[98] Xin et al. fabricated auxetic chiral metamaterials with tunable, programmable, and reconfigurable mechanical properties.[99] The non-linear J-shaped deformation modes based on the structural design enabled the printed metamaterial structures to match specific bio tissues/organs and to be converted to another biomaterial through programming. The authors further 4D-printed a pixel mechanical metamaterial by integrating collagen fiber–inspired helical ligament and a mechanical pixel array design.[100] With excellent programmability, the pixel metamaterial demonstrated excellent protection performance, thereby exhibiting great potential as a buffer device. For applications at high temperatures, a photosensitive aromatic polyamide–based SMP with high T_g was fabricated with enhanced thermal and mechanical properties.[101] This SMP maintained its high T_g and good shape memory properties after gamma radiation of 200 Gy.

Liquid metal (LM) exists in the liquid phase in an ambient environment, exhibiting intrinsic deformability which is advantageous for various printing techniques.[102,103] Zhang et al. grafted reversible addition–fragmentation chain transfer polymerization agents onto LM nanoparticles, which were directly printed by DLP.[104] This work provided a simple and efficient strategy for fabricating functional light-responsive LM–polymer composites.

It is worth mentioning that as a variation of DLP, digital light printing is another method to transform 2D films into 3D complicated shapes based on the stress mismatch from light-defined material heterogeneity. By using this method, various materials, including SMPs,[105] LCEs,[11] and hydrogels,[106] capable of highly designable motions could be fabricated.

2.1.2. Two-Photon Polymerization

TPP employs two-photon absorption of highly focused femtosecond laser pulses to polymerize a photosensitive liquid phase resin, thereby enabling the construction of arbitrary complex structures with nanometer accuracy.[107] Two-photon lithography (TPL) is a specific application of TPP, and multi-photon lithography (MPL) is related to the absorption of three or more photons at the same time.

A similar SMP formulation suitable for DLP was also found compatible with the TPP method, and various microstructures with fast printing speeds (1000 μm s^{-1}) were demonstrated.[65] Inspired by the nanoimprint lithography–assisted nanoscale patterns,[108] Zhang et al. employed TPL to fabricate SMP photoresist structures at the submicron level with a high resolution of ≈300-nm half pitch.[5] The upright grids on nanostructured SMPs served as a structural color filter that only transmitted some specific range of visible light, which became invisible when the nanostructures were flattened under the heat stimulus (**Figure 4a**).

A liquid crystalline network (LCN) is a class of smart materials that incorporate liquid crystalline molecules to build a highly crosslinked polymer network.[29] An LCN-based photoresist was printed by TPP where the mesogenic alignment was controlled by the aligned layers in the cell construct.[109] The 4D-printed photoresist together with the cell was further immersed in a warm solvent to remove unreacted monomers to build uniaxially aligned microstructures as illustrated in Figure 4b.

Different from directly incorporating dyes into the LC formulation, a two-step approach was proposed, which first used TPP to construct aligned LCEs and then incorporated different types of dyes into the printed microstructures by diffusion (Figure 4c).[110] This method avoided the incompatibilities of dye-containing inks and enhanced the performance of microstructures compared to using the conventional one-step method. The independent and arbitrary alignment control of LCs at 3D voxels could also be realized by applying homogeneous quasi-static electric fields of an arbitrary direction in situ during the MPL printing process.[111]

TPP has also been widely used to fabricate hydrogels. Nishiguchi et al. printed a bioinspired poly(N-isopropylacrylamide) (PNIPAM) / gold nanorod (AuNR) hydrogel structure with a defined 3D geometry and programmed

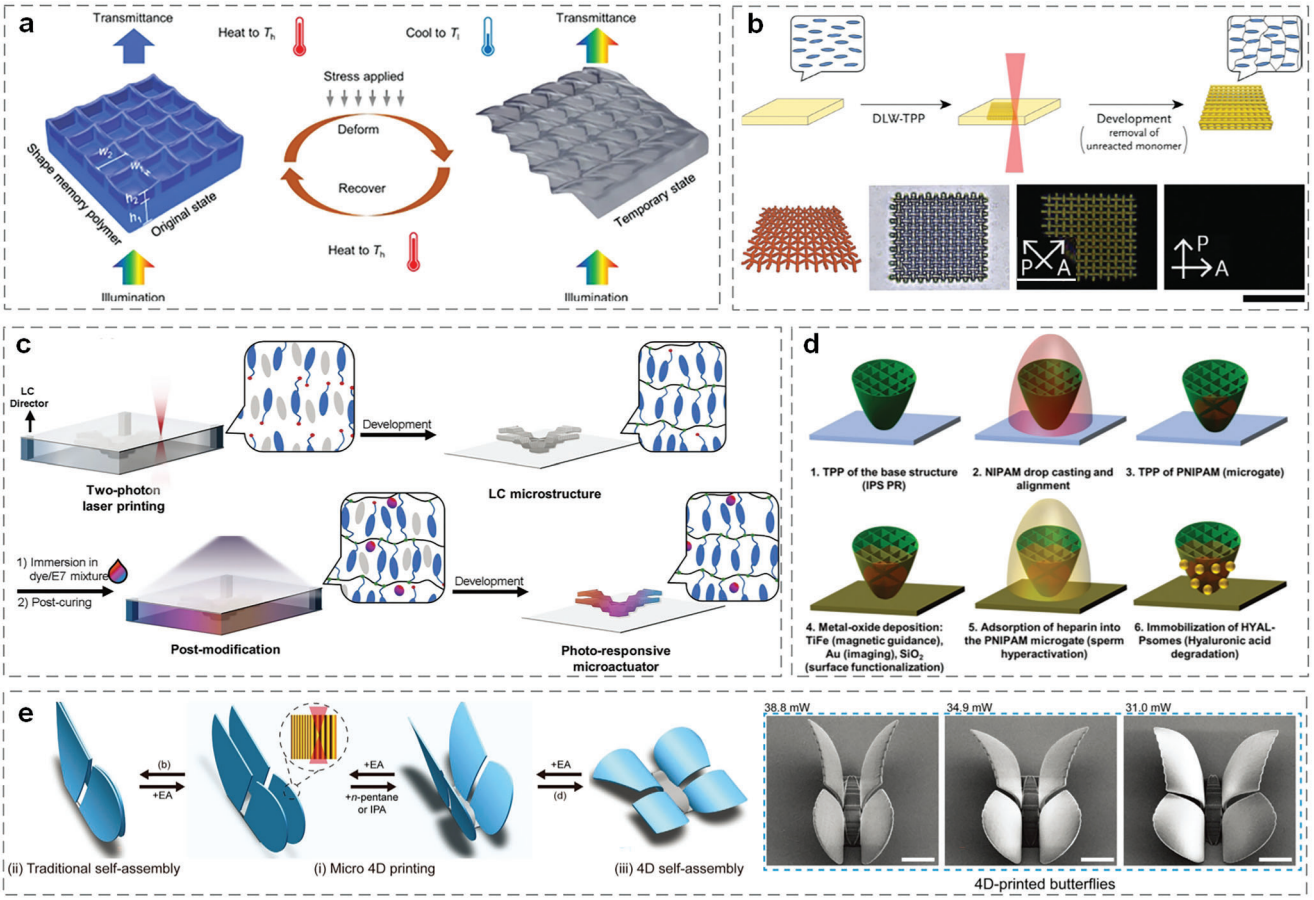

Figure 4. TPP-based 4D printing. a) Schematic diagram of the color and shape change of a TPL-printed nanostructured SMP. Reproduced with permission.[5] Copyright 2021, Springer Nature. b) Schematic diagram of the fabrication steps of an LCN-based photoresist through TPP and optical images of a uniaxially aligned microstructure under crossed polarizers. Scale bars, 4 μm. Reproduced with permission.[109] Copyright 2021, Wiley-VCH Verlag GmbH. c) Schematic approach of a two-step TPP method to construct LCE microstructures by diffusing different types of dyes and post-curing. Reproduced with permission.[110] Copyright 2022, Wiley-VCH Verlag GmbH. d) Schematic diagram of the fabrication process of TPP-printed hydrogel microcarriers. Reproduced with permission.[114] Copyright 2022, Wiley-VCH Verlag GmbH. e) Self-assembly of a 4D-printed butterfly structure with smooth morphology and controlled shapes at different laser power. Scale bars, 20 μm. Reproduced with permission.[115] Copyright 2021, Wiley-VCH Verlag GmbH.

printing density by MPL.[112] A series of multiarmed PNIPAM crosslinkers consisting of main-chain PNIPAM and a terminating allyl group was synthesized to enhance the printing resolution and promote the gelation efficiency. Hu et al. employed TPP to fabricate biomimetic hydrogel structures in a spatiotemporal domain.[113] Since the microstructure had a microscale size, the response frequency substantially increased. TPP-printed PNIPAM was integrated with a non-stimuli-responsive polymer to fabricate sperm microcarriers, following the fabrication process illustrated in Figure 4d.[114] After printing, a metallic layer was coated to increase the imaging ability of the microcarriers and then functionalized by loading heparin and immobilizing HYAL-Psomes.

TPP enables the fabrication of reversible self-assembly of microstructures based on spatially controlled asymmetric crosslinking densities. Figure 4e demonstrates the superiority of self-assembly realized by 4D printing over traditional assembly where the printed butterfly models exhibited smooth morphology and controlled shape at different laser power.[115] The vertical microstructures thus flexibly switched to curved shapes with desired thickness and curvature, which were hard to obtain directly by conventional 3D printing.

2.2. Material Extrusion

MEX is an AM technique where materials are extruded either in the form of filaments (FFF) or inks (DIW). **Table 3** summarizes the 4D-printed materials applicable to MEX together with their physical properties. MEX enables the printing of a wide variety of materials, including polymers, metals, ceramics, and multimaterials.

2.2.1. Direct Ink Writing

DIW is an extrusion-based AM method where a viscoelastic ink is extruded through a deposition nozzle and deposited along

Table 3. Overview of MEX-based 4D-printed materials with regard to composition, stimulus, and physical properties.

Printing method	Material type	Material composition	Stimulus	Physical property	Refs.
DIW	SMP	Acrylate β-CD PCL, EDDET, PETMP, Irgacure 819, TEA	Heat	T_m: 55.5 °C R_f: 98.0% R_r: 99.2%	[128]
		AuNPs/PU	Light	T_g: 40–44 °C	[120]
		Nano-hydroxyapatite (nHA) / PU	Heat	T_g: 38–46 °C	[121]
		AuNPs/nHA/PU	Light	T_g: 42.5 °C	[204]
		Poly(D,L-lactide-co-trimethylene carbonate), poly(trimethylene carbonate), Fe_3O_4	Magnetic field, heat	T_{g1}: ≈52 °C T_{g2}: ≈64 °C	[123]
		Poly(glycerol dodecanoate) acrylate	Heat	T_{trans}: 20–37 °C	[130]
	LCE	RM82, *n*-butylamine (*n*BA), Irgacure 651	Heat	T_{NI}: 89, 100 °C T_g: −18 °C	[145,146,157]
		RM82, A6A, EDDET, 1,8-diazabicyclo[5.4.0]undec-7-ene (DBU)/TEA, Irgacure 819	Heat, light	T_{NI}: 83 °C T_g: −31 °C $T_{N/SmC}$: 42 °C	[205]
		RM82, A6A, *n*BA, Irgacure784	Light	N/A	[206]
		RM257, EDDET, Irgacure 651	Heat	N/A	[150]
		RM82, *n*BA, butylated hydroxytoluene (BHT), Irgacure 651, eutectic gallium indium (EGaIn)	Electric field	T_{NI}: 127 °C	[151]
		RM257, EDDET, dipropylamine (DPA), Irgacure 2959	Heat	T_{NI}: ≈74 °C	[156]
		RM82, *n*BA, Irgacure 369	Heat	T_{NI}: 90–110 °C	[158]
		RM82, RM257, (3R,3aR,6S,6aR)-hexahydrofuro[3,2-b]furan-3,6-diyl bis(4-((6-(acryloyloxy)hexyl)oxy)benzoate), *N*,*N*-dimethylpropane-1,3-diamine, butylated hydroxytoluene, Irgacure 819	Humidity	T_{NI}: 72 °C	[162]
		RM82, A6A, EDDET, DBU, Irgacure 819, (3R,3aR,6S,6aR)-hexahydrofuro[3,2-b]furan-3,6-diyl bis(4-((6-(acryloyloxy)hexyl)oxy)benzoate)	Light	T_{NI}: 55 °C	[163]
		RM257, EDDET, Irgacure 651, titanium-based nanocrystal	Light	T_{NI}: ≈55–61 °C	[53]
		RM257, *n*BA, DMPA, Nigrosine B	Light	T_{NI}: 76 °C T_g: −0.6 °C	[159]
		RM257, EDDET, PETMP, TEA, 4-methoxyphenol, (2-hydroxyethoxy)-2-methylpropiophenone, 1,5-diazabicyclo[4.3.0]non-5-ene	Heat	T_{NI}: ≈75 °C	[153]
		RM257, RM82, A6A, EDDET, dimethylphenylphosphine, hexamethylene diisocyanate, TEA, 1,6-hexanedithiol	Heat, light	T_g: −16 °C T_m: 176 °C	[166]
		RM82, bismaleimide, 4,4'-bis(9-(acryloyloxy)nonyloxy)azobenzene, 2(6-isocyanatohexylaminocarbonylamino)-6-methyl-4[1H]pyrimidinone	Light, heat	T_g: 7 °C T_{NI}: 58 °C	[6]
		RM257, EDDET, DPA, Irgacure 2959	Heat	T_{NI}: 50–70 °C T_g: 14 °C	[207]
		RM82, EDDET, DBU, DMPA, BHT, AuNRs	Light	T_{NI}: 141 °C T_g: −8 °C	[155]
		RM82, RM257, EDDET, BHT, TEA, Irgacure 819, liquid metal	Eddy current	N/A	[208]

(*Continued*)

Table 3. (Continued)

Printing method	Material type	Material composition	Stimulus	Physical property	Refs.
	Multi-material LCE	RM257, *n*BA, EGaIn, Irgacure 369	Electric fields, light	N/A	[152]
	Hydrogel	Acrylamide (AA), *N*,*N*′-methylenebisacrylamide (Bis), yeast, phenyl-2,4,6-trimethylbenzoylphosphinate (LAP), cellulose nanocrystals	Biomolecules	*E*: 13–26 kPa	[167]
		Mxene, poly(3,4-ethylenedioxythiophene), poly(styrene sulfonate), dimethyl sulfoxide, sulfuric acid, sodium L-ascorbate	Heat	N/A	[168]
		Nanothylakoid, laponite, NIPAM, AA, Bis, LAP	Heat, light	LCST: 32 °C	[171]
		Methacrylated bovine serum albumin, NIPAM, dimethylaminoethyl methacrylate, LAP, F127	Heat, pH, enzyme	LCST: 32 °C	[173]
	Magnetic active materials	Polydimethylsiloxane (PDMS), silicone, NdFeB	Magnetic fields	N/A	[175]
		PDMS, silicone, NdFeB, SiO_2		N/A	[176]
		Magnetic soft materials: AUD, 2-phenoxyethanol acrylate, isodecyl acrylate, phenylbis (2,4,6-trimethylbenzoyl) phosphine oxide, SiO_2, NdFeB Magnetic SMPs: AUD, 2-phenoxyethanol acrylate, isobornyl acrylate, phenylbis (2,4,6-trimethylbenzoyl) phosphine oxide, SiO_2, NdFeB		N/A	[137]
		PDMS, NdFeB, dibutyl phthalate, SiO_2		N/A	[209]
	Shape memory material	Keratin protofibrils	Solvent	ε_b: 85% δ_s: 96.1 MPa σ_c: 137.2 MPa	[138]
	Elastomer composite	Silicone rubber, graphene plates, methanol	Light	N/A	[178]
	Multi-material metal	Cu–Ni	Heat	N/A	[180]
	Ceramics	Preceramic polymers, ZrB2 nanoparticles	Heat	T_g: 95 °C	[129]
		ZrO_2 particles, UV resin	Heat	N/A	[183]
FFF	SMP	PLA, carbon black	Light	T_g: 62, 79 °C	[186,210]
		PLA, CNTs/CFs	Electric fields	T_g: 90, 60 °C	[188,211]
		PLA, TPU, MXene	Heat	T_g: 50–54 °C	[187]
		PLA, poly(lactic-co-glycolic acid), acetyl tributyl citrate	Heat	T_g: 43 °C	[191]
		PLA, PEG, BaSO4	Heat	T_g: 44±3 °C	[192]
		PLA	Heat	*E*: 1.6 GPa σ_c: 50 MPa	[194]
		Poly(ether ether ketone) (PEEK)	Light	T_g: 152 °C R_r: >97%	[198]
		DGEBA, benzoxazine, CNTs	Heat	T_g: 179 °C R_r: ≈98%	[200]
		PLA, Fe_3O_4	Magnetic fields	N/A	[212]

ε_b: elongation at break

digitally defined paths to build 3D structures layer by layer under controlled flow rates.[33,36] Since the publication of the first work on 4D printing of hydrogels based on DIW,[9] this technique has garnered substantial attention within the realm of 4D printing.[116–119]

Thermoplastic SMPs and SMPCs are usually DIW-printed either by heating above T_m or being dissolved in a volatile solvent. Gold nanoparticle (AuNP)– and nano-hydroxyapatite (nHA)–reinforced PU has been printed at high temperatures.[120,121] The 4D-printed AuNP/nHA/PU composites possessed excellent computed tomography (CT) developability under X-ray contrast examination. In addition to fabricating homogenous SMPCs, co-extrusion of continuous metallic fibers embedded in poly(ether ether ketone) (PEEK) has been conducted, which exhibited electrical heating paths.[122] To extend the number of temporarily memorized shapes, a triple SMP consisting of poly(D,L-lactide-co-trimethylene carbonate)/poly(trimethylene carbonate) polymer blends embedded with magnetic Fe_3O_4 particles were prepared.[123] Multi-material SMPC structures with in-plane and out-of-plane shape changes were built by depositing thermoplastic polyurethane (TPU) / PCL and TPU/Fe_3O_4 together.[124,125]

DIW has been used to fabricate more thermoset SMPs than thermoplastics.[117,118,126–127] He et al. synthesized a photocurable SMP via UV light–assisted DIW based on the rapid thiol–acrylate click reaction of acrylate β-cyclodextrin PCL with dithiol or trithiol.[128] This biocompatible SMP served as a drug carrier for sustained drug release of everolimus through the host–guest coordination. Chen et al. synthesized a multifunctional preceramic polymer composite with reconfigurability and the SME.[129] This preceramic SMP underwent the sequential formation of two crosslinking networks during a stepwise curing process, resulting in its reconfigurability. During sintering, the reconfigured preceramic SMP pyrolyzed into lightweight ceramics with a uniform linear shrinkage of 28%, demonstrating a novel strategy to construct geometrically complex ceramics. Zhang et al. modified a poly(glycerol dodecanoate) acrylate–based SMP with T_{trans} in the range of 20–37 °C, close to body temperature.[130]

The extension of functionalities of DIW-printed thermoset SMPs have attracted increasing attention. The shear force could align stiff microfibers during printing, and the printed composites demonstrated multistability above T_g by having the directional and mismatched pre-stress encoded.[131] Chi et al. 4D-printed a graphene nanoplatelet (GNP) / epoxy–based SMPC that could be recycled and then used as a thixotropic agent to be printed again with unchanged properties for four cycles.[132] Weng et al. 4D-printed glass fiber–reinforced composites with large strain shape-shifting, high modulus (≈4.8 GPa), and anisotropic mechanical properties.[133]

Ever since the inception of 4D-printed magnetic soft materials (MSMs) comprising hard magnetic particles in soft polymeric matrices,[8] there has been a growing interest in the versatile capabilities of soft magnetic composites.[134,135] These advancements have particularly aroused interest in achieving untethered, rapid, and reversible actuation, along with the remarkable feature of shape locking, by embedding magnetic particles in SMPs (M-SMPs).[136] Ma et al. employed multi-material DIW printing to seamlessly incorporate an MSM and M-SMP into an intricate structural design (**Figure 5a**), which realized multimodal shape transformation and tunable materials properties.[137]

Different from synthetic SMPs, Cera et al. designed a hierarchically structured shape memory material inspired by the reversible keratin transition from α-helix to β-sheet, with long-range molecular order.[138] The keratin protofibrils extracted from animal hair spontaneously organized into a nematic phase during the extrusion process, resulting in the anisotropic protofibril alignment. By printing the protein dope in a hydrogel-based supporting and coagulation bath followed by oxidative treatment, geometrically complex structures were obtained.

DIW has been widely employed to fabricate LCEs with various deformation modes.[139–148] Taking the most commonly used main-chain LCEs as an example, a two-step polymerization method contains a chain extension reaction and subsequent photopolymerization to lock the shear force–aligned mesogens.[18,149] When the translational printing substrate was replaced by a rotating cylindrical substrate, the modified DIW apparatus enabled the fabrication of a 3D tubular LCE with highly programmed 3D alignment of mesogens.[150]

When a DIW printer was modified with a core–shell nozzle at a tilted angle, a coaxial core–shell LM–LCE structure was printed as shown in Figure 5b.[151] The presence of LM enabled the resistance and shape changes of the structure around T_{NI}. In addition to constructing the core–shell structure, LM was embedded into an LCE ink by adding a solvent to form dispersed droplets with desired sizes, which enabled sufficient filler content for electrical responses while maintaining the elastomeric mechanical properties.[152] To extend more diversified and arbitrary shape changes of LCE structures, Barnes et al. proposed a method that decoupled printing and programming processes into three steps.[153] A partially crosslinked printable LCE ink was printed into a catalyst bath to complete the thiol–acrylate reaction and then shape-programmed by mechanical deformation under UV light to trigger crosslinking of unreacted acrylate groups.

Since extrusion has an important effect on the performance of 4D-printed LCE structures, it is necessary to investigate the variable printing parameters in detail. The influence of printing parameters, including the printing temperature, gap size, nozzle diameter,[154] and printing speed,[155] on the actuation strain was systematically investigated. A unique core–shell alignment of LC was observed where the orientation was randomly aligned in the core but uniformly aligned along the printing path in the shell (Figure 5c), as validated by the polarized optical microscopy (POM) images at different printing temperatures.[154] The influence of the flow rate on the process–structure–property relationship was further studied for 4D-printed LCE sheets.[156] The mechanical and optical properties upon uniaxial tensile loading could be easily tuned by the mesogen orientation, loading direction, and temperature changes.

Ren et al. proposed that instead of changing the temperature which is time-consuming, various shape change modes of 4D-printed LCEs could be easily achieved by controlling the printing speed and printing path.[157] The interaction of multiple printing parameters on the filament width and shape-morphing behavior was further studied, including the printing speed, extrusion pressure, printing height, and UV light intensity.[158] Different printing parameters were investigated as one input based on the logic of AND gates. The influence of UV light intensity on T_{NI} and the actuation strain was revealed to design the threshold temperature.

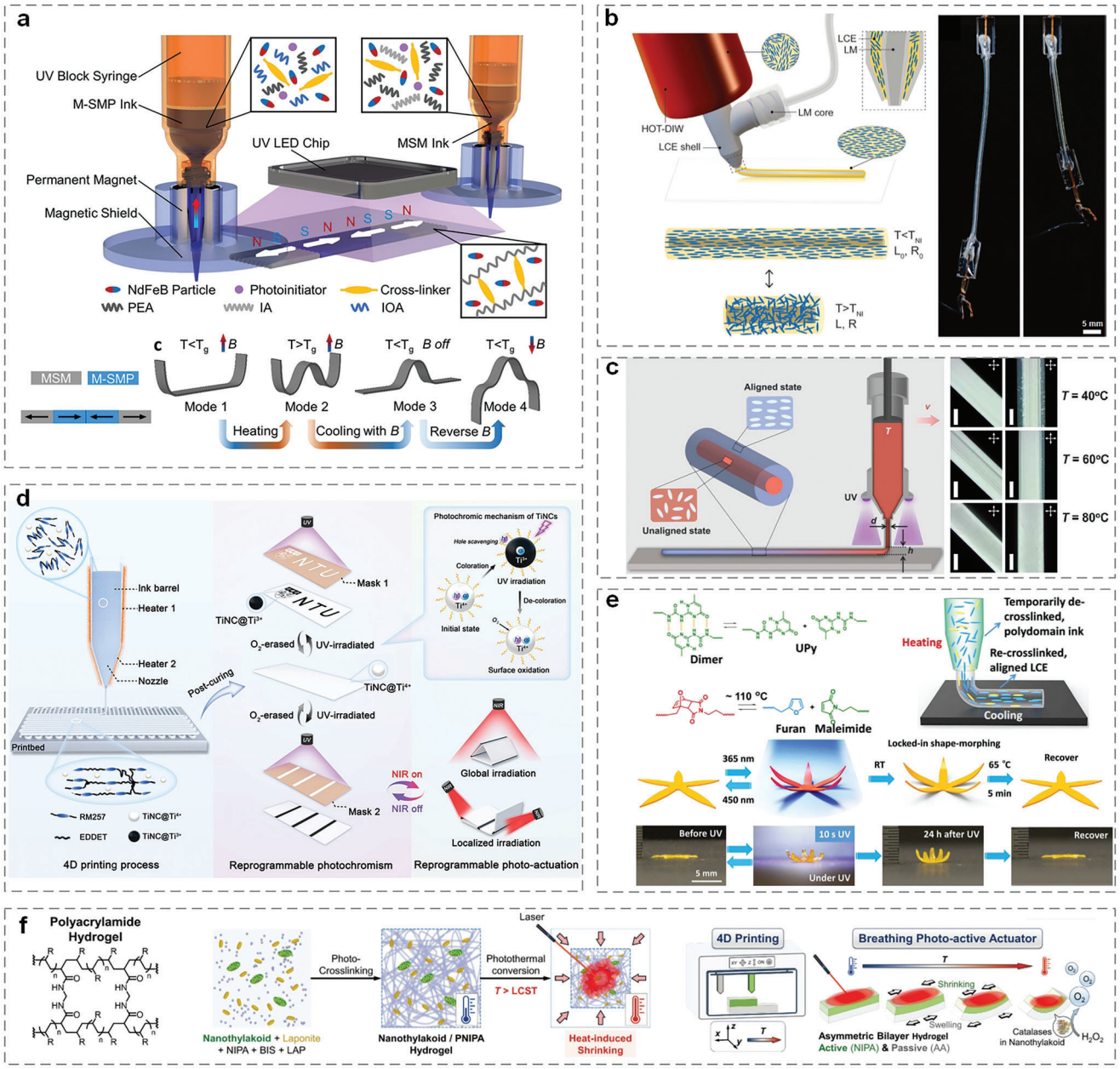

Figure 5. DIW-based 4D printing of SMPs, LCEs, and hydrogels. a) Schematic diagram of DIW printing of a magnetic SMP–based multi-material and the magnetization working principle. Reproduced with permission.[137] Copyright 2021, American Chemical Society. b) Schematic diagram of the core–shell printing of LCE–LM and actuation of the printed filament. Reproduced with permission.[151] Copyright 2021, Wiley-VCH Verlag GmbH. c) Unique core–shell LC alignment in an extruded filament and POM images at different printing temperatures. Scale bars, 0.5 mm. Reproduced with permission.[154] Copyright 2020, American Association for the Advancement of Science. d) Schematic diagram of the reprogrammable LCE composites with tunable photochromism and photoactuation capabilities, and the working mechanism for reversible color change. Reproduced with permission.[53] Copyright 2023, Wiley-VCH Verlag GmbH. e) Use of UPy hydrogen bonds and covalent DA bonds for the LC alignment and reconfigurability of a printed LCE under UV light. Reproduced with permission.[6] Copyright 2021, Wiley-VCH Verlag GmbH. f) Working principle and schematic transformation from H_2O_2 to oxygen by catalytic hydrogel structures. Reproduced with permission.[171] Copyright 2021, Wiley-VCH Verlag GmbH.

Chen et al. incorporated titanium-based nanocrystals (TiNCs) in an LCE with reprogrammable photochromism and photoactuation capabilities, as demonstrated in Figure 5d.[53] Because of the photoreduction of Ti^{4+} to Ti^{3+} species by photoexcited electrons, the LCE composites reversibly changed color between white and black upon UV irradiation and oxygen exposure, respectively. Moreover, the black structure absorbed light energy and converted it into heat with high efficiency. Yang et al. integrated highly luminescent perovskite quantum dots (PQDs) fabricated by inkjet printing with DIW-printed responsive LCEs.[159] Through siloxane covalent chemistry, the integrated device demonstrated free stretchability and foldability due to the robust

interface bonding. By tailoring the PQD ink formula, the fluorescence color could be tuned on demand and exhibited temperature dependence. Recently, Wang et al. proposed an off-center free-standing continuous fiber–reinforced LCE method to build 3D structures with high bearing capacity and enhanced deformation capacity and mechanical properties.[160]T

Cholesteric LCEs consist of chiral liquid crystal molecules oriented in a helical structure. Upon external stimuli, the molecular orientation and pitch of the helix change, leading to a change in color.[161] The incorporation of synthesized diacrylate chiral dopant endowed a 4D-printed LCE with cholesteric alignment.[162] The special ionic chain extender could have a positive charge, allowing water to swell the cholesteric elastomer. An azobenzene-functionalized cholesteric LCE was developed with three different mesophases, namely planar cholesteric, slanted cholesteric, and uniaxial pseudo-nematic states.[163] This method simplified the construction of multifunctional structures by tuning printing parameters instead of materials formulations, which shortened the fabrication time.

Dynamic covalent bonds are also employed in 4D-printed LCEs to achieve reconfigurability. Davidson et al. employed a special type of allyl dithiol to synthesize an LCE with light-triggerable dynamic bonds, where UV light can be used to achieve controlled network reconfiguration without an imposed mechanical field.[164] This method enabled the actuated shape to be locked under high-temperature UV exposure. Lu et al. synthesized a photoswitchable azobenzene-functionalized LCE based on both supramolecular UPy hydrogen bonds and dynamic covalent furan–maleimide Diels–Alder (DA) bonds.[6] During high-temperature printing, these two reversible bonds de-crosslinked so that the mesogen alignment was realized, as shown in Figure 5e. It was found that the UPy interactions made a great contribution to the shape-locking capability after the removal of the UV light, which could be activated to recover the original shapes by reheating.

Hydrogen-bonded supramolecular LCEs possess self-healing and recyclable properties. Lugger et al. synthesized a supramolecular PTU LCE, and the dissociation of hydrogen bonds at high temperatures enabled it to be printed by DIW.[165] The 4D-printed LCE strip demonstrated recyclability for several cycles of cutting and re-printing while the actuation strain diminished to some extent. Based on the same material, azobenzene photoswitches were then introduced to prepare light-fueled supramolecular LCEs.[166]

Hydrogels are another type of popular material for DIW.[9] Rivera-Tarazona et al. printed shape-morphing engineering living materials (ELMs) combining living cells with synthetic components.[167] Li et al. proposed a universal method for the construction of MXene hydrogels applicable to different MXene atomic layers and transition metal types.[168] Through a facile heat-stimulated self-assembly process, crosslinked MXene hydrogels with enhanced mechanical properties were obtained, exhibiting porous structures, large specific surface areas, and excellent electrical conductivity.

Multi-material DIW enables the fabrication of heterogenous hydrogel structures. The multi-material hydrogel consisting of cell-containing and cell-free polyacrylamide (PAA) inks enabled the spatial distribution of strain and concentration of yeast embedded within the printed objects.[167] Similarly, a multi-material bilayer hydrogel structure was built based on two hydrogels: high-swelling tyramine-functionalized hyaluronan (HAT) and low-swelling alginate/HAT composites.[169] Macroscopic anisotropy was realized by having varying magnetic-particle content in hydrogel precursors, and the highly structural-integrated multi-material hydrogels exhibited noncytotoxicity and biocompatibility.[170]

Inspired by natural plant-derived photothermal materials, Zhao et al. extracted nanothylakoids from spinach into bilayer PNIPAM/PAA hydrogel networks, as shown in Figure 5f.[171] The nanothylakoids not only served as a photothermal agent but also catalytically decomposed H_2O_2 into O_2 to mimic the actual botanical systems. This facile method enabled the 4D-printed structures to breathe accompanied by shape changes. Narupai et al. introduced methacrylated bovine serum albumin as a biodegradable building block into PNIPAM and poly(dimethylaminoethyl methacrylate) to fabricate protein-based Pickering emulsions.[172] To improve the mechanical properties, Laponite-based nanoclay was incorporated into a nanocomposite hydrogel as physical crosslinks, and a bilayer multi-material structure was fabricated.[173]

Although SMPs, LCEs, and hydrogels have made up the major materials for DIW-based 4D printing, other materials have also been employed. As a stimuli-responsive material, MSMs have garnered significant attention in tunable programmable robotics and metamaterials.[8,135,174] Wu et al. proposed a voxel-encoding DIW method for programming magnetic density and direction distributions at the voxel level, thereby enabling complex geometry variations and curvature distributions like a sidewinder (**Figure 6a**).[175] Taking each voxel containing three layers as an example, seven effective magnetization variations could be programmed by controlling the printing direction of each layer. Thus, variations in the intensity could be highly programmed. Ma et al. employed the same method to construct active programmable magneto-mechanical metamaterials by encoding eight printing layers.[176]

Liquid–vapor phase transition endows the printed elastomer structures with shape and functionality changes. Zhou et al. incorporated methanol microdroplets into an LM/silicone elastomer to construct shape-morphing multi-materials.[177] Similarly, Shao et al. introduced methanol microdroplets and graphene plates (GNPs) into an elastomer, achieving both local shape transformation and capacitance changes, as demonstrated in Figure 6b.[178] As a result of the photothermal effect, the temperature rose beyond the boiling point of methanol droplets, leading to the transition from liquid to vapor and a substantial alteration in both the shape and dielectric constant.

Recently, Xing et al. prepared a metallic gel consisting of Cu particles bridged by a soft eutectic gallium–indium alloy (EGaIn) in acidic conditions, and the 4D-printed parts with a metal content of 97.5 wt.% possessed a high electrical conductivity of 1.05×10^5 S m^{-1} without post sintering.[179] The shear force during DIW aligned the Cu–EGaIn ink, and the 4D-printed structures exhibited anisotropic shrinking upon heating as the residual water evaporated. Figure 6c demonstrates various structures with programmed Gaussian curvatures and excellent conductivity at the actuated state.

While polymers remain the predominant choice in DIW-based 4D printing, there is also a growing use of metals and

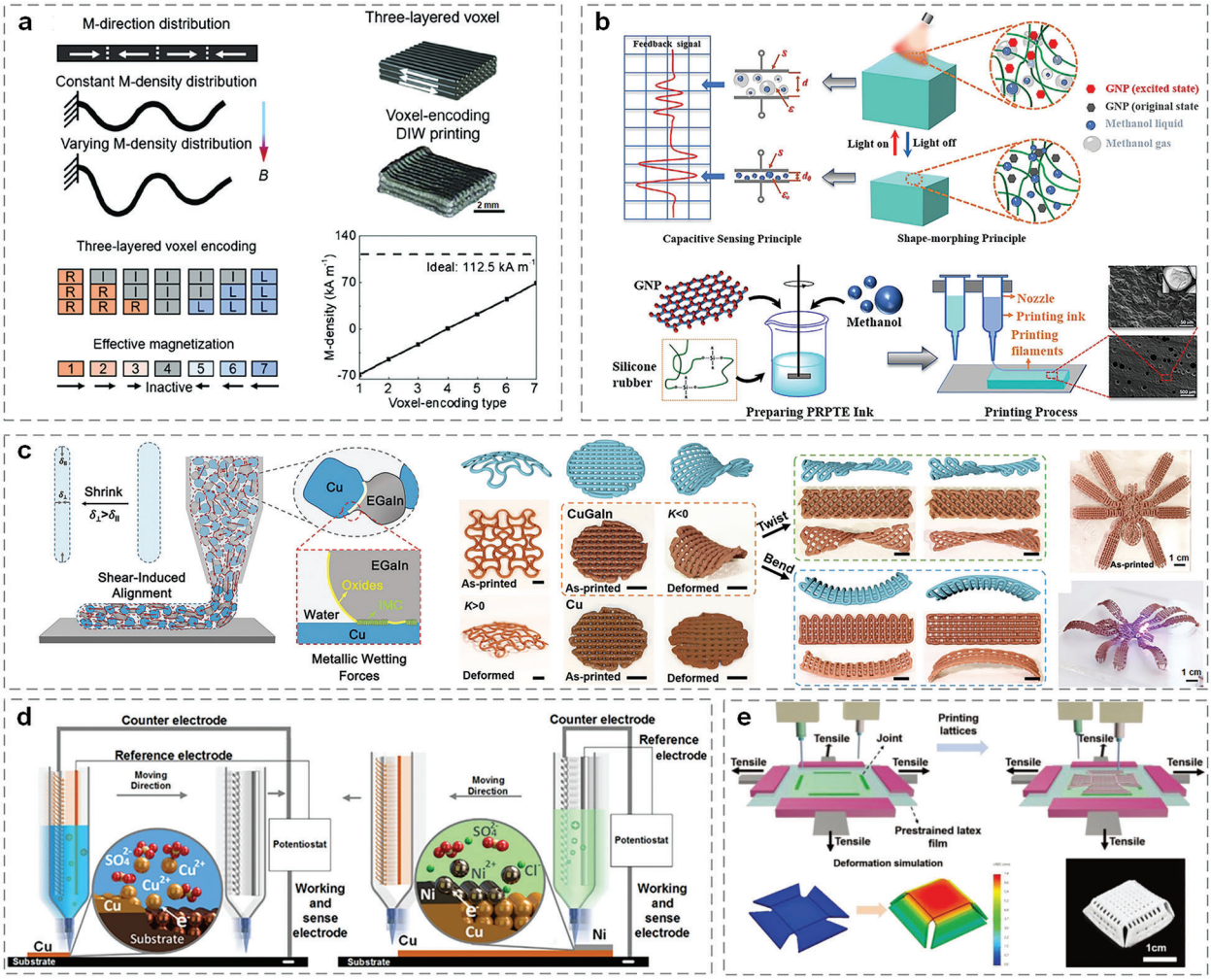

Figure 6. DIW-based 4D printing of other stimuli-responsive materials. a) Three-layered voxel-encoding-printed magnetic active materials with varying magnetic density and direction distribution. Reproduced with permission.[175] Copyright 2020, Wiley-VCH Verlag GmbH. b) Mechanism of local shape transformation and capacitance changes in a printed elastomer composite containing liquid–vapor phases. Reproduced with permission.[178] Copyright 2023, Elsevier. c) Anisotropic metallic gel structures with programmed Gaussian curvatures and high conductivity. Scale bars, 5 mm. Reproduced with permission.[179] Copyright 2023, Elsevier. d) Fabrication process of a multi-metal by using a modified electrochemical printer. Reproduced with permission.[180] Copyright 2019, Springer Nature. e) Prestrain method to achieve desired deformations of nanoceramics. Reproduced with permission.[182] Copyright 2022, Wiley-VCH Verlag GmbH.

ceramics. Chen et al. modified an electrochemical DIW printer and employed a meniscus-confined method with multiple syringes to construct thermally responsive multi-metal structures via 4D printing.[180] Figure 6d shows the schematic diagram of printing a copper–nickel bimetallic strip with a well-bound interface. An electrospun nanofiber nib was used to provide sufficient back pressure to the hydraulic head exerted by the electrolyte, and the deposition speed of both metals increased significantly. Compared to other techniques such as PBF, this method exhibited a huge advantage of cost-saving in printing metals.

Although ceramics are known to be brittle, their 4D printing can still be realized, via utilizing the shape-morphing behavior of their precursor polymers.[129,181] Li et al. manipulated a bioinspired microstructure design and adopted a programmable prestrain approach for 4D printing of nanoceramics with high inorganic content at 95 wt.%, as shown in Figure 6e.[182] After the prestrain was released, the nanoceramic lattice deformed into a box-like shape. By harnessing the stress mismatch between the top and bottom layer during sintering, a DIW-based 4D-printed ceramic green body was fabricated.[183] The shape-morphing process of the green body could be controlled by both the solid content of the ceramic ink and the printing path, thereby providing a new strategy for fabricating advanced ceramics.

2.2.2. Fused Filament Fabrication

FFF is an extrusion-based AM method where a spool of filament (usually thermoplastic materials) is loaded into a printer and then fed through to the extrusion head at a specific temperature. The hot nozzle deposits the molten material onto the build platform

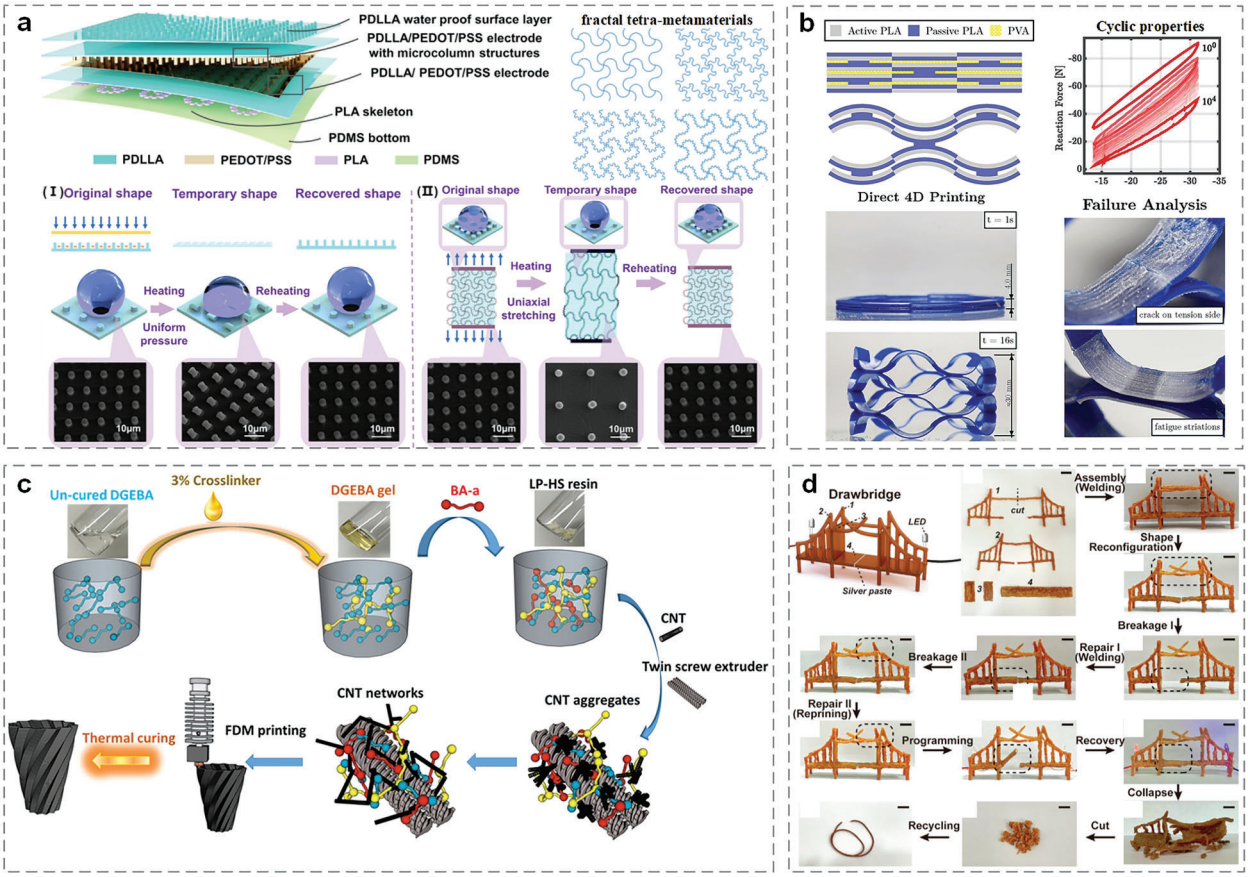

Figure 7. FFF-based 4D printing of polymer materials. a) Schematic diagram of a flexible sensor consisting of a 4D-printed fractal-inspired metamaterial skeleton and biomimetic electrodes with shape memory and tunable hydrophobic properties. PDLLA: poly(D,L-lactide acid). Reproduced with permission.[194] Copyright 2023, Elsevier. b) Structural design and direct 4D printing of a wave spring with exceptional performance under cyclic loading. Reproduced with permission.[196] Copyright 2023, Elsevier. c) Fabrication route of a shape memory thermoset. Reproduced with permission.[200] Copyright 2020, American Chemical Society. d) Multifunctionality of a 4D-printed SMP vitrimer structure, including self-healing, weldability, reprocessability, and reprintability. Scale bars, 1 cm. Reproduced with permission.[201] Copyright 2021, Wiley-VCH Verlag GmbH.

layer by layer, and as it cools down, it solidifies and fuses with the previous layer.

The high processability and excellent SME of polylactic acid (PLA) make it the most frequently used filament material for FFF-based 4D printing. The influence of the infill pattern, printing angle, and printing temperature on the mechanical and shape memory properties of PLA have been investigated.[184,185] Bioinspired by the gap structure of scorpions, a 4D-printed shape memory PLA / carbon black (CB) structure with gradient gaps from the bottom to top layers was fabricated, and the electrical resistance of the structure was sensitive to compression forces.[186] The introduction of low loadings of MXene flakes into a TPU/PLA-based SMPC improved the mechanical properties and response speed.[187] By modifying an FFF printer with dual feed channels, a continuous CF–reinforced shape memory PLA composite was fabricated, and the bending strength and flexural modulus were systematically studied.[188] Based on the same material, modified rectangular horseshoe lattice structures were constructed that exhibited temperature-dependent equivalent stiffness and peak loading capacity.[189] Cellular structures based on continuous Kevlar fiber–reinforced PLA exhibited improved mechanical properties compared to structures based on pure PLA.[190]

As a biodegradable polymer, PLA demonstrates good shape memory capability, but its T_g is usually too high to meet the requirement for implantable devices. To solve this issue, many methods have been adopted to decrease T_g while maintaining high R_r and biocompatibility. For example, by introducing acetyl tributyl citrate as a biocompatible plasticizer into the polymer blends of PLA/poly(lactic-co-glycolic acid), T_g was decreased to 43 °C.[191] Lin et al. incorporated radiopaque fillers, namely barium sulfate (BaSO4) and polyethylene glycol (PEG), into PLA, which lowered T_g to around body temperature.[192]

By modifying an FFF printer with an add-on rotating device, reconfigurable PLA structures were constructed on curved surfaces with high complexity and versatility of 3D-to-3D shape changes.[193] In addition to homogenous PLA-based materials, the integration of a printed fractal-inspired metamaterial skeleton and lotus-inspired microcolumn electrodes was realized as a flexible sensor, as demonstrated in **Figure 7a**.[194] This device possessed both out-of-plane and in-plane SME along with tunable hydrophobic microarray patterns.

Table 4. Overview of 4D printing by PBF, BJT, MJT, and DED techniques with regard to the composition, stimulus, and physical properties.

Printing technique	Printing method	Material type	Material composition	Stimulus	Physical property	Refs.
PBF	SLS	SMP	1,12-dodecanedioic acid, 1,12-dodecanedioic amine, polyetheramine, silica	Heat	T_g: ≈48 °C ε_b: 200% E: 124 MPa σ_c: 13.7 MPa	[217]
			PA1212 salt, DA, polyetheramine, silica, sodium hypophosphite	Heat	T_m: ≈25 °C	[218]
			PU with DA bonds, CNTs	Light	T_g: 42–65 °C	[216]
		Elastomer Composite	TPU, NdFeB, SiO_2	Magnet	σ_c: 9.9–14.5 MPa	[215]
	SLM	SMA	Ni–Ti	Heat	N/A	[220]
			Fe–Mn–Si	Heat	δ_s: >230 MPa	[222]
			Cu–Al–Ni	Heat	N/A	[223]
BJT	BJT	SMA	Ni–Mn–Ga SMA	Magnetic fields	MFIS: ≈0.01%	[226]
			Ni-based superalloy 625	Time	Density: >99%	[227]
MJT	PolyJet™	SMP	VeroBlue	Heat	T_g: 60 °C	[50,238]
			VeroClear, AgNPs	Heat	T_g: 60 °C	[239]
DED	Laser DED	Alloy	Fe–Ni–Ti–Al maraging steel	Time	ε_b: 8.1% σc: 1538 MPa	[241]
	Electron beam DED	SMA	Ni–Ti	Heat	N/A	[242]

In addition to realizing shape change after printing, graded built-in strain could be embedded during the printing process. For example, by setting different printing speeds along the thickness direction, the shrinkage strains between different layers resulted in a bending behavior.[195] Consequently, various complex shapes were obtained with flexibility and high fidelity. Similarly, the prestrain imbalance between bilayers enabled a 4D-printed wave spring to change configurations from flat to deployable upon heating, and the bilayer structural design for the spring is shown in Figure 7b.[196] This spring could also be redeployed using cold programming and withstand at least 10^4 cyclic loading cycles without failure, avoiding the typical delamination issues. Wang et al. designed a bi-material composite consisting of TPU and PLA with prestrain to construct 4D-printed reversible structures.[197]

PEEK exhibits high T_g and enhanced mechanical properties compared to PLA and has become one of the popular engineering materials. Yang et al. 4D-printed PEEK with high R_r (>97%) and a fast recovery speed.[198] PCL-based FFF-printed SMP structures exhibited a high strain at break of over 1200% because of the orientation of the semi-crystalline and micro-phase-separated domains, and the existence of PCL contributed to the self-healing properties.[199]

To improve the thermal stability, a high-performance shape memory thermoset was constructed by formulating low-temperature thermoplastic benzoxazine/epoxy composites suitable for printing at 100 °C by FFF, which was then post-cured into a high-temperature thermoset at 200 °C (Figure 7c).[200] Joe et al. developed a PCL-based SMP vitrimer with a dynamic network rearrangement suitable for FFF.[201] The 4D-printed drawbridge structure demonstrated multifunctionality, including self-healing capability, weldability, reprocessability, and reprintability, with great promise for recycling, as shown in Figure 7d.

The combination of FFF with other polymer processing methods allows it to fabricate functional structures. Inspired by the mechanism of hygroscopic dispersion of natural seeds, a 4D-printed functional structure was constructed by integrating FFF-printed PCL with coaxial electrospinning hygroscopically active core–shell fibers, which exhibited geometrical sizes and biomechanical properties comparable to those of the seeds.[202] FFF-based 4D printing is also applied to fabricating metal materials. A functional 4D-printed Ni–Ti shape memory alloy (Ni–Ti SMA) consisting of thermoplastic binder and metal powder showed a shape memory strain of 1.9%.[203]

2.3. Powder Bed Fusion

PBF is a printing technique where an energy source (such as laser, infrared light, or electron beams) is employed to induce fusion of polymer or metal powder particles into solid objects.[213] Based on the different melted materials, PBF can be further categorized into selective laser sintering (SLS) and selective laser melting (SLM). An overview of 4D printing via the two PBF methods is presented in **Table 4**.

2.3.1. Selective Laser Sintering

In SLS, powder particles are heated by high-power laser so that they fuse together layer by layer to create a solid 3D object.[214] It has the benefits of having no requirement for support, a high material utilization rate, fast processing, and high precision. An NdFeB/TPU composite structure fabricated by SLS 4D printing followed by post-magnetization demonstrated excellent mechanical strength, and the magnetic-induction intensity distribution was thoroughly analyzed, as

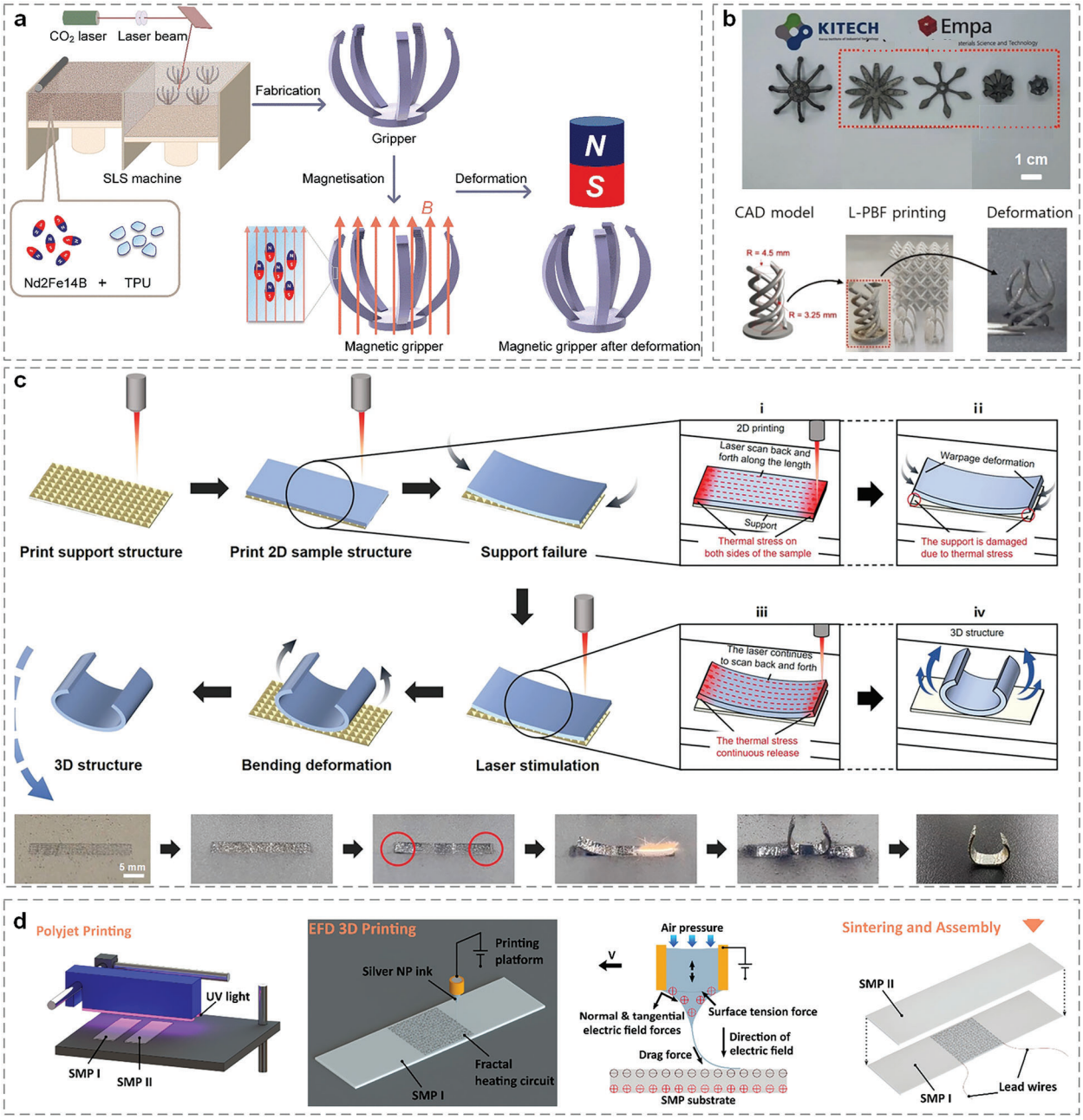

Figure 8. PBF- and MJT-based 4D printing of polymers and metals. a) Schematic fabrication process of SLS-printed magnetic composites and post-magnetization. Reproduced with permission.[215] Copyright 2021, American Chemical Society. b) Fe–Mn–Si-based SMA structures printed via SLM and their deformation behavior. Reproduced with permission.[222] Copyright 2022, Wiley-VCH Verlag GmbH. c) Schematic diagram of the fabrication process of conventional metallic shape-morphing structures and SLM-printed stainless steel. Reproduced with permission.[224] Copyright 2023, Wiley-VCH Verlag GmbH. d) Illustrative PolyJet™ printing process of SMP-integrated stretchable heating circuits with fractal motifs. Reproduced with permission.[239] Copyright 2021, American Chemical Society.

shown in **Figure** 8a.[215] A novel shape memory PU with DA bonds suitable for SLS was fabricated, and the dynamic covalent networks endowed the printed parts with self-healing capability.[216]

A polyamide 1212 (PA1212)–based thermoplastic elastomer was synthesized by one-pot melt polycondensation followed by freeze crushing into powder particles, and the SLS-printed structure demonstrated good mechanical properties under optimized printing parameters.[217] It was further found that the hard crystalline PA1212 and soft polyether segments served as physical crosslinking points and the actuation phase, respectively.[218] This materials combination enabled the two-way SME based on CIE and MIC.

2.3.2. Selective Laser Melting

In SLM, metallic powder particles are selectively melted and fused by high-power density laser to form a near-net-shape part of up to 99.9% relative density.[219]

Ni–Ti SMAs, known for their peculiar SME and hyperelasticity, stand as the most extensively employed active metallic materials in SLM-based 4D printing. By controlling the processing parameters, such as the energy source power, scan speed, and hatch distance, Ma et al. modulated the microstructures of a 4D-printed Ni–Ti SMA based on the thermal history, thereby achieving the target spatial and functional responses.[220]

The martensitic transformation temperature of Fe–Mn–Si-based SMAs is less sensitive to materials composition, and they have therefore been regarded as a more efficient candidate for SLM than Ni–Ti SMAs.[221] They also show superiority by having low cost, high recovery stress, and easy processibility, making it easier to construct complicated shapes. Kim et al. have successfully designed and printed Fe–17Mn–5Si–10Cr–4Ni (Figure 8b) with different shapes and functions.[222] A high yield strength of over 230 MPa and an elongation of 45% were obtained after a post heat treatment at 800 °C for 30 min.

A novel 4D-printed Cu–Al–Ni SMA consisting of two parts with different hardness and recovery temperatures was found to exhibit high recovery ratios because of the damping behavior of the harder section.[223] The SLM printing method was also employed in the 4D printing of non-shape-memory metallic materials through the introduction of internal thermal stress during the printing process, as illustrated in Figure 8c.[224] Because of the failure of the support layer by laser scanning, the two sides of the sample layer were broken so that the structure could bend, thereby forming the expected shape.

2.4. Binder Jetting

BJT is a layer-by-layer manufacturing process that involves dispensing a liquid binding agent onto a powder bed in each layer, resulting in the layers binding together to form the final solid product.[225] A summary of studies employing BJT 4D printing is presented in Table 4.

Magnetically actuated SMAs can transform to a martensitic in response to a magnetic field and produce a magnetic field–induced strain (MFIS). Caputo et al. adopted BJT to print a Ni–Mn–Ga SMA with a complicated configuration and reversible martensitic transformation.[226] The parts manufactured using powders via spark erosion in liquid nitrogen exhibited the highest porosity (70.43%) owing to their hollow morphology. Zheng et al. employed gas-atomized nickel-based superalloy 625 powders for BJT printing followed by isothermal sintering at subsolidus and supersolidus temperatures.[227] The printed parts sintered at the supersolidus liquid phase realized better densification and mechanical properties.

2.5. Material Jetting

Stratasys PolyJet™ is an MJT-based process that dispenses multiple photoreactive and sacrificial support materials simultaneously while continuously exposing them to UV light, resulting in the creation of 3D objects layer by layer.[228] MJT enables the production of intricate parts with high resolution and smooth surfaces. Because of the capability to fabricate multi-materials, most of the early studies on 4D printing adopted MJT.[3,4,229–233] Table 4 provides the details of parts 4D-printed by the MJT technique.

Bioinspired hierarchical architecture offers opportunities for improved performance and customization.[234–237] Thus, it has attracted applications in 4D printing. Wang et al. adopted MJT to realize controllable shape changes in 4D-printed horseshoe structures.[238] They further designed a digital tool to program the mechanical properties of fractal metamaterials.[50] By regulating the geometric parameters, bionic stress–strain matching with large stretchability (≈360%) and imperfection insensitivity could be flexibly programmed. Figure 8d demonstrates the fabrication process that integrated PolyJet™ printing of SMPs and electric field–driven microscale 3D printing of a circuit with fractal motifs.[239] This stretchable heating circuit could be steadily tensioned in both uniaxial and biaxial directions, thus providing stable heating of the SMP to transform it into a shape-morphing structure under low voltage.

2.6. Directed Energy Deposition

As another powder-based near-net-shape production technique, DED involves a high-power energy source, either laser or an electron beam, to continuously direct melted metal powder or wire through nozzles into the melt pool.[240] This technique not only produces a fully dense structure with highly complex geometric features but also has a fast deposition speed, especially for manufacturing large-scale or complex components. The summary of alloys 4D-printed by DED is presented in Table 4.

A novel Fe–Ni–Ti–Al maraging steel was fabricated by DED.[241] It was found that during the printing process, the intrinsic heat treatment effect triggered the in situ precipitation, and the post heat treatment could be therefore avoided. Electron beam–based DED was employed to fabricate a Ni–Ti SMA, and the microstructure evolution, phase transition temperature, mechanical properties, and SME were systematically studied.[242]

2.7. Hybrid Printing

Hybrid printing is a manufacturing process that integrates multiple printing methods and multiple materials together to fabricate a single part.[33] It offers many advantages over traditional printing methods, including enhanced design flexibility, boosted geometry complexity, improved functionality, reduced waste, and improved efficiency. **Table 5** summarizes the materials for hybrid 4D printing.

A hybrid printing system for multi-materials was built based on DLP and DIW to print LCE-based composite structures in a single printing job.[243] Using the same system, 4D-printed LCE–SMP bilayer structures were realized, with the LCE and SMP being printed via DIW and DLP, respectively.[244] As **Figure 9a** depicts, the shape configurations were highly dependent on the cooling rate because of the unique thermo-mechanical properties of the SMP and LCE. The nematic-to-isotropic transition of the LCE and glass transition of the SMP were first-order and

Table 5. Overview of hybrid 4D printing with regard to the composition, stimulus, and advantages.

Hybrid method	Material type	Material composition	Stimulus	Advantages	Refs.
DIW+Inkjet	Multi-material LCE	DIW: LCE (RM257, EDDET, TEA, Irgacure 651), soft elastomer (AUD, BA, PCL, SiO_2, glycidyl methacrylate (GMA)), glassy polymer (AUD, GMA, SiO_2, Irgacure 819) Inkjet: conductive ink (DuPont ME603), acrylate-based polymer	Heat	Tunable functionality, high resolution	[142]
DIW+DLP	Multi-material LCE	DIW: LCE (RM257, EDDET, TEA, Irgacure 819), photocurable ink (GMA, AUD, Irgacure 819, blue dye, SiO_2), silver nanoparticles DLP: elastomer (AUD, GMA, isodecyl acrylate, Irgacure 819, Sudan I), plastic (ToughPoint)	Heat	High resolution, low cost, tunable functionality	[243]
	Multi-material LCE	DIW: LCE (RM257, RM82, EDDET, pentaerythritol triacrylate, PI 784) DLP: acrylate-based resin (IBOA, tricyclodecane dimethanol diacrylate, PI 819, Sudan I)	Heat	High resolution, high complexity, one-step process, freestanding on-the-fly fabrication	[51]
	LCE–SMP	DIW: LCE (RM257, RM82, EDDET, TEA, Irgacure 369) DLP: SMP (aliphatic diacrylate, IBOA, BA, Irgacure 651, thermochromic dye)	Heat	Large, rapid, and reversible shape change, tunable shape morphing behaviors	[244]
SLS+SLM	Multi-material	SLS: TPU, NdFeB, SiO_2 SLM: 316L stainless steel	Pressure	Integrated property and functionality	[245]
DIW+PolyJet^{TM}	Multi-material	DIW: hydrogel PolyJet^{TM}: elastomer	Heat	Voxel-based modeling, interlocking block assembly	[246]
FFF+electrospinning	Multi-material	FFF: PCL Electrospinning: polyethylene oxide, cellulose nanocrystals (CNCs)	Humidity	Integrated functionality	[202]

second-order transitions, respectively, and they thus had different dependence on the temperature changing rate. This method not only inherited the reversible actuation of LCEs but also harnessed the high stiffness of SMPs at low temperatures to lock the deformed shape.

A new hybrid AM system was developed by Peng et al. for the 4D printing of freestanding LCE structures in a one-step process based on top–down DLP and DIW with an in situ laser-curing module, as depicted in Figure 9b.[51] Since the hybrid printing process was performed by alternating the DIW and DLP platforms successively, it was important to separate the individual polymerization to avoid their interference. To solve this problem, visible-light and UV-light photoinitiators with absorption at different wavelengths were incorporated into the DIW and DLP inks, respectively. The introduction of CO_2 gas into the resin vat purged undesired oxygen, which enabled the printed DLP ink to completely cure and dry to achieve strong adhesion with the extruded LCE filaments within the multi-material structure. Wu et al. integrated a conductive helix structure printed by SLM and a magnetic porous structure printed by SLS and assembled them with two flat plates into a 4D-printed multifunctional device, as shown in Figure 9c.[245]

Benyahia et al. proposed a computational design to fabricate desired shape-morphing multi-material structures by assembling interlocking blocks printed separately using a single AM method.[246,247] As shown in Figure 9d, the multi-material assembled from active and passive blocks printed by DIW and PolyJet^{TM}, respectively, exhibited a shape change as expected in the design and simulation stages. This computational design could achieve automatic interlocking, unlike manufacturing via expensive assembly design methods.

3. Stimuli

Stimuli play a crucial role in driving the dynamic and adaptive behaviors of 4D-printed structures. By incorporating specific triggers, these structures can undergo shape changes, self-assembly, or property alterations over time. Commonly used stimuli include heat, light, electric fields, magnetic fields, solvents, and humidity. Other stimuli include pH changes, chemical, pressure changes, laser, and their combinations. The successful integration of these stimuli in 4D printing offers exciting possibilities for creating intelligent and responsive materials capable of self-regulation and adaptability. **Table 6** summarizes an overview of typical stimuli for 4D printing with regard to the mechanism, printing material, printing method, and applications.

3.1. Heat

Heat stands as the predominant and widely employed stimulus for 4D-printed materials, including SMPs, LCEs, hydrogels, and other stimuli-responsive materials. It relies on a direct heat source or environmental factors, such as a hot plate, a heating gun, a water bath, or an oven. This process involves direct transformation of the thermal energy from an external source to the 4D-printed structures.

Thermally responsive SMPs have received the most extensive attention among all SMPs mainly due to their high level

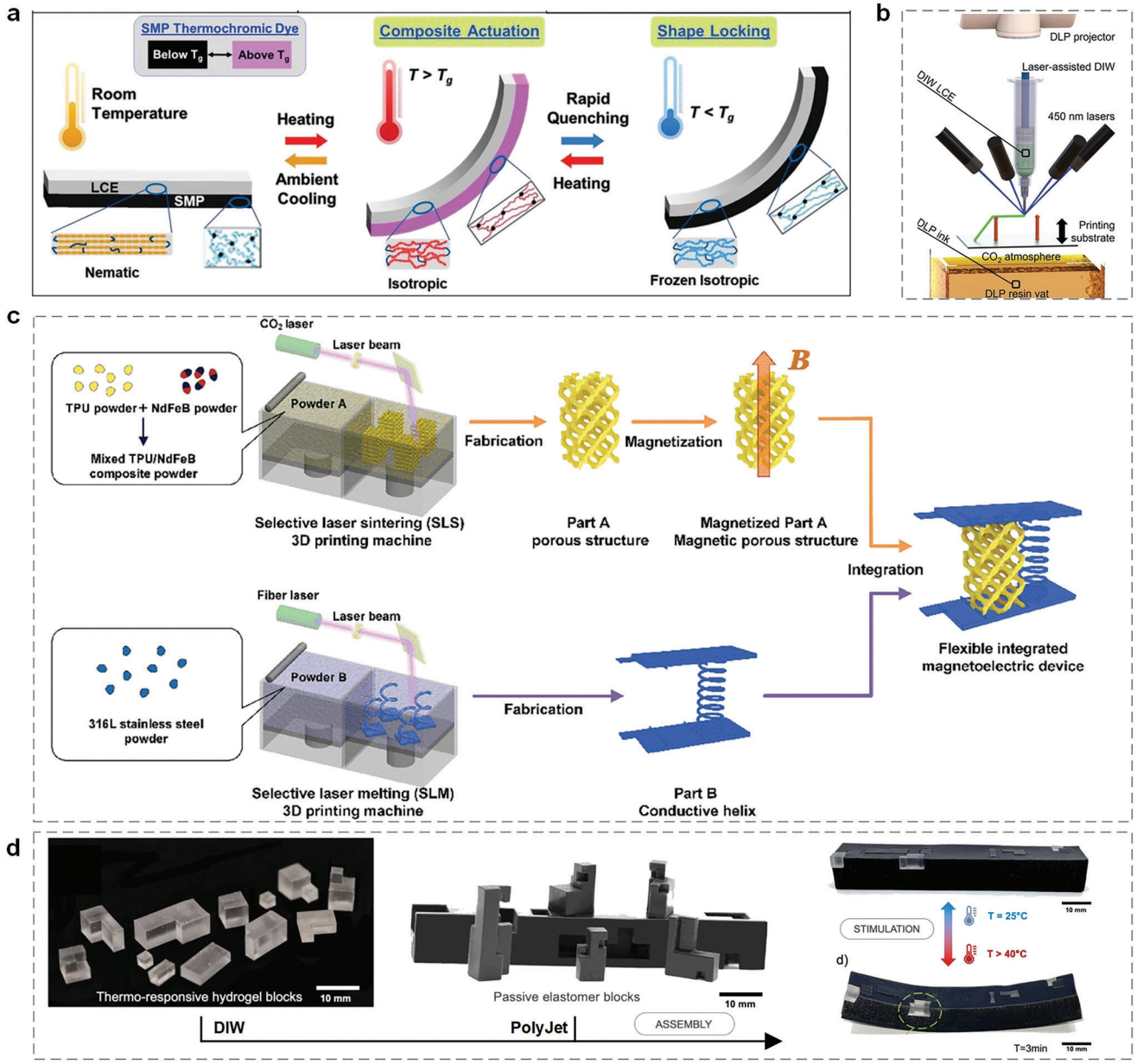

Figure 9. Hybrid 4D printing. a) Schematic diagram of the actuation mechanism of an LCE–SMP bilayer composite. Reproduced with permission.[244] Copyright 2022, Wiley-VCH Verlag GmbH. b) Schematic diagram of a hybrid printing system employing DLP and laser-assisted DIW. Reproduced with permission.[51] Copyright 2022, Wiley-VCH Verlag GmbH. c) Schematic diagram of a hybrid printing method combining SLS and SLM for fabrication of magnetoelectric devices. Reproduced with permission.[245] Copyright 2020, Wiley-VCH Verlag GmbH. d) 4D-printed multi-material assembly from active and passive interlocking blocks based on a computational design method. Reproduced with permission.[246] Copyright 2022, Elsevier.

of tunability of T_{trans} and mechanical properties and the convenience of triggering the SME through the direct-heat stimulus. SMP structures fabricated by various 4D-printing methods have demonstrated fast responses to temperature, including DLP,[67,68,73,76,78,99,100] DIW,[121,128,204] SLS,[217,218] FFF,[187,191,192,194] and TPP.[5,65]

Yue et al. 4D-printed flat SMP sheets with a symmetrical hinge design and used the cold programming method to fabricate transformable panels via grayscale DLP.[72] **Figure 10**a demonstrates the various shape-morphing structures including buckled-up and buckled-down configurations by setting different stretching directions and hinge locations. Additionally, more complex geometry could be obtained by through-hole assembly. Meurer designed a supramolecular SMP, and the 4D-printed butterfly structure recovered to the initial shape in a few seconds at 130 °C.[66] The XB bonds contributed to its remarkable resistance against water.

Besides demonstrating the commonly known programmable shape recovery, 4D-printed semi-crystalline SMPs could exhibit reversible actuation around T_m due to the two-way shape memory mechanism based on CIE and MIC.[73,218] Additionally, the

Table 6. Overview of typical stimuli for 4D printing with regard to the mechanism, printing material, printing method, and applications.

Stimulus	Mechanism	Printing material	Printing technique (method)	Applications
Heat	Shape memory effect Nematic-to-isotropic transition Phase transition based on LCST Anisotropic thermal expansion Liquid–vapor phase transition	SMP, SMA LCE, LCN Hydrogel Elastomer composite Metal, alloys Ceramics	VPP (DLP, TPP) MEX (FFF, DIW) PBF (SLS, SLM) BJT MJT DED	Biomedical engineering Electronics Robotics and actuators Photonics Aerospace Information encryption Orthopedics Decoration
Light	Photothermal effect Photochemical effect	SMP LCE Hydrogel Elastomer composite	VPP (TPP) MEX (FFF, DIW) PBF (SLS)	Biomedical engineering Electronics Robotics and actuators Photonics Information encryption
Electric field	Joule heating	SMP LCE Hydrogel Elastomer composite	MEX (FFF, DIW)	Biomedical engineering Electronics Robotics and actuators Aerospace
Magnetic field	Magnetization Induction heating	SMP, SMA Magnetic active materials	MEX (FFF, DIW) PBF (SLS) BJT	Biomedical engineering Robotics and actuators Magnetic sensors Energy dissipation devices
Solvent	Swelling/Deswelling Asymmetric crosslinking densities	Photopolymer LCN Hydrogel	VPP (TPP, DLP)	Biomedical engineering Robotics and actuators Microfluidic devices
Humidity	Differential hygroscopic swelling Interaction between functional groups and water molecules	LCE, LCN Fiber composite	MEX (FFF)	Robotics and actuators Orthopedics
pH	Swelling/Deswelling	Hydrogel	VPP (TPP)	Biomedical engineering Photonics
Pressure	Anisotropic modulus Electromagnetic introduction Coupled triboelectrification and electrostatic induction	SMP LCE Hydrogel Magnetic active materials with alloys	MEX (DIW)	Electronics Energy dissipation devices

permanent shape could be erased when the structure was heated above the higher T_m value because of elimination of the chain segment orientation. Figure 10b shows the diversified shape change of 4D-printed cartoon structures upon heating and cooling in two different shape programming modes.[73] Other 4D-printed structures based on semi-crystalline SMPs also demonstrated similar two-way actuation.[75,218]

The heat-shrinkable property of printed polymers inspires advancements in 4D printing.[248] Unlike structures requiring post-printing programming through an external force, as-printed SMP structures with spatially varying anisotropies under optimized printing paths and parameters could exhibit programmed shape-shifting behavior.[193] This behavior was attributed to the rapid cooling of extruded filaments which shrank along its longitudinal direction upon heating. Figure 10c demonstrates a series of out-of-plane and in-plane deformations by designing the distribution of specific unit cells in the passive and active layers.

Chen et al. developed an SMPC-based ceramic precursor, and the 4D-printed structures first underwent shape recovery and then transformed into ceramics during sintering.[129] Figure 10d demonstrates the reconfiguration and active shape transformation to self-shaping ceramics. The finite element analysis (FEA) simulation of the shape recovery process corresponded well with the experimental findings where the maximum strain occurred at the root of the petal.

The molecular orientation along the printing path endows DIW-printed LCEs with various shape changes upon heating, including volumetric contraction, snap-through transformation, thermal springing, and planar-to-3D and 3D-to-3D shape transformations.[139–145,147] A novel reactive printing method enabled the symmetry-breaking transformation of an LCE, which was hard to obtain via traditional printing methods.[153] In addition to the two-way shape memory behavior due to the nematic-isotropic phase transition, complicated shape changes of LCE structures could be designed by combining the glass transition process.[207] Based on hybrid 4D printing, various freestanding 3D active lattices made from LCEs with structural or removable supports were constructed with reversible large actuation under the heat stimulus.[51]

By liquid-assisted printing and programmed structural design, complex deformations such as out-of-plane bending were realized. The temperature gradient and curvature between the

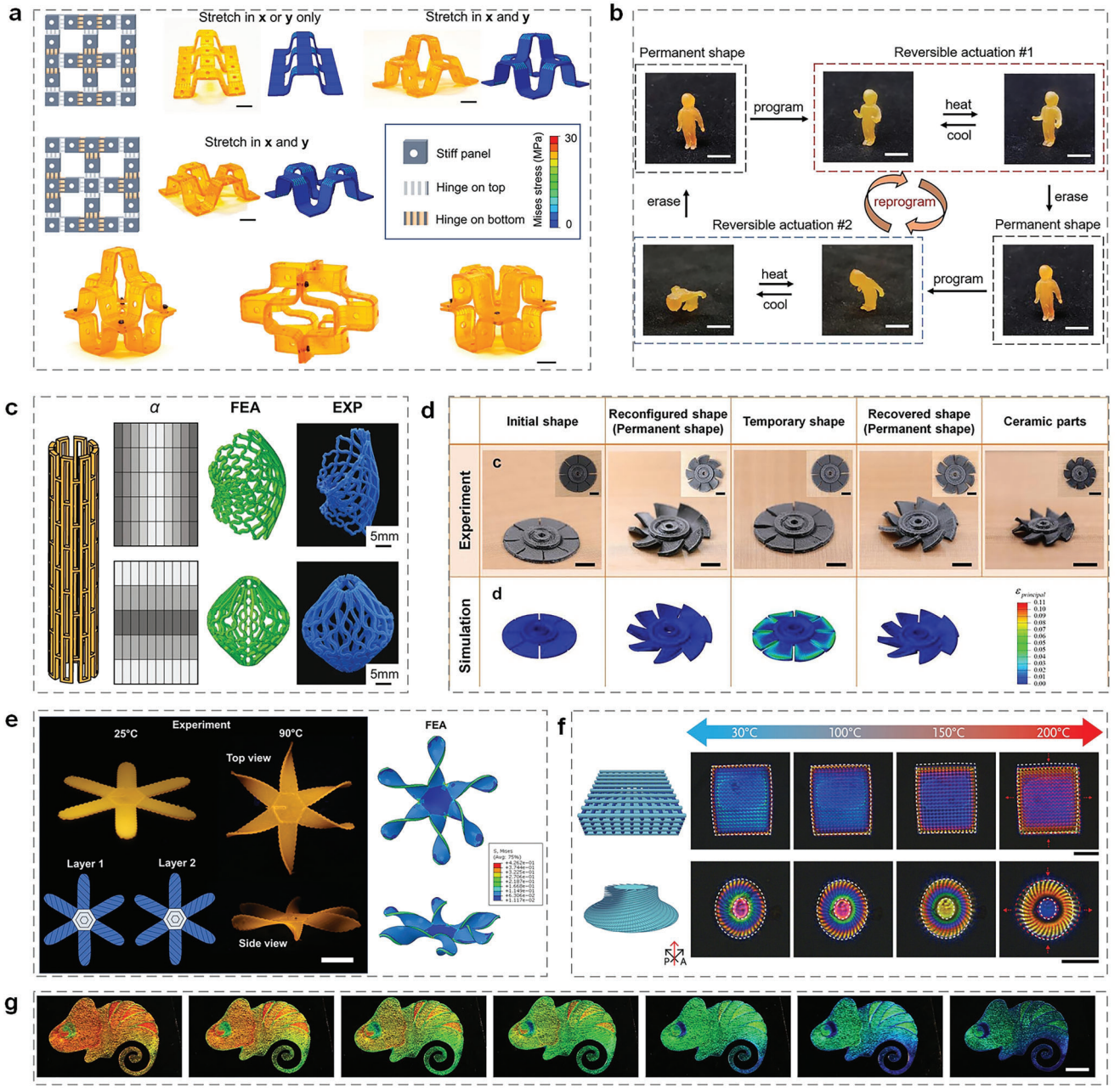

Figure 10. Temperature-based stimulus responses of 4D-printed structures. a) Cold-programmed transformable panel structures with different stretching directions, hinge patterns, and through-hole assembly. Scale bars, 1 cm. Reproduced with permission.[72] Copyright 2023, Springer Nature. b) Two reversible deformation modes of a cartoon structure based on semi-crystalline SMPs. Scale bars, 1 cm. Reproduced with permission.[73] Copyright 2021, Elsevier. c) Various transformations of an SMP based on unit cell designs. Reproduced with permission.[193] Copyright 2021, Springer Nature. d) Transformation of preceramic polymers to self-shaping ceramics and FEA simulation of the shape recovery. Scale bars, 1 cm. Reproduced with permission.[129] Copyright 2023, Elsevier. e) Shape change of a functional gradient bilayer LCE structure with FEA simulation. Scale bars, 2 cm. Reproduced with permission.[154] Copyright 2020, American Association for the Advancement of Science. f) Anisotropic shape and polarized color changes of an LCN microstructure. Scale bars, 20 µm. Reproduced with permission.[109] Copyright 2021, Wiley-VCH Verlag GmbH. g) Color-morphing process of a biomimetic chameleon from colloidal photonic crystals. Scale bars, 2 mm. Reproduced with permission.[249] Copyright 2022, Elsevier.

bottom and top layers endowed a 4D-printed LCE film with untethered self-propelling actuation on a hot plate.[146] Based on a comprehensive understanding of the processing–structure–property relationship between LCE filaments and sheets, Wang et al. presented a simple method to construct various morphing bilayer structures with functional gradients upon heating above 90 °C (Figure 10e).[154] This flexible approach allowed simultaneous control over both the direction and magnitude of the actuation strain and helped to mitigate stress concentration near the soft–hard material interface.

By adjusting the printing speed and printing path at specific locations, gradient parameter–embedded printing could produce complex deformations, such as locally programmed popping-up, self-assembling, oscillating, and curling behaviors.[157] Distinct localized shape change was realized by multiparameter-encoded programming, which enabled on-demand control of the local shape instead of using hybrid materials.[158] By harnessing different printing speeds of LCE filaments, a cellular lattice structure demonstrated sequential actuation, exhibiting the potential as a roller launcher.[51] Similar to LCEs, 4D-printed LCN microstructures exhibited evident anisotropic shape changes and simultaneous polarization color changes due to the increased molecular disorder (Figure 10f).[109] These changes enabled the identification of different geometries and self-sensing of the microstructures with great promise as anti-counterfeiting microdevices.

In addition to shape change, color change under the heat stimulus has recently attracted more attention. Liao et al. developed colloidal photonic crystals and 4D-printed structures featuring both digitally defined macroscale configurations and structural colors because of the ordered structures at the sub-micron scale.[249] Figure 10g demonstrates the color-morphing process of a biomimetic chameleon at different temperatures.

SMAs have also been widely used in 4D printing.[220] A 4D-printed Fe-based SMA in the shape of a flower and spring exhibited obvious shape changes at 300 °C.[222] When combined with structural design, a printed 2D Fe SMA metamaterial structure not only possessed pronounced shape recovery but also simultaneously showed the self-healing capability to close cracks.

4D-printed multi-materials exhibit thermal responsiveness as well. The contraction of LCE layers embedded in elastomers could change the geometry of various printed structures, including mimicking flower blooming and crawling actuation.[243] Roach et al. found that the cooling rate influenced the shape of a 4D-printed LCE–SMP metamaterial structure as the structure maintained its deformed shape after quenching and reverted to the as-printed shape upon ambient cooling conditions.[244]

In addition to employing responsive materials directly, shape-morphing structures can be fabricated by using other methods. For example, when the printing paths were deliberately set along different directions within a single thermoplastic material, the anisotropic thermal deformation caused a bending behavior.[185] Similarly, a buckyball actively self-folded from a 2D hexagonal lattice sheet.[94] Since copper and nickel have different thermal expansion coefficients, a pronounced bending deformation of printed bimetallic strips was observed upon heating from 50 to 300 °C.[180] A pattern of "ICL" was demonstrated by changing the layer thickness and geometric arrangement in each layer. A bilayer structure integrating swellable and support layers exhibited controlled shape-morphing architecture upon heating due to the swelling ability of microliquid chambers.[177]

3.2. Light

The photoresponse of 4D-printed structures is realized through two mechanisms: photochemical and photothermal effects. The photochemical mechanism involves chemical changes upon exposure to specific wavelengths of light. For example, the chemical bonds of ketone and ether have strong absorption in the UV wavelength range, and the printed shape memory PEEK thus exhibited remotely controllable actuation under both UV light and natural sunlight focused by a convex lens.[198] To avoid oxidation under UV light, a thin layer of gold was coated with enhanced anti-UV oxidation performance.

The isomerization of azobenzene moieties from trans to cis configurations under UV light enabled LCEs with programmed deformation through both photochemical and photothermal effects.[6,163,205–206,250] The blue light conferred the isomerization back from cis to trans states. At room temperature, the printed LCE strip bent away from the UV light because of the phase transition from smectic C to smectic A.[205] However, at high temperatures, it bent toward the UV light. When azobenzene was incorporated into physically crosslinked LCEs, various shape changes were obtained, including a 2D film, a re-entrant structure with a honeycomb unit cell, and a spiral structure under illumination of UV and blue light (**Figure 11a**).[166] This reversible shape change could be observed both in air and underwater while the actuation strain of the latter was smaller. Similarly, azobenzene-containing LCE structures demonstrated contraction actuation under light in a biological buffer.[250] By integrating three mesophases, a 4D-printed LCE multicomponent was printed on a polyetherimide (PEI) foil, and the bilayer structure exhibited multimodal bending deformations under illumination of UV and blue light (Figure 11b).[163]

The photothermal effect relies on the introduction of functional particles with a strong conversion ability from light to heat. GNPs, CB, and carbon nanotubes (CNTs) enabled 4D-printed SMPs to respond to near-infrared (NIR) or far-infrared (FIR) light with local and selective shape recovery.[82,210,216,251] A smart alarm fabricated from an SMPC consisting of CNTs and PTU could be activated by high temperature or NIR light illumination for fire warning.[82] The introduction of AuNPs endowed shape memory PU with an obvious photothermal effect under 520 nm.[120]

The photothermal effect of additives also endows LCEs with photoresponse under NIR light. A 4D-printed PQD–LCE film containing a passive polydimethylsiloxane layer demonstrated a reversible bending behavior.[159] A low PEG-modified-AuNR content of 0.1 wt.% in an LCE realized rapid response and large actuation strains.[155] As depicted in Figure 11c, the petals of an LCE flower could globally or separately bloom under localized irradiation. The incorporation of 71 wt.% LM into an LCE led to an obvious photothermal effect.[152] When different types of dyes, including azobenzene, donor–acceptor Stenhouse adducts, and anthraquinone derivates, were incorporated into an LCE microstructure, the ability to absorb light of various wavelengths in the visible range (400–700 nm) endowed it with multi-photo responses, as depicted in Figure 11d.[110]

AuNRs endowed PNIPAM-based hydrogels with obvious photothermal effects under 808 nm.[112] Figure 11e demonstrates the NIR light–triggered anisotropic twisting and falling behaviors of a core–shell helix microstructure attributed to different swelling ratios between the passive static polymer layer and active dynamic hydrogel layer. Similarly, a 4D-printed CNT/PNIPAM hydrogel microclamp device consisting of a circular array of six micropillars exhibited controlled actuation under NIR light with diversified laser power (Figure 11f).[252]

The photothermal agent also endows 4D-printed non-stimuli-responsive materials with photoresponse. For example, the

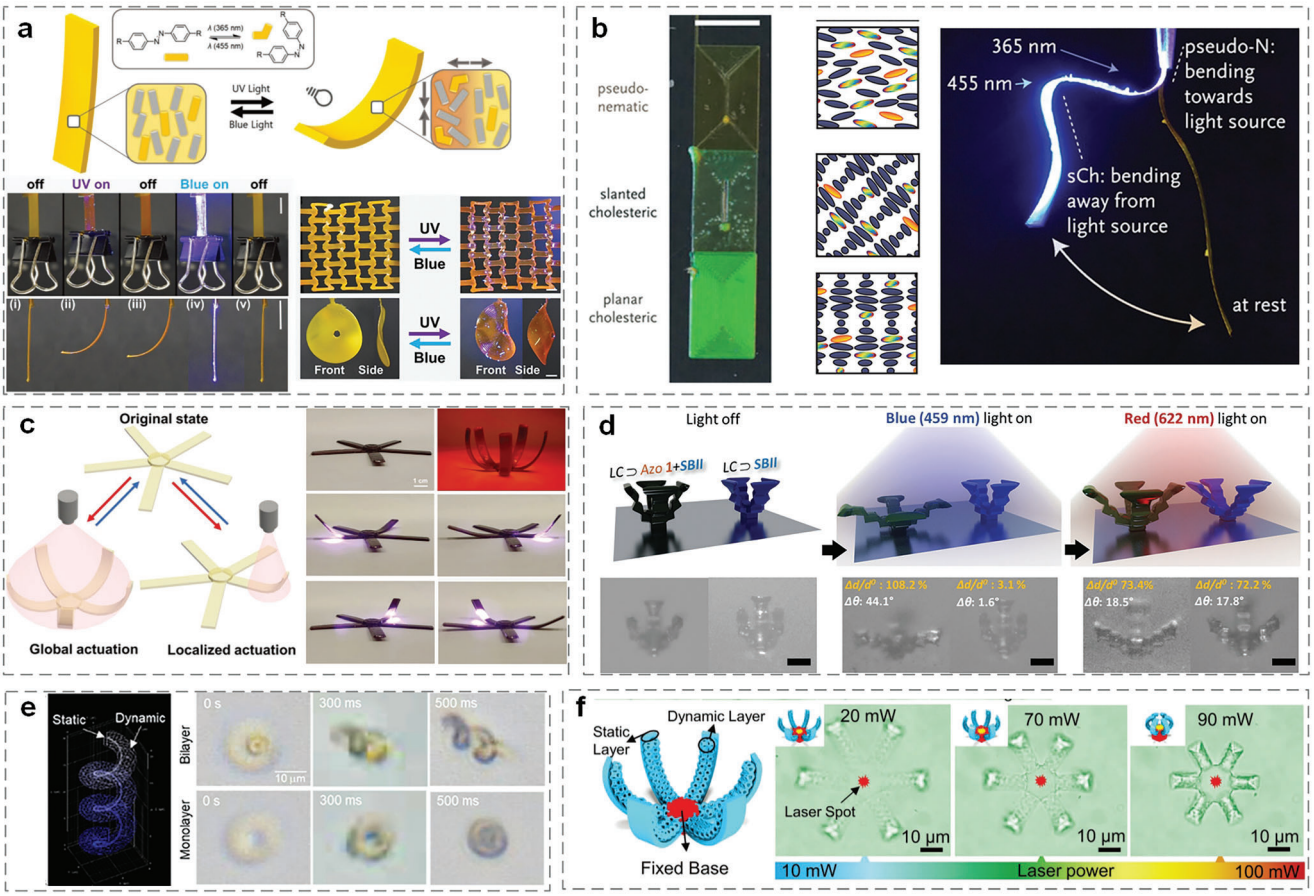

Figure 11. Light-based stimulus responses of 4D-printed structures. a) Reversible shape transformation of various LCE structures under UV and blue light based on the trans–cis mechanism of azobenzene moieties. Scale bars, 5 mm. Reproduced with permission.[166] Copyright 2022, Wiley-VCH Verlag GmbH. b) Simultaneous multiple bending behaviors of a multi-mesophase LCE–PEI bilayer film under UV and blue light. Scale bar, 6 mm. Reproduced with permission.[163] Copyright 2022, Wiley-VCH Verlag GmbH. c) Global and localized blooming of an LCE flower under NIR irradiation. Reproduced with permission.[155] Copyright 2022, Wiley-VCH Verlag GmbH. d) Multi-photoresponsive actuation of an LCE microstructure containing different types of dyes. Scale bars, 25 μm. Reproduced with permission.[110] Copyright 2022, Wiley-VCH Verlag GmbH. e) NIR light–triggered shape changes of core–shell hydrogel-based helix microstructures. Reproduced with permission.[112] Copyright 2020, American Chemical Society. f) NIR light–triggered bending actuation of a hydrogel microclamp device at different laser power. Reproduced with permission.[252] Copyright 2023, Wiley-VCH Verlag GmbH.

introduction of GNPs significantly improved the thermal conductivity and mechanical properties of 4D-printed elastomers, which exhibited selective shape-morphing behavior under NIR light, including bending, grabbing, and creeping motions.[178]

3.3. Electric Field

An electric field is a stimulus that can induce dynamic changes in 4D-printed structures, altering both their shapes and functions. Electric fields can be employed to induce dynamic shape changes via indirect heating, especially when the use of an external heat source is impossible. The generated Joule heating effect could elevate the operating temperature beyond T_{trans} of SMPs or T_{NI} of LCEs to trigger the shape recovery and reversible change, respectively.

The incorporation of electrically conductive fillers, such as CFs,[188] CNTs,[211,253] CB,[254] and silver nanowires,[255] endowed 4D-printed SMP structures with electrical responses of changing from temporary to original shapes by the Joule heating effect. The resistance change during actuation could also be used to monitor real-time deformation modes.[188] **Figure 12a** depicts the electroactive responses of an SMP structure under a voltage of 25 V.[211] Besides the overall shape actuation, the modular and stepwise shape recovery has been demonstrated, by connecting two adjacent electrodes at desired locations, as shown in Figure 12b.[253] In addition to directly applying voltage to the conductive SMP, the SMP matrix could be actuated to recover its original shape through Joule heating generated by an embedded conductive circuit.[239]

An electric field could also trigger color change together with shape change. When CB and a thermochromic pigment–reinforced SMP were integrated together, the Joule heating effect produced by the electroactive part could transfer heat to the thermochromic part, and the 4D-printed multi-material structure thus exhibited both shape and color changes (Figure 12c).[254]

The incorporation of LM has endowed LCEs with reversible electroactive actuation by Joule heating. A 4D-printed

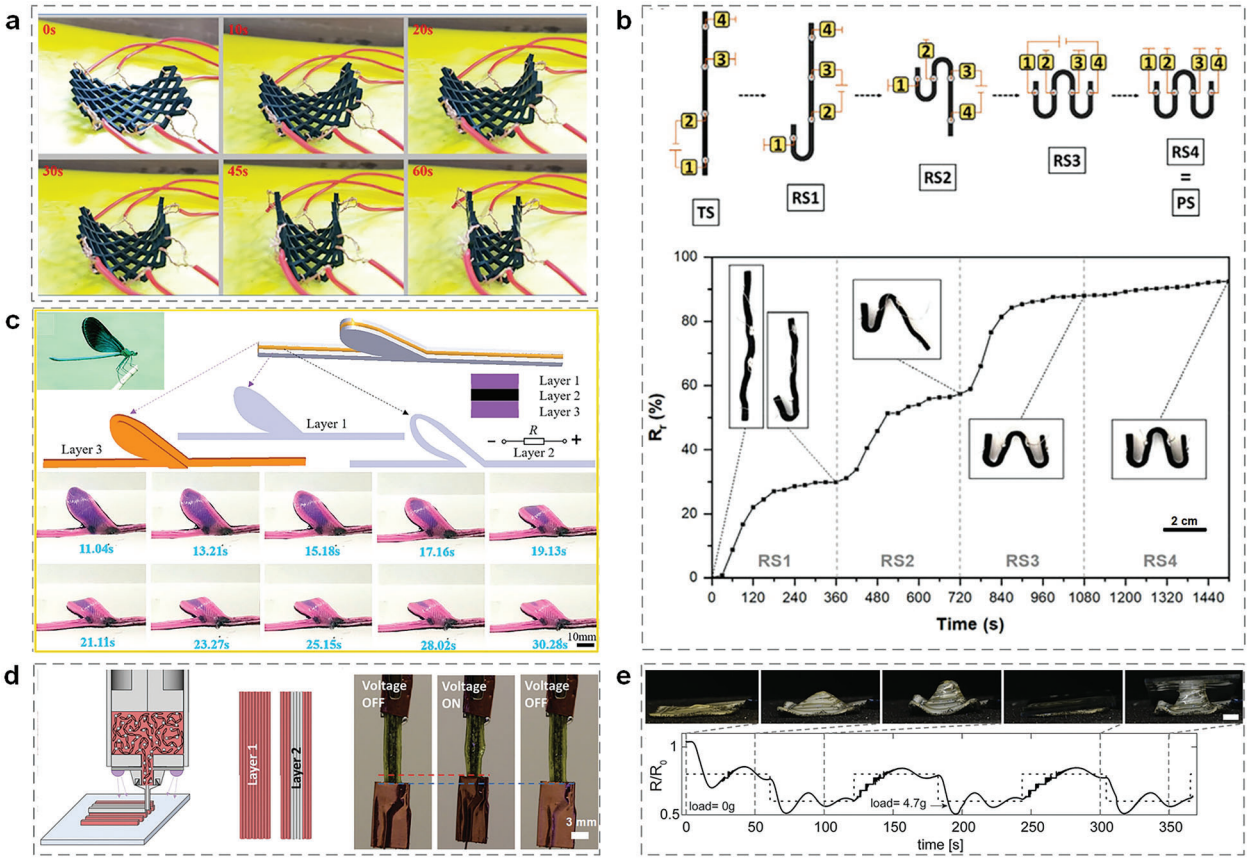

Figure 12. Electric field–based stimulus responses of 4D-printed structures. a) Shape recovery of an SMP structure. Reproduced with permission.[211] Copyright 2022, Elsevier. b) Stepwise actuation of a multistage SMP structure. Reproduced with permission.[253] Copyright 2021, Wiley-VCH Verlag GmbH. c) Structural design and concurrent shape and color changes of a multi-material SMP structure. Reproduced with permission.[254] Copyright 2021, Elsevier. d) Structural design and reversible actuation of a multi-material LCE strip (red and gray represent LCEs with LM contents of 0 and 88 wt.%, respectively). Reproduced with permission.[152] Copyright 2021, American Chemical Society. e) Shape change of an innervated LCE actuator and concomitant resistance change with closed-loop control. Scale bar, 5 mm. Reproduced with permission.[151] Copyright 2021, Wiley-VCH Verlag GmbH.

multi-material LCE structure consisting of 0 and 88 wt.% LM demonstrated reversible actuation under a low direct-current voltage (Figure 12d).[152] A core–shell LM–LCE structure exhibited concomitant resistance changes, even with a large bias load.[151] Using this method to program 2D director patterning into 3D structures, an out-of-plane shape transformation of an innervated LCE actuator was realized as shown in Figure 12e. The resistance profile with closed-loop control was capable of self-sensing.

3.4. Magnetic Field

The magnetic field stimulus provides precise control, remote operation, and versatility. The realization of magnetic responses usually relies on embedding magnetic particles into both smart materials and soft materials. Magnetic particles are generally classified into two categories: soft magnetic and hard magnetic. Soft-magnetic particles, such as iron-, nickel-, and silicon-based alloys, are characterized by high magnetic susceptibility and saturation magnetization but relatively low remanence and coercivity, which are strongly attracted to a magnet. By contrast, hard-magnetic particles, such as NdFeB, exhibit a large coercivity, enabling the realization of complex shape transformations under magnetic actuation.

The incorporation of Fe_3O_4 could generate heat in an alternating magnetic field, thus triggering the SME,[123,212,256–257] or serve as an active filler in soft polymers and hydrogels with magnetically driven capabilities in a magnetic field.[113,258–260] **Figure 13a** demonstrates the magnetically driven shape recovery process of an expanding SMP stent.[212] Kuhnt et al. synthesized anisotropic magnetic Fe_3O_4 from hematite templates, and the embedded hydrogel nanocomposite scaffold demonstrated unpaired actuation by controlling the distinct orientations of magnetic particles (Figure 13b).[259] Cao et al. embedded carbonyl iron particles in thermoplastic rubber to fabricate 4D-printed biomimetic structures with programmable actuation, and the FEA simulation showed consistent results, as illustrated in Figure 13c.[261]

NdFeB is another typical kind of magnetic particle that could align along the direction of an external magnetic field through the magnetization process, thereby achieving controllable magnetic deformation with growing interest in both SMPs and soft elastomers.[8,136,173,175,215,262–264] Inspired by the crawling motion of an inchworm, Wu et al. designed a 50-mm-long biomimetic

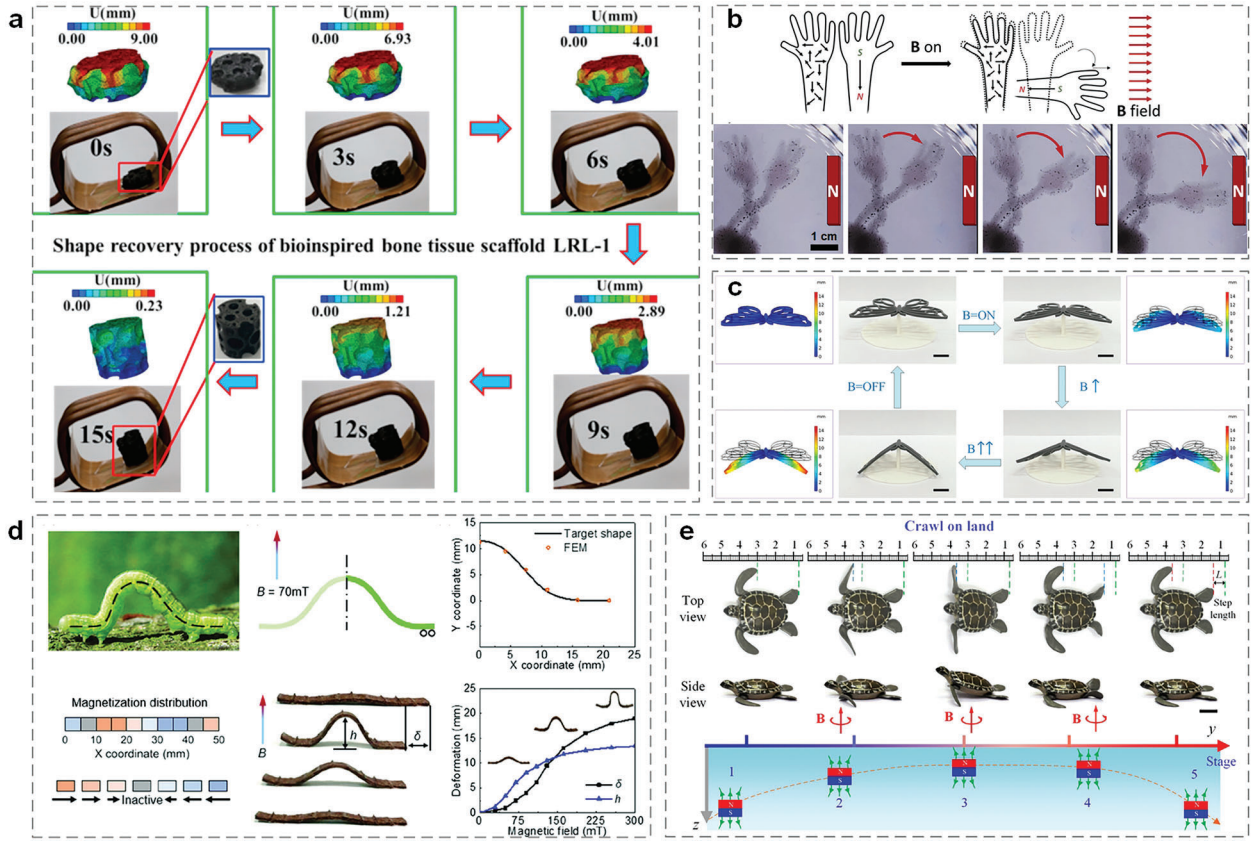

Figure 13. Magnetic field–based stimulus responses of 4D-printed structures. a) Shape recovery process of an SMP stent described by both experiments and simulations. Reproduced with permission.[212] Copyright 2021, Elsevier. b) Unpaired movement of a hydrogel composite structure.[259] c) Shape transformation of a biomimetic butterfly and its simulation. Scale bars, 1 cm. Reproduced with permission.[261] Copyright 2021, American Chemical Society. d) Inchworm-inspired crawling robot with the designed magnetization distribution to construct desired curvatures. Reproduced with permission.[175] Copyright 2020, Wiley-VCH Verlag GmbH. e) Various self-locomotion behaviors of a soft turtle structure. Reproduced with permission.[209] Scale bar, 1 cm. Copyright 2021, American Chemical Society.

crawling robot consisting of ten three-layered 5-mm-long voxels with designed magnetization distribution (Figure 13d).[175] Thus, the robot enabled a biomimetic directional crawling motion, accompanied by both height and distance changes under a periodic magnetic field. Although not directly printed, 2D magnetic soft active metamaterials were magnetized using a 3D-printed PLA mold as the fixture under an impulse magnetic field, demonstrating tunable area density with area-preserving capability.[264]

Through an enhanced origami-based magnetization process, 4D-printed magnetic-responsive soft materials exhibited improved magnetism and a spatial magnetization profile.[209] This enhancement enabled reversible shape changes and controllable locomotion. Figure 13e demonstrates the crawling behavior of a bionic turtle structure consisting of a rigid body and four magnetoactive soft flippers. Based on a mechanically-guided 4D-printing process, various complex magnetic structures were obtained across different length scales.[262] Other commonly used magnetic particles such as strontium ferrite and nickel-coated CFs were introduced into silicone elastomers or photosensitive resins.[265,266]

Without the addition of magnetic particles, 4D-printed alloys intrinsically possess magnetic responses. It was shown that in a rotating magnetic field of 0.97 T, a reversible MFIS of ≈0.01% was observed in a printed Ni–Mn–Ga SMA because of the twin variant rearrangement.[226] Magnetic SMA particles could also be embedded into polymers to achieve magnetic responses. The incorporation of Ni–Mn–In–Co metamagnetic SMA particles into a photocurable polymer enabled tunable damping capability under a small magnetic field below 100 kA m^{-1}, providing the design for 4D-printed magneto-mechanical damping devices.[267]

3.5. Solvent

The solvent stimulus involves the use of various solvents, such as water or other liquids, to cause changes in the shapes and properties of 4D-printed structures. It is usually employed in hydrogels because of the swelling behavior of their 3D networks.

The swelling behavior of a superabsorbent hydrogel upon the stimulus of water produced internal stress to fold the electrode bilayer structure around small peripheral nerves (100–200 µm).[92] Cheng et al. adopted the centrifugal printing method to fabricate mechanically tunable digital materials consisting of spatially distributed hard and soft voxels.[97] When the multimaterial hand was immersed in water, the integrated hydrogel

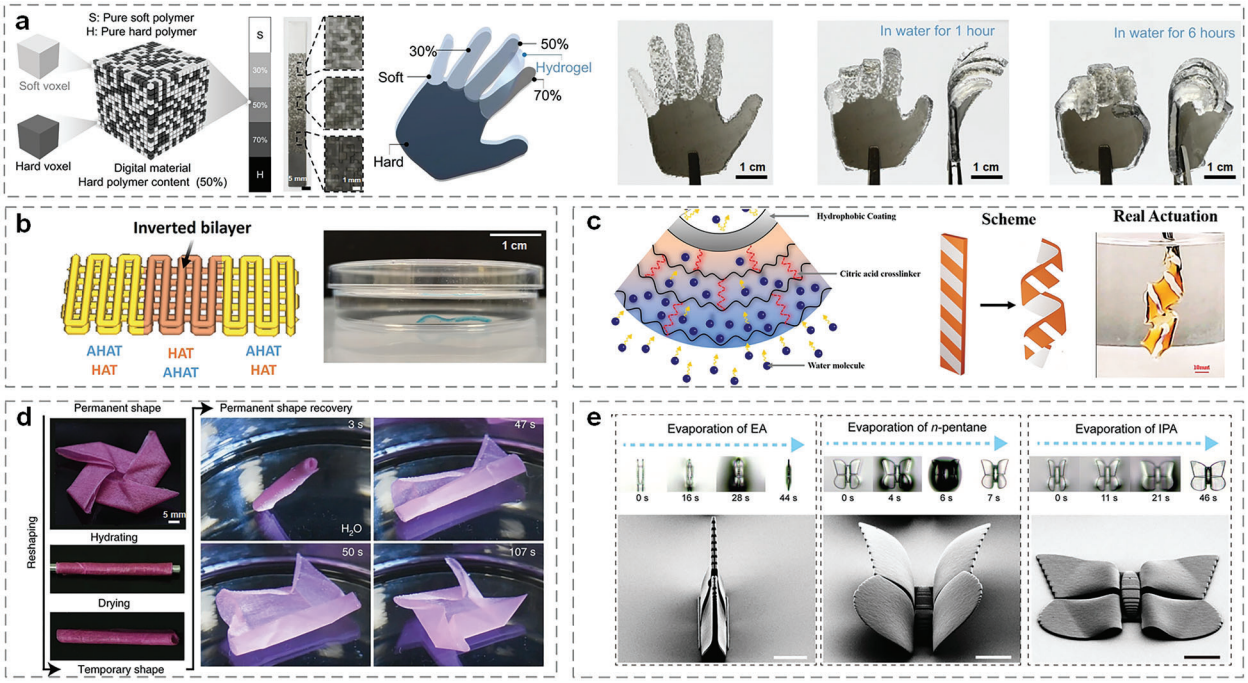

Figure 14. Solvent-based stimulus responses of 4D-printed structures. a) Bending behavior of a multi-material hydrogel hand in water. Reproduced with permission.[97] Copyright 2022, Springer Nature. b) Alternating bending behavior of biphasic hydrogel scaffolds. HAT: tyramine-functionalized hyaluronan. AHAT: alginate with HAT. Reproduced with permission.[169] Copyright 2022, Wiley-VCH Verlag GmbH. c) Shape-morphing mechanism and actuation of hydrogel structures with hydrophobic coatings. Reproduced with permission.[268] Copyright 2023, Elsevier. d) Shape recovery process of an origami structure in water. Reproduced with permission.[138] Copyright 2020, Springer Nature. e) Three shape configurations of a microstructure when immersed in different solvents, including ethyl acetate, *n*-pentane, and isopropyl alcohol. Scale bars, 20 μm. Reproduced with permission.[115] Copyright 2021, Wiley-VCH Verlag GmbH.

layer swelled, which triggered the five fingers to bend at various angles because of their different moduli (**Figure 14a**). Similarly, different swelling between two types of hydrogels enabled the autonomous multistage bending behavior of biphasic scaffolds upon immersion in water as depicted in Figure 14b.[169] When applying hydrophobic silane coatings on one side of printed chitosan hydrogels, controlled shape deformations were achieved.[268] Figure 14c demonstrates the mechanism of shape-morphing due to concentration gradients and actuation of a spiral structure by water, which could be reversed upon immersion in ethanol. Mao et al. designed a patterned film consisting of hydrophilic chitin and a non-responsive polymer, which could be transformed into complicated multidimensional architecture when immersed in water.[269]

Besides the intrinsic swelling behavior of hydrogels, there are other methods to realize solvent responses. The strain-induced phase transition from coiled α-helix to metastable β-sheets enabled the shape recovery of a printed hierarchically structured material, triggered by hydration, as depicted in Figure 14d.[138] When microstructural pillars were immersed in different evaporating solvents, they exhibited three configurations, namely the coalesced cluster, curved shape, and assembled shape toward the curving directions (Figure 14e).[115] These configurations were attributed to the different net capillary forces caused by asymmetric crosslinking densities during the TPP process. Inspired by amyloid fibrils, Zhang et al. 4D-printed water-induced self-assembly zein gel in a Carbopol supporting bath with various water concentrations where the hydrophobic and hydrogen bonding were controlled.[270] The 4D-printed butterfly demonstrated asymmetrical shape changes in its wings, along with controlled drug release.

The anisotropic shrinkage along the thickness of printed parts also enabled solvent responses. The bending behavior of a 4D-printed re-entrant structure was due to light attenuation, where the upper sheet possessed lower crosslinking densities than the lower part.[93] The subsequent removal of unreacted monomers by solvents and evaporation caused higher shrinkage in the upper part. By controlling the layout, transport in the lateral/forward directions was easily programmed. Ren et al. designed 4D-printed structures with aligned magnetic fibers, which were fabricated using a magnetic-assisted printing method and demonstrated anisotropic shrinkage when dissolved in acetone.[266]

3.6. Humidity

Unlike the solvent stimulus, which relies on using different types of liquids, humidity responses involve the absorption or release of moisture from the surrounding environment. The stimulus of relative humidity (RH) has attracted increasing attention for various types of materials, from LC materials to fiber composites.

Upon immersion in acetone, the aggregated non-reacted 4′-Pentyl-4-biphenylcarbonitrile triggered by PIPS left gradient

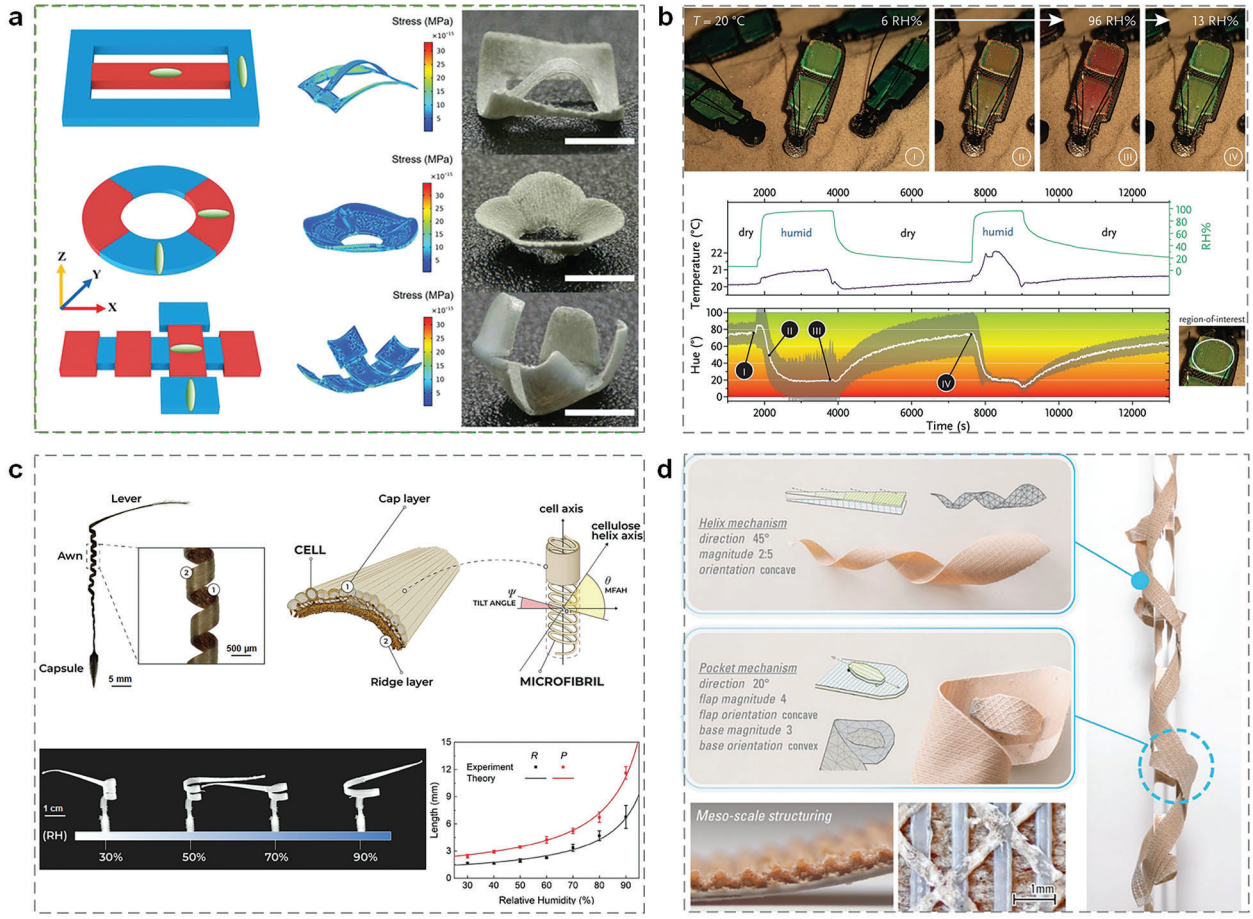

Figure 15. Humidity-based stimulus responses of 4D-printed structures. a) Programmable spatial actuation of LCN structures with programmed LC and SiC alignment. Scale bars, 5 mm. Reproduced with permission.[88] Copyright 2022, Wiley-VCH Verlag GmbH. b) Color changes of a beetle-like LCE actuator under different RH and hue evolution during two drying/humidifying cycles. Reproduced with permission.[162] Copyright 2022, Wiley-VCH Verlag GmbH. c) Shape-morphing of a natural awn–inspired artificial seed at different RH. Reproduced with permission.[202] Copyright 2023, Wiley-VCH Verlag GmbH. d) Transfer of the mechanisms of bioinspired motions to multifunctional hygroscopic structures. Reproduced with permission.[273] Copyright 2021, Wiley-VCH Verlag GmbH.

pores in LC-crosslinked networks, which collapsed after drying and induced a bending behavior.[88] Various humidity-responsive actuations were realized by programming-aligned LCs and SiC in desired positions in single or multiple layers, as shown in **Figure 15a**. By protonating the pendant amine groups of the cholesteric LCE with a hydrochloric acid solution, a hygroscopic ammonium group was generated, thereby realizing humidity responses.[162] Figure 15b demonstrates the color changes of a 4D-printed cholesteric LCE structure on a substrate under a complete cycle of humidity. The 4D-printed biomimetic scallop-like actuator could also reversibly open and close. Similarly, by activating one side surface of a dimethylamino-functionalized LCE, the produced cations on the surface enabled asymmetric hydrophilicity.[271]

The hydrophilic properties of cellulose fibers could cause water molecules to be trapped between intermolecular hydroxyl groups through hydrogen bonds. When electrospun core–shell fibers containing cellulose nanocrystals and printed biodegradable polymers were combined together, the biomimetic structure could mimic the movement of natural seeds under humidity changes, as demonstrated in Figure 15c.[202] Inspired by the pinecone, 4D-printed bilayer structures consisting of a wood polymer composite and acrylonitrile butadiene styrene with differential hygroscopic swelling characteristics exhibited programmable hygroscopic multiphase movement.[272]

Cheng et al. adopted the same material strategy and introduced computational design tools to evaluate the mechanisms of bioinspired motions.[273] Based on the helix and pocket biomechanics of natural plants to generate forces, they transferred the same principle to 4D-printed multifunctional structures, as demonstrated in Figure 15d. Similarly, 4D-printed hygromorph biocomposites containing continuous flax fibers or pulp fibers with hygroscopic responsiveness were constructed.[274,275]

3.7. Other Stimuli

Besides the above-mentioned traditional stimuli, there are other stimuli in 4D printing, such as pH changes,[113,276–278] chemicals,[84,167] pressure,[150] laser,[224] and microwave.[279,280]

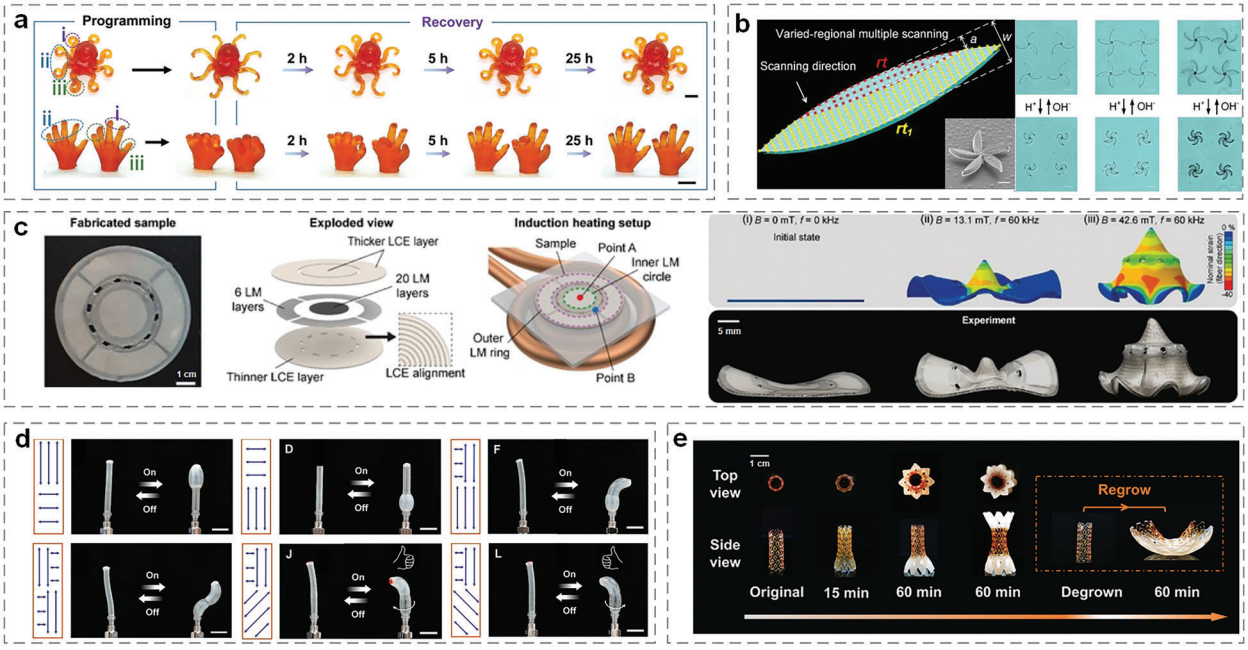

Figure 16. Other stimulus responses of 4D-printed structures. a) Autonomous morphing of an octopus structure and a hand structure with programmable temporal evolution. Scale bars, 5 mm. Reproduced with permission.[83] Copyright 2021, Wiley-VCH Verlag GmbH. b) Diverse pH-triggered shape transformations of micro hydrogel structures. Scale bar, 20 μm. Reproduced with permission.[113] Copyright 2019, Wiley-VCH Verlag GmbH. c) Untethered ultrafast pop-up deformation of LCE–LM structures under eddy current induction heating. Reproduced with permission.[208] Copyright 2023, Wiley-VCH Verlag GmbH. d) Integrated LCE alignment to execute complex motions under pressure. Scale bars, 1 cm. Reproduced with permission.[150] Copyright 2023, Royal Society of Chemistry. e) Spatiotemporal shape changes through localized growth, degrowth, and regrowth under chemical interactions. Reproduced with permission.[84] Copyright 2023, Wiley-VCH Verlag GmbH.

It is found that 4D-printed structures can exhibit different changes spontaneously as time passes.[83] The strong time–temperature dependence of a supramolecular SMP enabled the versatile off-equilibrium shape-morphing pathways through localized programming conditions. The self-evolving process of an octopus structure and a hand structure (**Figure 16a**) indicated that not only the shape change could autonomously occur with time but the morphing sequence could also be programmed in precision. This temporal morphing could be activated or locked by changing the temperature across T_g.

4D-printed microscale hydrogel structures could demonstrate reversible expansion, contraction, torsion, and complex geometrical shape changes under various pH environments, as shown in Figure 16b.[113] This behavior was attributed to the non-uniform crosslinking densities at different locations achieved by accurately controlling the laser scan direction, which resulted in various swelling ratios.

Untethered actuation is highly desired, especially in constrained or enclosed environments. Recently, Maurin et al. developed LCE–LM composites with ultrafast untethered, and highly programmable actuation in milliseconds by eddy current induction heating generated by high-frequency magnetic fields.[208] Figure 16c shows the multimodal sequential deformation of a pop-up structure by spraying different LM layers within the DIW-printed LCEs to program the spatial intensity of the eddy current. Selective actuation was realized by moving the magnetic field to control the eddy current distribution.

The alignment of LCs could also induce programmed mechanical anisotropy. Fundamental motions, such as contraction, elongation, bending, and twisting, can be achieved through inflation by increasing the pressure (Figure 16d).[150] Based on the principle of electromagnetic introduction, an integrated 4D-printed multi-material device exhibited piezoelectric properties under external pressure, enabling the conversion from mechanical energy to electrical energy.[245]

The presence of special chemicals can also lead to responses. Based on the regenerative living method, printed homogenous parts were transformed into different heterogeneous derivatives by controlling the localized growth, which could be further degrown and regrown into a new shape (Figure 16e).[84] The genetics of yeast encapsulated in a 4D-printed ELM could be leveraged to proliferate in the presence of specific biomolecules, which resulted in a macroscopic shape change accompanied by a volumetric increase of up to 370%.[167] By employing this method, sequential and multiple shape changes with the presence or absence of specific biochemicals were realized.

3.8. Multi-Stimuli

Multi-stimuli responses refer to the capability of printed structures to respond to multiple external stimuli, including heat, light, magnetic fields, electric fields, humidity, and pH changes. The integration of multiple stimuli makes printed structures highly versatile and suitable for a wide range of applications.

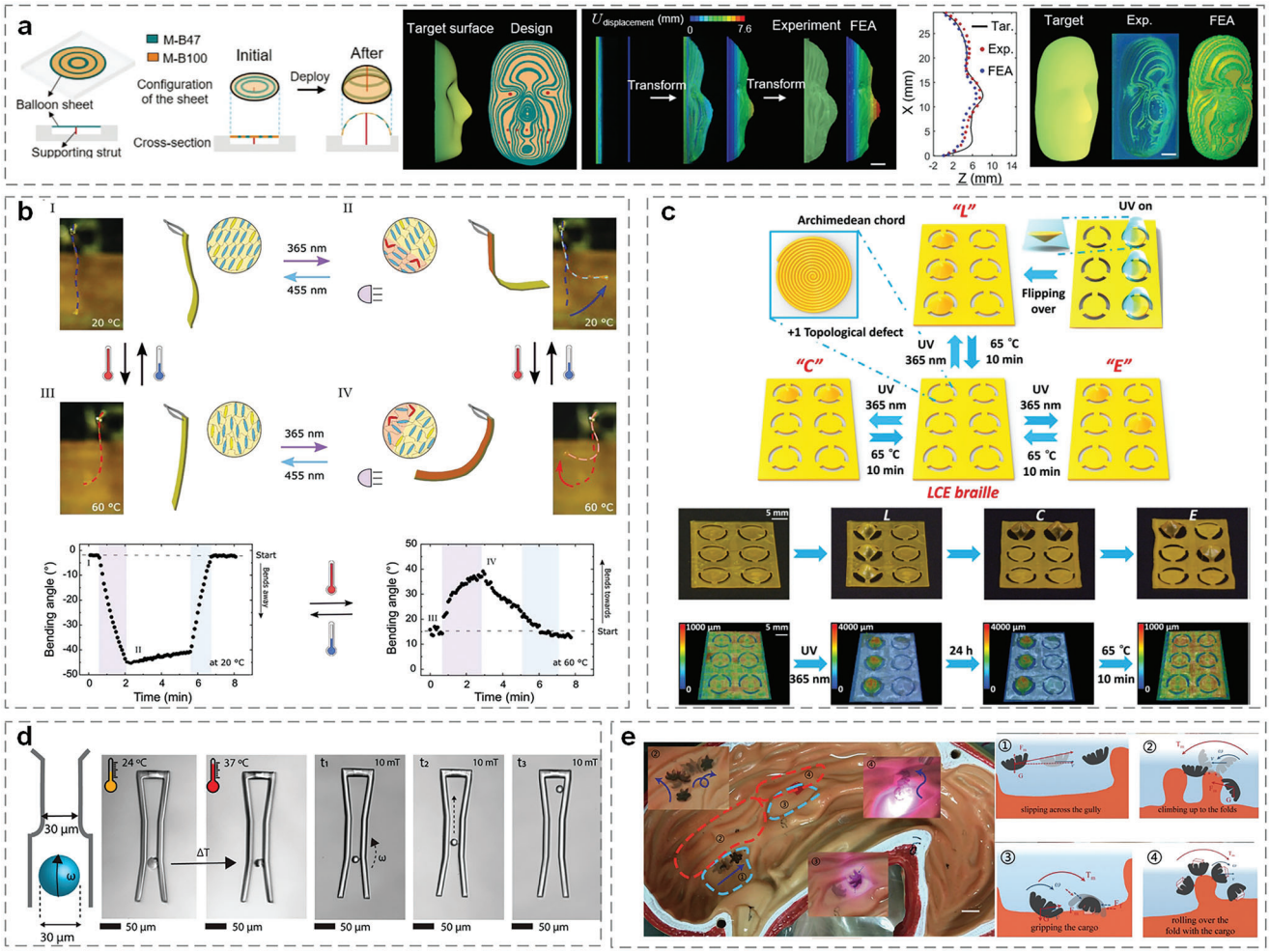

Figure 17. Multi-stimuli responses of 4D-printed structures. a) Shape transformation of a 2D SMP balloon into a 3D human face contour under thermo-pneumatic stimuli. Scale bars, 3 mm. Reproduced with permission.[71] Copyright 2021, Wiley-VCH Verlag GmbH. b) Schematic diagram of the mesogen alignment and shape-morphing behavior of an LCE film under thermo-photo stimuli. Reproduced with permission.[205] Copyright 2020, Wiley-VCH Verlag GmbH. c) On-demand shape transformation of a Braille-like actuator under thermo-photo stimuli. Reproduced with permission.[6] Copyright 2021, Wiley-VCH Verlag GmbH. d) Actuation of a hydrogel microroller that passed through a channel with spatial adaptability under thermo-magnetic stimuli. Reproduced with permission.[10] Copyright 2020, American Chemical Society. e) Actuation of hydrogel structures in a stomach model under photo-magnetic stimuli. Scale bar, 6 mm. Reproduced with permission.[173] Copyright 2022, Elsevier.

A multi-material crane-like structure with triple SME exhibited quintuple complex shape transformation under magnetic and heat stimuli with sequential and accurate controllability.[123] Isophorone diisocyanate was incorporated, which could react with water to form the –NHCONH– moiety and serve as a self-healing agent for thermo-magnetic stimuli-responsive SMP structures.[281] A thermoplastic SMPC structure was designed to possess a thermo-magnetic response based on a multi-material design.[124,125] By heating a multi-material SMP from T_{g1} to T_{g2}, pneumatic blowing enabled the fabrication of a shape memory balloon with a predefined intricate shape and local control, as proven by both experiments and FEA.[71] **Figure 17a** shows a representative shape-morphing process of a 2D balloon structure into a highly sophisticated 3D human face contour with the target shape. A 4D-printed conductive SMP integrated with a magnetorheological elastomer composite exhibited bi-directional and bistable actuation with enhanced stability under electro-magnetic stimuli.[265]

Figure 17b demonstrates the thermo-photo stimuli–responsive bending behavior of a 4D-printed LCE film at 20 °C and 60 °C in water.[205] The increase in temperature reversed the bending direction under UV light. In both circumstances, upon illumination with a 455-nm blue light, the actuation was reversible because of back isomerization, which could be repeated several times. Based on the comprehensive understanding of the relationship between the LCE network and shape-switching behavior, a 4D-printed Braille-like actuator with Archimedean chord patterns demonstrated repeatable on-demand shape transformations under the UV light and heat stimuli (Figure 17c).[6] The shape locking did not require a continuous power supply, which paved the way for practical applications.

The permeability of the functionalized membrane of Psomes could be tuned by pH changes, and the shrinkage behavior of

the PNIPAM microgate upon heating triggered the release of heparin.[114] The presence of nanothylakoid and PNIPAM endowed a 4D-printed bilayer hydrogel with light and thermal responsiveness, respectively.[171] When subjected to NIR irradiation, nanothylakoid transformed the laser energy into heat. When heated above the lower critical solution temperature (LCST), the thermal-sensitive PNIPAM layer contracted while the PAA layer remained swollen, resulting in a bending behavior of the bilayer. The existence of PNIPAM, acrylic acid, and Fe_3O_4 endowed the hydrogel composite with thermo-, pH-, cation-, and magnetic-responsiveness.[10] Figure 17d demonstrates the actuation of a 4D-printed hydrogel microroller that passed through the channel by manipulating the temperature and rotating magnetic field.

A 4D-printed protein-based hydrogel possessed distinct shapes under multiple external stimuli, demonstrating reversible shape changes upon heating and irreversible shape changes with an enzyme.[172] The complex shape changes also facilitated the development of delivery and release systems, exemplified by a 4D-printed shellfish-like robot demonstrating cargo transport on a wrinkled stomach surface model under NIR light irradiation and magnetic responses (Figure 17e).[173] The shrinkage and swelling behaviors of alginate-based hydrogel structures could be actuated by both pH changes and divalent cation chelators.[282] Similarly, a biocompatible hydrogel structure containing citric acid–coated superparamagnetic iron oxide nanoparticles could flexibly perform gripping, delivering, and releasing behaviors under electromagnetic actuation.[283]

4. Computational Structural Design

With reference to the summary of various printing methods and stimuli, it is apparent that the design of materials and structures is the key to 4D printing and the basis for the controllable changes of shape, property, and functionality of the printed parts. Harnessing its advantage plays an important role in enabling intelligent printing and advancing various engineering applications.[284–287] The design of materials encompasses selecting materials with suitable properties, such as thermal, electrical, and mechanical properties, to ensure the desired performance upon an external stimulus. For instance, the incorporation of conductive materials influences the electrical conductivity and performance of 4D-printed electronic components. The structural design involves the geometry, porosity, and interconnectivity of the printed parts, and optimizing these structural parameters can enhance the design efficiency and properties of the parts. For example, designing hierarchical structures with controlled porosity can facilitate the diffusion of stimulus chemicals throughout the material, thereby promoting uniform and sensitive actuation.

Although this knowledge-based design could meet the fundamental demands of various applications, it is intuitive and highly depends on the designers' experience and expertise, which poses challenges for multi-material structures.[288] To achieve a more complicated target shape (or function) change, determining the spatial material distribution plays an important role. In this section, we elucidate the essential role of computational structural design in advancing the 4D printing technology, particularly in the realm of multi-material fabrication.

Topology optimization (TO)[289] is a method that optimizes the geometric features to achieve certain objectives, such as maximizing the structural properties and minimizing the weight. It has found significant applications in 4D printing.[290–298] However, TO has the drawbacks of complicated mathematical derivations and computationally expensive simulations, especially in design problems with geometric and material nonlinearities.

The history of machine learning (ML) dates back to the late 1950s when simple statistical algorithms were proposed.[299] With the revolution in the running speed and reduced cost in modern computer systems, recent advancements in ML algorithms offer more opportunities for various fields. Given the tremendous design space in 4D printing, conventional methods pose significant challenges in workload and design efficiency when seeking optimal designs for desired shape changes. In this context, ML stands out for its high efficiency in solving these problems, especially in inverse material design for 4D-printed structures with desired properties or functionalities. Additionally, FEA tools are usually combined to accurately simulate experimental results as training data for ML algorithms. Currently, ML has made great progress in the flexible design of 4D-printed smart materials and metals.[43,300]

As a natural selection–inspired optimization algorithm, the evolutionary algorithm (EA) is capable of simulating the behavior of biological populations. Hamel et al. adopted the ML–EA method combined with FEA to design active composite structures with target shape-shifting responses.[301] They designed and optimized the composite structures consisting of equally sized voxel units that were made of either a passive or an active material. The agreement between the target shapes and the ML-simulated shapes was well achieved, which demonstrated the high potential of ML for the design of 4D-printed active composite structures. This approach was recently further developed to consider void as a design element.[302] An optimized EA-based ML tool was employed to obtain the stress–strain curves of a 4D-printed fractal metamaterial.[50]

Based on the robust EA-guided inverse design method, Wu et al. achieved complex nonintuitive magnetization distributions with desired curvature and deformations.[175] By integrating DIW printing and the EA-guided design strategy, complex and dexterous dynamic motions under magnetic fields were realized, such as the biomimetic dog trot gait as shown in **Figure 18a**. Ma et al. developed an inverse design framework where a deep residual network substituted conventional FEA for acceleration of the design process, achieving predefined global strains of metamaterials under magnetic actuation.[176] Figure 18b demonstrates the use of deep learning for designing magnetization distribution and fabricating targeted complex magnetic soft metamaterials.

Sun et al. proposed a novel paradigm for predicting the mechanical responses and inverse design of a 4D-printed active composite beam.[303] A recurrent neural network (RNN)–based ML model was employed to predict the forward shape change of a 1D cantilever with training datasets obtained by FEA simulations. When EA and ML were combined, the optimal design was able to be found inversely for various target shape changes with high efficiency. By integrating computer vision (CV) algorithms, hand-drawn lines could be identified as target shapes to inversely find the optimal materials distribution. Following slicing, the transformed grayscale patterns were imported into a DLP

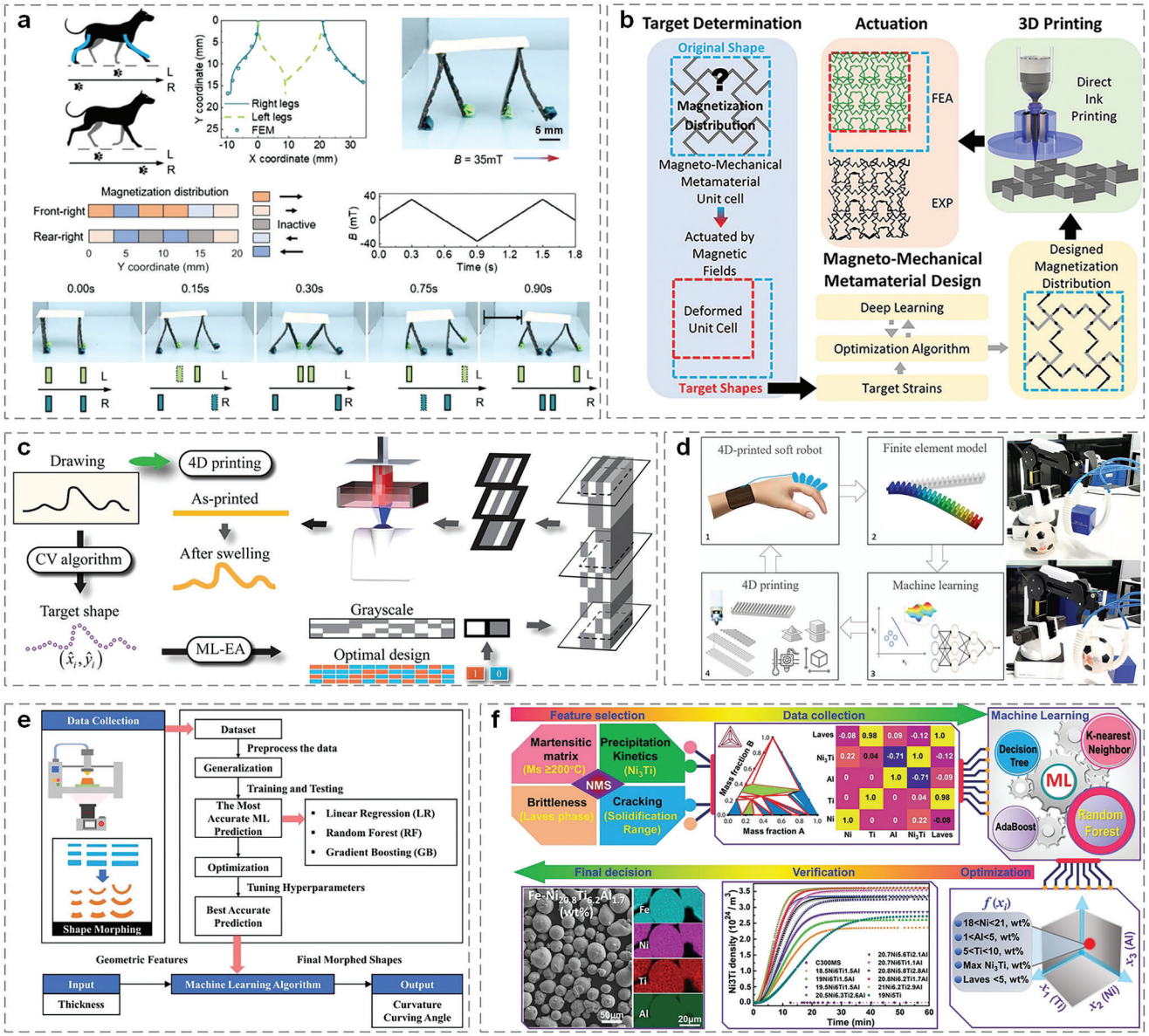

Figure 18. Use of ML in 4D printing. a) Biomimetic dog trot gait based on the EA-assisted design of magnetization distribution. Reproduced with permission.[175] Copyright 2020, Wiley-VCH Verlag GmbH. b) Deep learning–based design process for tunable magneto-mechanical soft metamaterials. Reproduced with permission.[176] Copyright 2022, American Chemical Society. c) Workflow of the CV algorithm integrated with EA for the design of an active beam. Reproduced with permission.[303] Copyright 2021, Wiley-VCH Verlag GmbH. d) Optimized ANN-based design process of a soft pneumatic actuator to realize the grasping behavior of different objects with specific bending angles. Reproduced with permission.[305] Copyright 2021, Elsevier. e) Schematic flow chart using ML models to predict shape-morphing behaviors of 4D-printed active structures. Reproduced with permission.[306] Copyright 2020, IOP Publishing. f) Schematic of the ML-assisted fabrication of novel Fe–Ni–Ti–Al maraging steel. Reproduced with permission.[241] Copyright 2023, Wiley-VCH Verlag GmbH.

printer to construct a 1D beam with two differentially polymerized material phases. Upon swelling, the printed active beam automatically transformed into drawn profiles because of the volumetric mismatch between the two phases. The whole process is schematically illustrated in Figure 18c. Recently, Sun et al. presented a seamlessly integrated approach combining ML and sequential subdomain optimization, which exhibited superior performance in terms of optimization accuracy and speed, delivering results within seconds.[304] Additionally, when augmented with a splicing strategy, this approach demonstrated the capacity to design varied lengthwise voxel configurations, thereby exhibiting remarkable adaptability to complex target shapes while maintaining high levels of speed and accuracy.

An accurate simulation of actuation was developed based on the FEA of a hyperelastic material, which was used to obtain training data for ML modeling.[305] Based on the optimized artificial neural network (ANN) method, the geometrical requirements of 4D-printed soft pneumatic actuator robots were

predicted to achieve the necessary bending angles for different objects (Figure 18d). Three different ML regression models, including gradient boosting, random forest (RF), and multiple linear regression, together with three-time series forecasting algorithms, were employed to predict the shape-morphing behavior of 4D-printed active materials.[306] Figure 18e illustrates the schematic flow chart of the ML models for quantitatively geometrical shape-morphing structures with desired curvatures and curving angles. Similarly, R_f and R_r of a PNIPAM hydrogel were employed to train the algorithm and optimize the best materials formulation, demonstrating the potential of the approach for innovative smart drug delivery systems.[307] Yu et al. used an ML model based on a polycube-based RF regressor to obtain different complex shapes, with the simulation 20 times faster than hybrid isogeometric analysis–FEA simulations.[308]

An ML-assisted strategy was employed in the fabrication of novel Fe–Ni–Ti–Al maraging steel, as demonstrated in Figure 18f.[241] Among various ML algorithms, the most accurate RF method was employed to design the alloy composition. Compared to 3D printing, ML-assisted 4D printing exhibited high energy efficiency and sustainability due to a synchronous combination of geometry shaping and time-dependent precipitation hardening.

The design approaches discussed above are often ad hoc and case-specific. 4D printing is a highly interdisciplinary field that involves AM, smart materials, and mechanics. To establish a more generalized design methodology, it is necessary to develop common core knowledge in 4D printing. Toward this direction, Dimassi et al. pioneered the effort to develop an ontology-based framework that formalizes knowledge about 4D printing with regard to AM processes and techniques, smart materials, stimuli, and shape transformation.[309,310] This framework categorized and described the common knowledge in 4D printing in a computer-interpretable manner so that it could be reused for product design.

5. Applications

As a rapidly growing technology, 4D printing has found many potential applications owing to its dynamic capability, tunable responsiveness, highly customized complexity, integrated functionalities, and reduced assembly steps for fabricated parts. In previous review articles, it has been shown that 4D printing attracts extensive attention in soft robotics, biomedicine, tissue engineering, electronics, defense, and security.[46,311] This section focuses on the most relevant applications of the 4D-printing technology during the last three years, including biomedical engineering, electronics, robotics and actuators, photonics, aerospace, and information encryption.

5.1. Biomedical Engineering

The autonomous adaptability brought by 4D printing provides enhanced customization to different patients, thus making biomedical devices more appealing, especially in the fields of smart medical implants, drug delivery systems, self-expanding stents, and tissue engineering. Moreover, 4D printing introduces additional functionalities, including the self-healing capability, improved controllability to reach less accessible regions readily under a stimulus, and the ability to facilitate targeted therapies.

The programmability of 4D-printed biodegradable SMP structures enables them to be smaller for easier implantation and on-demand actuation under the specific stimulus, thus demonstrating great potential in minimally invasive surgeries. A biocompatible SMP scaffold exhibited photo-triggered expanding behavior and efficiently realized local breast tumor ablation by hyperthermia treatment.[120] A soft tissue engineering scaffold demonstrated good void-filling capability.[77] The self-deploying actuation around body temperature could support stenotic lesions, and the loaded drug also inhibited the proliferation of endothelial cells and enhanced inflammatory responses.[128] An anastomosis ring with a designed grid and hook lock structure could be easily implanted into the intestine, demonstrating good mechanical properties and being able to excrete within one month after healing.[191] Inferior vena cava filters self-deployed in warm water and simulated the thrombi-capturing behavior.[76] Both in vitro stenting and in vivo vascular grafting have demonstrated good mechanical adaptability.[130]

Inspired by bionic structures, the structural optimization of SMP structures demonstrates enhanced mechanical properties. A cartilage scaffold inspired by the mangrove structure could be actuated at body temperature, showing its potential to treat articular cartilage defects.[121] Owing to the bionic design with honeycomb pore structures and its outer contour as scanned by the CT reconstruction method, an orbital stent at the recovered state offered a higher volume filling rate of nearly 150% than traditional stents (**Figure 19a**).[204] The three-month postoperative follow-up revealed promising outcomes in terms of orbital tissue growth, offering significant potential for the personalized treatment of enophthalmos. Lin et al. fabricated various ventricular septal defect occluders (VSDOs) with wavy bionic structures that mimicked the mechanical responses of biological tissues to adapt to defects at different locations.[192] Additionally, these biocompatible devices avoided the drawbacks of alloy occluders, such as wear, displacement, perforation, and embolism, and demonstrated overall radiopacity (Figure 19b). Lotus root–bioinspired 4D-printed scaffolds exhibited improved cell attachment and proliferation ability for bone regeneration.[212]

Biocompatible SMP and hydrogel structures are widely co-cultured with cells. Based on the optimization of the microgroove width, coculturing three different types of cells that mimicked the cellular composition of the human heart resulted in homogeneous cell alignment, which was challenging to achieve on curved scaffolds because of the influence of gravity. (Figure 19c).[251] The high electrical conductivity of graphene within the curved tissue construct enhanced myocardial maturation, which contributed to improved cardiac functions. Mimetic trachea tissue containing two types of cells was constructed from a silk hydrogel, and its implantation into a rabbit for 2 months was proven for treatment of a damaged trachea.[312] Biopolymer- and microgel-based cell-laden gradient hydrogels with programmable shape changes facilitated the formation of bone-like and cartilage-like tissues.[277,282,313] By leveraging the exchange reactions between 4D-printed PTU and hydrophilic or hydrophobic sulfhydryl compounds, the surface wettability could be flexibly tuned, thus regulating the cell adhesion performance.[82]

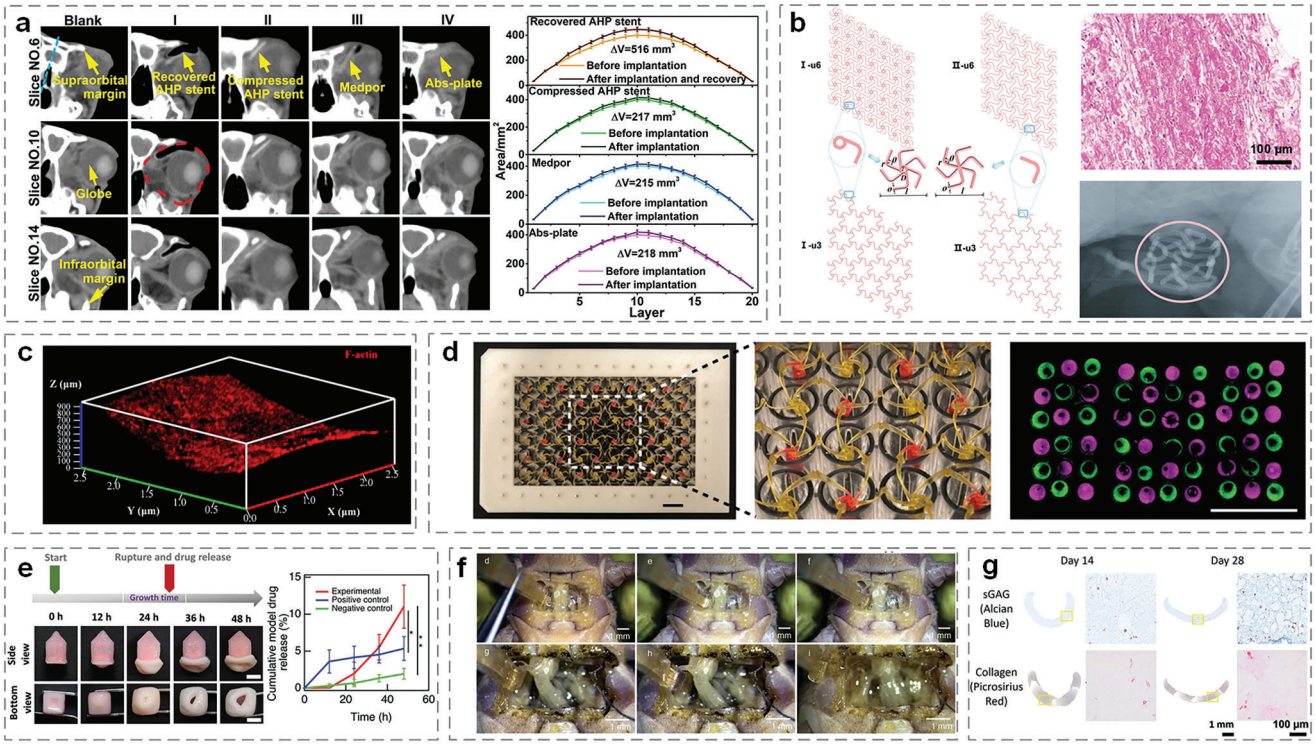

Figure 19. Biomedical applications of 4D-printed structures. a) Comparison of CT slides between SMP and commercial stents and their orbital volume increments after implantation. Reproduced with permission.[204] Copyright 2022, Elsevier. b) Wavy structural design, biocompatibility, and in vivo radiopacity of VSDO. Reproduced with permission.[192] Copyright 2022, Wiley-VCH Verlag GmbH. c) Immunofluorescence staining of cells on curved cardiac constructs with cell alignment after shape transformation. Reproduced with permission.[251] Copyright 2021, American Chemical Society. d) High-throughput cell culturing and histology with a transformable tube array. Scale bars, 10 mm. Reproduced with permission.[49] Copyright 2020, Wiley-VCH Verlag GmbH. e) On-demand drug delivery by a capsule device in response to a particular biomolecule. Scale bars, 5 mm. Reproduced with permission.[167] Copyright 2021, Wiley-VCH Verlag GmbH. f) In vivo implantation and extraction of an electrode interfacing with the peripheral nerve of an insect. Reproduced with permission.[92] Copyright 2023, Wiley-VCH Verlag GmbH. g) Staining of cartilage-containing molecules during the cell culturing of hydrogel scaffolds. Reproduced with permission.[169] Copyright 2022, Wiley-VCH Verlag GmbH.

An SMP-based transformable tube array consisting of a series of cell culture tubes was built, where the bottom cell chambers and upper helical arms were used for cell culturing and shape transformation, respectively.[49] The 3.6-time difference in the lateral size enabled the temporary shape to match the 96-well plate for cell culturing while the recovered shape transferred all cells to the standard histology cassette (Figure 19d). This high-throughput parallel histology examination method was believed promising for disease modeling and drug screening to save time and labor costs.

4D-printed hydrogel structures also demonstrated great potential in biomedical applications. Figure 19e shows the adoption of a 4D-printed reservoir-based drug delivery capsule with an embedded probiotic mutant for on-demand drug delivery.[167] In response to a particular biomolecule, the capsule ruptured, and a model drug was released to the surrounding environment. Figure 19f demonstrates the in vivo implantation and extraction process of a 4D-printed cuff electrode interfacing with the peripheral nerve of a locust.[92] When immersed in an electrolyte, the conductive electrode wrapped around the nerve with good contact to reliably stimulate and record neural signals. The force of the electrode could be easily tuned so that it could be simply pulled off without causing damage. The safe removal from the nerve highlights the great potential of the electrode for clinical applications in peripheral nerve interfacing. A 4D-printed nanocomposite hydrogel structure could decrease the undesired leakage of drugs into the environment because of the contraction of the hydrogel networks.[173]

A multifunctional hydrogel microcarrier enabled the transportation and delivery of multiple motile sperm cells to increase fertilization rates, local release of heparin, and facilitation of the HA–cumulus complex degradation.[114] This device offered a new strategy for in vivo fertilization by improving the sperm–oocyte interactions. Hydrogel structures containing human bone marrow cells showed high cell viability and exhibited cartilage-like matrix production after 28 days in culture, as visualized by Alcian blue and Picrosirius red staining (Figure 19g).[169]

5.2. Electronics

The tunable conductivity and stretchability of 4D-printed structures enable them to function in the field of electronics as smart electronic devices through materials, process, and structure integration. The dynamic characteristics of 4D printing bring augmented functionality in electronics, such as the enhanced

monitoring range of tunable sensors, improved sensitivity of electromechanical sensors, adaptive properties of shape-changing sensors, and sensor–actuator integration. Moreover, the conductivity along with shape-changing capability allows the switch of a circuit to be controlled by different stimuli.

Based on the temperature gradient along the thickness direction upon FIR light irradiation, a CB-containing SMP structure bent toward the light, lighting up light-emitting diode (LED) bulbs sequentially.[210] An integrated sensor–actuator device demonstrated a heat-triggered active touching behavior with self-perception capability by recording the resistance signals.[186] The strain isolation characteristics in a digitally heterogenous SMP not only endowed the stretchability of nonstretchable electronic devices but also demonstrated autonomous shape transformation, thereby exhibiting great potential toward complex shrinkable electronics.[105]

Based on the structural design and optimization of 4D-printed metamaterials, tunable stretchability could be obtained. The integration of imperfect fractal metamaterial lattices allowed an assembled bionic electromyogram sensor to match the J-shaped stress–strain behavior of human skin, thereby demonstrating its great potential for the detection of bioelectrical signals.[50] Throughout the stretching process of a shape-reconfigurable metamaterial structure, an LED light connected to the structure remained lighted, demonstrating the great promise of the metamaterial structure in the field of reconfigurable flexible electronics (**Figure 20a**). Similarly, the introduction of fractal auxetic metamaterials led to high elongation, tunable water contact angles, and capacitance changes, thereby endowing the health-monitoring sensors with improved sensitivity, as shown in Figure 20b.[194]

Conductive LCE and hydrogel components also play an important role in integrated electronic devices. A multi-material bilayer LCE actuator that integrated electrothermal and photothermal responses could be employed as an electrical switch to control the circuit on/off under NIR irradiation, as shown in Figure 20c.[152] The activation of an LED light gave feedback for real-time monitoring of the actuators. Zhao et al. constructed 4D-printed MXene hydrogel structures with remarkably effective pseudocapacitive energy storage, excellent mass loading, impressive resistance to low temperature (−20 °C), and outstanding areal energy/power densities (92.88 μWh cm^{-2}).[168] Figure 20d demonstrates the cyclic performance at −20 °C and the voltammetry curves of the different micro-supercapacitors with the implementation of four capacitors in a series tandem device, which powered three LED bulbs.

The hybrid multi-material method enabled not only irregular out-of-plane electronic patterns with high efficacy but also strain sensors with good sensitivity and repeatability to be fabricated.[243] A 4D-printed multi-material device generated a maximum output voltage of 18 μV when subjected to external pressure, thereby demonstrating its great potential as a self-powered pressure sensor with quick responses and good sensitivity (Figure 20e).[245] A free-standing helical structure printed using tough conductive hydrogels encapsulated by an SMP could respond to the heat stimulus and hence drive the whole structure to close a circuit and power an LED light.[314] The high sensitivity of conductive hydrogel sensors during tension and compression enabled them to monitor diverse human motions.[315] A 4D-printed self-recovered triboelectric nanogenerator (TENG) was capable of harvesting mechanical energy with a maximum output power density of 56 mW m^{-2}.[316] This device could detect the bending angles of human joints as self-powered sensors, as shown in Figure 20f.

4D-printed metallic and ceramic structures also demonstrated electronic applications. The mechanical deformation of a bimetallic strip under the heat stimulus showed great potential as a high-temperature sensor.[180] When the temperature was increased to 300 °C, the strip exhibited a bending behavior, thus closing a circuit to light an LED bulb to indicate a temperature change. The semiconducting property of a 4D-printed polymer-derived ceramic allowed it to function as a temperature sensor based on the one-to-one correspondence between electrical resistance and temperature.[129] This sensor not only showed a wide test range from 25 to 750 °C but also detected irregular surfaces with uneven curvatures because of the reconfigurability of its preceramic polymers. Inspired by spider silk, Xing et al. 4D-printed a highly stretchable metallic gel touch sensor located on a ''spider web'' composed of LM microfibers.[179] When pressure was applied to the fiber, the regional strain caused an increase in resistance and a decrease in voltage so that the connected LED bulb turned off, which could be utilized for monitoring the strain variation in multiple directions (Figure 20g).

5.3. Robotics and Actuators

Robotics and actuators have emerged as another key application of 4D printing, such as capturing devices and smart switches. The shape-changing capability of 4D-printed devices enables them to perform autonomous actuation, complex movements, and multifunctional tasks. Moreover, with careful design of multi-materials distribution, they can simultaneously show integrated sensing–actuating functionality and facilitate human–robot interaction.

The shape recovery of an SMPC device was proven to be useful in capturing devices.[78] **Figure 21a** shows the selective releasing behavior of carrots from an SMP gripper attached to a transport belt under different UV light irradiation sites.[198] While conventional SMPs could not exhibit reversible shape changes, the integration of dynamic covalent bonds enabled shape memory PTU to reconfigure its permanent shape, allowing for reversible functions such as unloading and grabbing loads (Figure 21b).[82] A dexterous electric-driven soft robot consisting of an active dielectric elastomer artificial muscle and 4D-printed chiral-lattice foot was developed, which exhibited immediate changes in forward, backward, and turning motions under a single voltage input.[317] Using the shape reconfiguration of the 4D-printed chiral-lattice design under the heat stimulus, the soft robot demonstrated complex functions such as forming S-shaped trajectories or passing through narrow tunnels. The integration of the SME into the chiral structural design provided promising potential for the next-generation soft robots with dexterous locomotion.

The reversible deformation modes of 4D-printed LCEs demonstrated great potential as actuators to lift loads and perform mechanical work.[166] An amphibious LCE film presented different deformation modes triggered by heat and light in both air and underwater for the fabrication of light-fueled actuators.[205] Due to the high orientational order of mesogens, an LCE bending

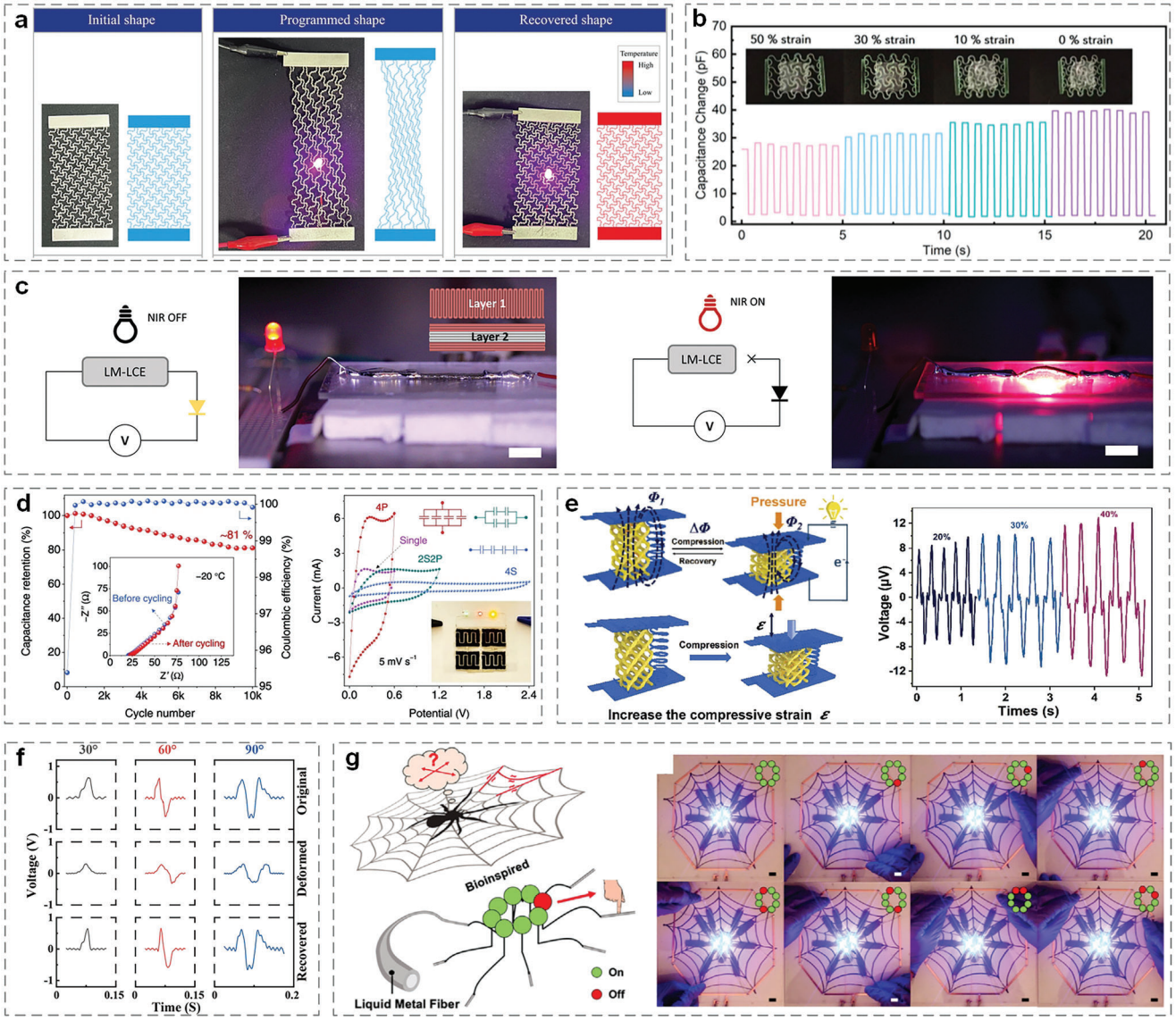

Figure 20. Electronics applications of 4D-printed structures. a) Shape reconfigurability and high stretchability of an optimized lattice structure connected to an LED light. Reproduced with permission.[50] Copyright 2022, Wiley-VCH Verlag GmbH b) Tunable electrical properties of flexible sensors integrated with auxetic metamaterials. Reproduced with permission.[194] Copyright 2023, Elsevier. c) Use of an LCE actuator as an electrical switch to control a circuit. Scale bars, 5 mm. Reproduced with permission.[152] Copyright 2021, American Chemical Society. d) Cyclic performance at −20 °C and voltammetry curve of various hydrogel micro-supercapacitors with the capability to power LED bulbs. Reproduced with permission.[168] Copyright 2022, Springer Nature. e) Electrical output of an integrated device as a pressure sensor. Reproduced with permission.[245] Copyright 2020, Wiley-VCH Verlag GmbH. f) Use of a 4D-printed TENG as a self-powered sensor to detect the bending angles of finger joints. Reproduced with permission.[316] Copyright 2021, Elsevier. g) Strain monitoring capability of a 4D-printed highly stretchable sensor with different touching directions. Scale bars, 10 mm. Reproduced with permission.[179] Copyright 2023, Elsevier.

actuator generated a specific work capacity at 63 J kg^{-1}.[89] A 4D-printed humidity-responsive actuator could serve as a smart gripper for cargo pick-up and release, a high-speed crawler, and an indicator for acetone leaks.[88]

With precisely controlled mechanical anisotropy, a tubular LCE structure performed diverse tasks, such as grabbing objects and mixing inks, as depicted in Figure 21c.[150] This approach offered a new perspective for the design and fabrication of soft pneumatic actuators without incorporating any other materials or heterogeneous structures. Besides in situ shape changes, tactile perception behavior has been demonstrated by LCE structures. For example, an untethered soft LCE robot demonstrated rolling on a slope, climbing over or reversing the direction toward obstacles, and transporting cargo (Figure 21d).[146] This autonomous actuation paved the way for a combination of machine perception and artificial intelligence. Under local NIR irradiation, a soft LCE robot climbed on an inclined ratchet surface with a fast locomotion speed.[155]

LCEs have also been integrated with other materials for advanced robotics.[243] The large and reversible actuation of LCEs

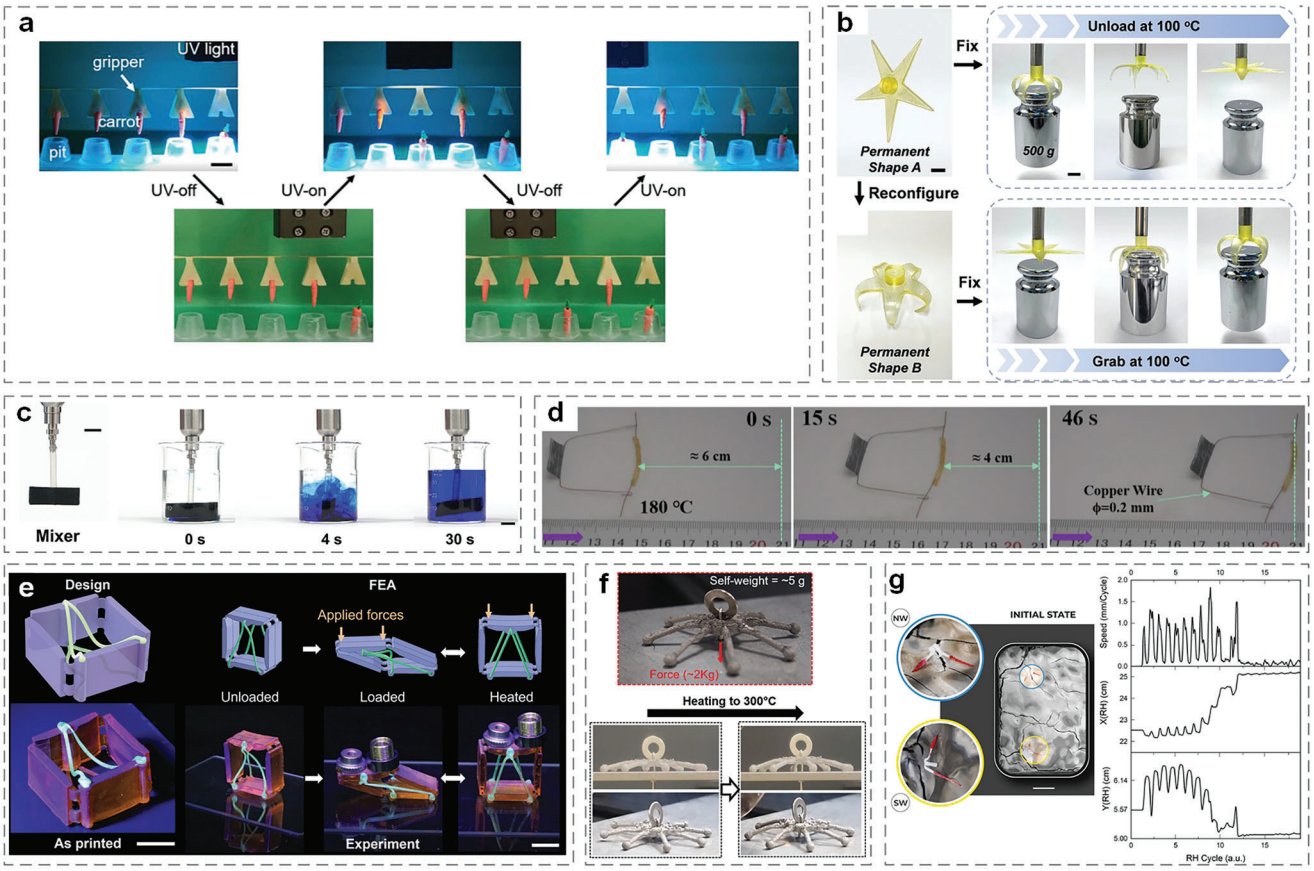

Figure 21. Robotics applications of 4D-printed structures. a) Selective delivery of carrots from an SMP gripper when moving the exposure positions of UV light. Scale bar, 1 cm. Reproduced with permission.[198] Copyright 2022, Wiley-VCH Verlag GmbH. b) Reconfigurability of an SMP structure to unload or grab loads. Scale bars, 1 cm. Reproduced with permission.[82] Copyright 2022, Wiley-VCH Verlag GmbH. c) Use of an assembled LCE-based soft pneumatic actuator to mix inks at an inflation pressure of 80 kPa and a frequency of 0.5 Hz. Scale bars, 1 cm. Reproduced with permission.[150] Copyright 2023, Royal Society of Chemistry. d) Cargo transportation capability of an untethered LCE robot based on the self-propelling actuation. Reproduced with permission.[146] Copyright 2021, Elsevier. e) Actuation of an active multi-material tensegrity structure fabricated by hybrid printing to lift a load. Scale bars, 1 cm. Reproduced with permission.[51] Copyright 2022, Wiley-VCH Verlag GmbH. f) Shape recovery of a spider-like SMA structure lifting a heavy load at 300 °C. Reproduced with permission.[222] Copyright 2022, Wiley-VCH Verlag GmbH. g) Use of a seed-like robot to explore soil. Scale bar, 5 cm. Reproduced with permission.[202] Copyright 2023, Wiley-VCH Verlag GmbH.

enabled a multi-material structure to serve as a smart gripper to pick and place.[142] Based on the hybrid printing method, an active actuator consisting of a flexible square part and redundant LCE fibers possessed tunable structural stability.[51] When placing a load, the hybrid structure fell because of its low stiffness, as shown in Figure 21e. Upon heating, the LCE fibers were actuated to shrink, which produced a tensile force that lifted the structure and the load, in close agreement with the FEA simulation.

4D-printed hydrogels with expansion/contraction or bending/unbending deformations also contribute to the development of soft robotic devices. A four-arm flower-like bilayer hydrogel structure demonstrated reversible opening/closing behavior upon heating/cooling, which could tightly capture and move a load.[171]

The high stiffness and SME of SMAs enabled them to be applied as actuators. A spider-like SMA structure with a load ≈400 times its own weight tied to each leg recovered to the original shape upon heating at 300 °C, inducing the bending behavior as shown in Figure 21f.[222] In the meantime, the high recovery stress during the shape recovery process could be used to lift heavy loads against its gravitational force, demonstrating the superior mechanical properties of this SMA structure compared to polymer-based robots. A twisting actuator consisting of a Nitinol-based SMA and static flexible rubber could actuate within 4 s under a current of 28 A, making it promising as a robotic arm.[318]

The ultimate goal in enhancing the experience of human–robot interaction is to create a soft-robot system that can not only adjust its own movements but also perceive real-time signal feedback, thereby maximizing the potential for effective interaction. A 4D-printed muscle-like actuator recorded its capacitance change during the expansion/contraction motions under NIR light for accurate actuation control.[178] The seed-like robots not only lifted loads upon changes in environmental humidity but also moved, explored, and adapted their configuration to the soil, thereby demonstrating potential as wireless tools for environmental topsoil monitoring (Figure 21g).[202]

In addition to macroscopic structures, 4D-printed microstructures have demonstrated significant potential for

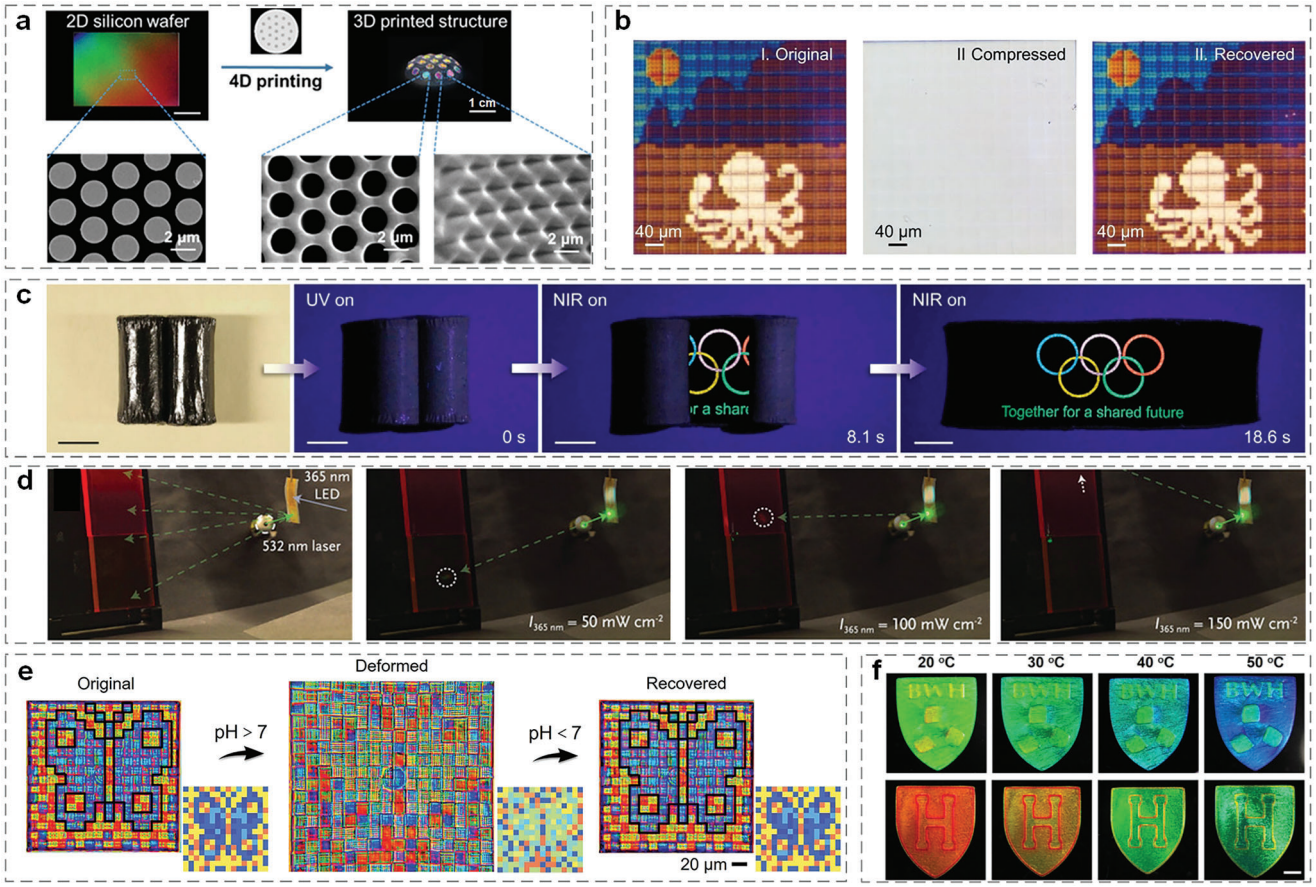

Figure 22. Photonics applications of 4D-printed structures. a) Nano-photonic device integrating a digital SMP and 2D silicon wafer. Reproduced with permission.[105] Copyright 2019, American Chemical Society. b) Information encryption and decryption using nanostructured SMP photonic devices. Reproduced with permission.[5] Copyright 2021, Springer Nature. c) NIR-triggered self-deployable process of a PQD–LCE painting with fluorescent colors under UV light. Scale bars, 5 mm. Reproduced with permission.[159] Copyright 2023, Elsevier. d) Selective reflective-light control of an LCE actuator. Reproduced with permission.[163] Copyright 2022, Wiley-VCH Verlag GmbH. e) Transformation of a butterfly painting based on pH-responsive microscopic hydrogel structures. Reproduced with permission.[278] Copyright 2022, Wiley-VCH Verlag GmbH. f) Highly tunable colloidal photonic crystals with diverse multicolor patterns as intelligent color displays. Scale bar, 2 mm. Reproduced with permission.[249] Copyright 2022, Elsevier.

self-assembly applications, including autonomous patterning, two-way origami, and switchable wetting behavior.[115]

5.4. Photonics

The dynamic capability of 4D-printed structures could be harnessed in photonics applications to fabricate adaptive optical devices or tunable photonic structures. The utilization of altering structural colors enhances their visualization and identification, thereby serving purposes such as information encryption/decryption and smart actuation. Moreover, integrated multimaterial 4D printing introduces improved functionalities to photonic devices, such as temperature sensing and indicating capabilities.

When a digital heterogenous SMP was projected onto a nanostructured 2D silicon wafer with a specific projection pattern, the shape-shifting behavior of the SMP transformed the planar wafer to exhibit a nano-photonic 3D geometry, as demonstrated in **Figure** 22a.[105] In addition to this passive color transformation, a multicolor painting fabricated from a nanostructured SMP autonomously became invisible in the compressive state and recovered upon heating, attributed to the interaction of the nanostructures with light (Figure 22b).[5] These examples indicated great promises as tunable photonic devices for temperature labeling and information encryption.

The integration of LCEs with other materials has made them promising photonic devices. Inspired by Chinese scroll painting, a 4D-printed PQD–LCE film was fabricated, which spontaneously curled into a roll at room temperature and demonstrated Olympic rings with fluorescent green texts under UV light (Figure 22c).[159] This reversible and on-demand control of visualization demonstrated its great potential for next-generation advanced photonics and optoelectronics. The multiple bending deformations of LCE–PEI photonic devices enabled a fluorescent detector plate behind them to respond to external light sources that tuned their transmissive or reflective properties, as demonstrated in Figure 22d.[163]

Color change can also occur in environments other than air conditions. A submerged 4D-printed microscopic hydrogel

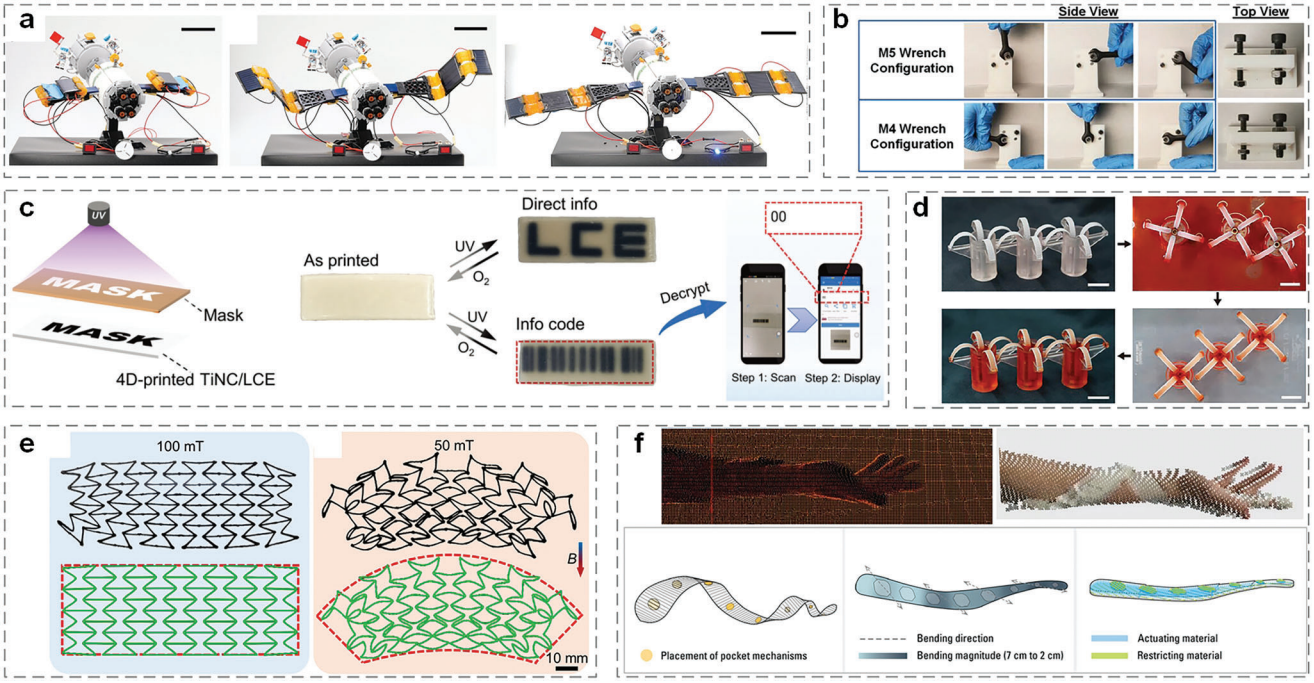

Figure 23. Other applications of 4D-printed structures. a) Self-deploying process of solar panels triggered by the shape recovery of smart hinges with aerospace applications. Scale bars, 5 cm. Reproduced with permission.[52] Copyright 2021, Wiley-VCH Verlag GmbH. b) Use of a reconfigurable wrench to tighten bolts of different sizes. Reproduced with permission.[244] Copyright 2022, Wiley-VCH Verlag GmbH. c) 4D-printed rewritable LCE paper with UV-assisted reprogrammable color patterning for information encryption and decryption. Reproduced with permission.[53] Copyright 2023, Wiley-VCH Verlag GmbH. d) Scalable oil–water separation of a microfluidic device. Scale bars, 2 cm. Reproduced with permission.[93] Copyright 2023, Wiley-VCH Verlag GmbH. e) Tunable magneto-mechanical metamaterials with targeted strain and tunable Poisson's ratio under a magnetic field. Reproduced with permission.[137] Copyright 2021, American Chemical Society. f) Construction process of an adaptive tightening orthotic splint as a wearable device. Reproduced with permission.[273] Copyright 2021, Wiley-VCH Verlag GmbH.

structure consisting of submicron woodpile structures demonstrated nearly the entire red–green–blue color range in the chromaticity diagram.[278] Figure 22e shows the pH-triggered size change together with the structural color transformation of a butterfly pattern due to the interaction of pendant carboxylic groups with acid or basic solutions.

The incorporation of thermochromic powder into non-stimuli-responsive materials endowed a 4D-printed fresnel lens with selective color focusing and temperature sensing capabilities.[319] Liao et al. fabricated colloidal photonic crystals featuring a wide range of desirable functions and mimicked the color manipulation of hierarchical structures, with great potential as intelligent color displays.[249] By varying the curing time, projected pattern, or ink color, diverse multicolor patterns could be highly tuned, as demonstrated in Figure 22f.

5.5. Other Applications

The on-demand shape change and dynamic properties of 4D-printed structures also demonstrate great potential in aerospace, information encryption, microfluidic devices, morphing structures, decoration, orthopedics, etc.

In space-limited aerospace applications, the self-assembly of 4D-printed structures is of great interest, especially from the perspective of time and cost efficiency. The challenge of high expenses of replacing parts in aerospace can be alleviated by 4D printing because of its flexible design, lower assembly costs, and reduced fabrication time. Zhang et al. assembled an SMP structure as smart hinges to mimic the self-deploying process of solar panels.[52] The hinge was designed with microchannels, where the wire was filled so that the produced Joule heating effect triggered the shape recovery when the device was powered on, as shown in **Figure 23a**. Similarly, Chen et al. designed shape memory ceramic precursors integrated with screen printing for a self-deploying process in a programmed sequence.[129] They envisioned that the in situ conversion from SMP precursors to ceramics in orbit showed great promise for future applications due to the high-temperature tolerance of ceramic materials.

Because of the limited resources at the International Space Station, it is essential to manufacture multipurpose tools with diverse functions. A 4D-printed reconfigurable wrench was employed to achieve multiple configurations, allowing for the application of torque to bolts of various sizes.[244] Figure 23b shows that by simply tuning the cooling rate, the wrench was capable of tightening bolts of two different sizes, and it possessed high stiffness at low temperatures. This multifunctional component fabricated using a single structure was capable of performing multiple tasks, demonstrating a facile method for on-demand use with a simple and readily available stimulus.

Information encryption and decryption can be achieved by not only color changes as mentioned above but also shape changes

in 4D-printed structures. The torsion of pixel mechanical SMP metamaterials under deformation upon heating enabled the decryption of the letter "H", which could be transformed to the encrypted state when heated again.[100] Chen et al. used a photomask to locally tune the color patterns by irradiating 4D-printed TiNCs-containing LCE with patterned UV light, which could be erased in the air, thereby enabling direct information display and information encryption.[53] Figure 23c shows the photorewritable process from a letter pattern to a high-resolution barcode with good stability after 12 h of storage under ambient conditions.

The re-entrant structures with self-propelled capability of ultra-wide-angle liquid transportation showed great promise in microfluidic devices for liquid mixing, liquid evaporation on large surfaces, and treatment of oily water.[93] Figure 23d demonstrates the oil–water separation at a large scale, which led to the collection of 20 mL oil within 20 minutes. A 4D-printed sample pretreatment device, consisting of a solid-phase extraction column and a thermally responsive flow-actuated valve, was capable of extracting ions from high-salt content samples, displaying comparative analytical performance.[320]

Morphing devices based on tunable metamaterial configurations are another application of 4D-printed structures. Figure 23e demonstrates the wide tunability of magneto-mechanical multimaterial metamaterials based on both FEA and experiments using an hourglass design.[137] It was further shown that the on-demand design framework enhanced the multifunctionality of metamaterials, thereby enabling greater control of the deformation, stiffness, acoustic band gap, and electromagnetic properties.[176] 4D-printed LCE lattice foam demonstrated a notable increase in energy dissipation efficiency at room temperature, reaching up to 3.9 times greater than its counterparts based on non-LCE materials under cyclic mechanical loading.[86]

The adaptive tightening characteristics of a bioinspired tensioning helix structure made it promising as a wrist–forearm orthotic splint device.[273] Figure 23f demonstrates that by 3D scanning the entire arm and reconstructing the deductive flat printable geometry with the desired radius based on the assembly of motion mechanisms, a wearable device could fold upon the humidity stimulus and adapt to human arms.

Decoration is another important application. When a piece of smart furniture consisting of a table and eight hinges was heated, the hinges recovered to their original shape, and its high stiffness allowed it to bear heavy loads.[52] When the furniture was not in use, the hinges could be programmed to exhibit a packed 2D shape to save space for storage and transportation purposes. The hybrid printing method has combined the individual properties of the constituent materials and demonstrated multicolor prototypes.[243] The color and texture change of a curcumin-integrated lotus root during microwave heating could provide consumers with a different sensory experience, thus contributing to a novel method for food printing.[279]

The magnetic sensing performance of a printed fiber tip polymer microcantilever made it promising as a magnetic sensor at various magnetic-field intensities with high repeatability and a sensitivity of up to 119 pm mT^{-1} in the range of 0–90 mT.[321] Based on this Lab-on-Fiber process, this functionality-integrated optical fiber showed superiority in detecting weak or microspace magnetic fields at high spatial resolutions.

6. Conclusion and Perspective

As evident from the concepts and embodiments outlined in this review, a wide range of 4D-printing techniques for the fabrication of polymers, metals, ceramics, and multi-materials have been explored. We reviewed the progress by first introducing various printing techniques and working principles, together with their applicable materials, which are the basis for achieving desirable excellent structural properties. Then, we systematically summarized the diverse stimuli, including heat, light, electric fields, magnetic fields, solvent, humidity, and multi-stimuli, which laid a good foundation for environmental adaptability. Owing to the multifunctionality of 4D-printed structures, we finally summarized their great application potential in biomedical engineering, electronics, robotics, photonics, aerospace, etc. Complex and dynamic structures that are difficult to fabricate with traditional processing technologies can be easily designed and realized by 4D printing. Despite the considerable progress achieved by 4D printing, there are still many challenges that need to be overcome in the future to develop high-value application products.

6.1. Materials Development

To fulfill the requirements of multifunctionality, developing materials and ink formulation with excellent properties is essential for further applications of 4D printing. To date, the fast advancement in stimuli-responsive materials, including SMPs, LCEs, hydrogels, and SMAs has witnessed not only dramatic shape changes with the time dimension but also multifunctionality, such as reconfigurability, self-healing, degradability, and color shifting capabilities. Some new functionalities may also be considered in the future, such as long-term storage stabilities and anisotropic properties.[322] Additionally, the compatibility of novel materials with printing methods needs to be better understood.

Most 4D-printed SMPs possess one-way shape transformation, and the repetitive actuation requires another external programming step. Nevertheless, with the flexible chemical or physical design of SMP networks, two-way, thermal adaptive, and semi-interpenetrating networks have been explored, which are adaptable to various printing methods to enable more complicated shape deformations. The fabrication of SMP structures at the microscale or nanoscale has achieved typical structural color transformations during the shape recovery process. It is envisioned that the integration of two-way or thermal adaptive structures with microscale printing will definitely pave the way for fabricating tiny functional 4D-printed SMP devices.

For LCEs, both physically and chemically crosslinked networks have been developed. Owing to the dynamic characteristics of hydrogen bonds or dynamic covalent bonds, the reconfigurability and recyclability of 4D-printed LCEs have been achieved. The specific orientational change of LC domains affects the polarization and contributes to the different structural colors. However, developing LCE materials with improved properties, such as higher actuation strains, faster responses, and especially enhanced mechanical strength, remains a challenge. Additionally, the mesogen alignment in 4D-printed LCE actuators at high thickness is hard to achieve, thus restricting their structural complexity and actuation work.

The design of double network, supramolecular network, and nanoparticle-reinforced 4D-printed hydrogels has also demonstrated superior mechanical properties and multi-functionalities. The structural color change in hydrogels relies on the incorporation of microscale or nanoscale structures upon the swelling or shrinking behavior. However, 4D-printed hydrogel structures exhibit slow printing speeds and limited resolution. Thus, scaling up the production of 4D-printed hydrogels remains a big challenge.

In addition to the utilization of the intrinsic responsiveness of smart materials under an external stimulus, there are other common strategies, including having anisotropic crosslinking densities during the printing process, non-uniform deformation between multi-materials, liquid–vapor phase transition, magnetization profile, interaction of functional groups with specific chemicals, and anisotropic fiber alignment. Developing a wider range of strategies for 4D printing is essential to expanding its applications and achieving more complex functionalities. For example, the integration of functional particles with LM enhances its functionality, such as the ability to undergo magnetic manipulation when LM is combined with magnetic particles. These strategies further show great potential for 4D-printed multifunctional LM materials.[323,324] In contrast to hard materials, the unique fluidic nature of LM prevents dramatic changes in the mechanical properties and allows for the deformation of LM within the polymer matrix to further improve the shape recovery behavior.

The development of metal-based 4D printing still faces many challenges, such as limited printing parameter space due to element volatilization and the existence of only a single actuation method. It is also necessary to explore the mechanism behind AM of metals to provide further technical support for the research and application of 4D-printed metal structures.

Since materials and ink formulations are highly relevant to the actuation methods, mechanical properties, response speed, sensitivity, stability, and repeatability of 4D-printed structures, developing novel materials with excellent properties is essential. Although diverse stimuli have been explored, little attention has been paid to the mechanical properties that are comparable to those of traditionally built parts and accurate control of shape and functionality changes upon these stimuli. Developing materials that could reliably and predictably respond to external stimuli with precise well-defined control is still challenging. Most 4D-printed materials and structures are only responsive to one stimulus, which limits their use in complex environments and inhibits multi-stimuli responsive behavior. The development of composites and multi-materials will definitely extend the actuation to a variety of stimuli. The reprogrammability of 4D-printed materials is highly desired to achieve multiple cycles of transformation rather than a one-time, irreversible process.

Although the current 4D-printing technology primarily focuses on a single printing method with a single material, the use of multi-materials that incorporate multiple materials together enables the fabrication of more complicated and multifunctional structures. Multi-material 4D printing is still in its infancy, and its development poses many challenges, such as selection of compatible materials, good adhesion between different materials, integration of different printing methods, and precise control of the workflow. Ensuring proper adhesion, bonding, or interlocking between these materials can be challenging, as they may have different thermal, chemical, or mechanical characteristics. Developing suitable material combinations and effective bonding tools is essential for successful multi-material 4D printing.

6.2. Printing Techniques

Among the major categories of AM, six printing techniques, namely VPP, MEX, PBF, MJT, BJT, and DED, have been employed in 4D printing. As shown in Table 1, different printing techniques are applicable to specific material types with respective advantages and disadvantages. It could be seen that a single printing method is relatively easy to manipulate as long as the printing material is adjusted to meet the compatibility requirements of a specific printing technique. Several methods have been adopted to modify 3D printers to extend the functionalities of the printed structures, such as replacing the deposition platform,[150,193] adding feed channels,[151,188] and setting an electric field during printing.[88,325] There were only a limited number of printing methods applicable to 4D printing (mainly FFF, SLA, PolyJet™, DIW, SLS, and DLP) before 2019, but the recent three years have witnessed an explosive growth in various printing methods or techniques (TPL, SLM, DED, TPP, and BJT).

The VPP technique is primarily limited to printing photosensitive materials, with the majority being SMPs and a small portion being LCEs and hydrogels. The intrinsic difference in the heterogenous crosslinking density along the z axis enables the as-printed polymers to change configurations. Among MEX techniques, FFF requires thermoplastic or thermoset filaments with post-curing, while DIW is easier to print various types of materials including multi-materials. The PBF technique suitable for 4D printing has been reported to be compatible with both plastic and metal powder, while it is limited by its inherent single-material fabrication capability. To achieve multi-material fabrication in PBF, it necessitates the integration with other printing methods. Although the PolyJet™ method under MJT is a commercial multi-material printing method, both its hardware and software are proprietary, making it challenging to modify or expand. BJT is often employed to fabricate metals, especially SMAs, but achieving multi-material fabrication and high resolution are still big challenges. In contrast, the deposition efficiency and power energy of DED are better so that a more decent microstructure uniformity can be obtained. Nevertheless, the size of parts built by DED is too hard to realize obvious change with time. It thus poses challenges for the 4D printing of SMAs.

To the best of our knowledge, there is still no work on 4D printing using the SHL technique or on certain printing methods, such as continuous liquid interface production (CLIP), multi-jet fusion, and electron beam melting. CLIP is an innovation of DLP that introduces continuous and rapid printing capabilities, thereby reducing layering artifacts and enabling the creation of complex, high-resolution objects in significantly reduced time.[326] Despite the rapid advancements in CLIP, it has not been utilized in 4D printing. Additionally, many 4D-printing methods have a relatively low printing resolution and low geometric precision, which limits the accuracy and complexity of the printed structures and affects their applications. At the same time, the slow printing speed and limited printing size also restrict commercial applications. It is believed that the integration of new

printing methods with high accuracy and resolution will create new possibilities for the fast development of 4D printing.

Even if a single-material formulation is printed using a single printing method, diversified combinations of printing parameters are beneficial to realizing heterogeneous printed structures, especially gradient 4D-printed structures with multiple local shape-changing behaviors. For example, by using a single recipe of LCE, various shape transformations with fast responses to an external stimulus were realized by simply changing the printing parameters during DIW printing.[154,156,157] This method highly simplifies the fabrication process of complicated 4D-printed structures with site-specific responses in comparison to integrating different synthesized materials within one structure. In the future, to develop this concept for more diverse applications, gradient-boosting parameters must be translated into codes compatible with 3D printers. It can be envisioned that updated software tools with parameter information codes will definitely offer expanded design space for 4D printing that is free of geometric and materials constraints.

Hybrid printing is considered a future trend toward 4D printing as it leverages the strengths of different printing methods to overcome the limitations of each method and create more complex and functional structures. It dramatically simplifies the fabrication of functional multi-material structures with intricate geometries that are challenging to achieve with only one printing method. Hybrid printing is therefore expected to play a significant role in unlocking new possibilities in the field of 4D printing. However, hybrid printing faces some challenges. First, it may cause possible contamination between different materials systems. Thus, an extra auxiliary setup is usually needed to clean the built part. The second challenge is the seamless integration between different printing methods, which involves the development of hardware and software systems to coordinate and synchronize with each other for smooth transitions.

Process scalability and complexity also need to be considered. As the complexity of the printing process increases, it becomes more challenging to scale up the production and maintain consistency. Optimizing the process parameters, enhancing the automation and control systems, and streamlining the post-processing and assembly steps are areas that require attention to enable the efficient and scalable production of hybrid structures.

6.3. Design

Designing structures that can undergo controlled and predictable shape transformations requires a deep understanding of the materials, their behavior, and the activation mechanisms. It involves factors such as material elasticity, stress distribution, and the desired shape-changing effect to achieve functional and reliable transformations.

Customizable printed geometries enable the construction of desired mechanical properties of 4D-printed structures, which may in turn exhibit excellent stretchability although the constituent materials might be stiff. Diversified metamaterials, such as auxetic, chiral, and fractal designs have witnessed broad tunability and reconfigurability in a dramatically large range.[50,99–100,176,194,264,327] Origami and kirigami structures have attracted great attention over the past years as they possess the high tunability of versatile mechanical properties like metamaterials, which will be continuously employed in 4D printing to build functionally active structures.[328,329]

Multiscale design may also be a future direction in 4D printing, which integrates structures at micro and macro scales together with enhanced functionalities and robustness. Designing for these multiscale features and ensuring their compatibility and interaction pose challenges. Improving the overall performance of the structure while considering the behaviors at different scales and their interactions requires attention.

6.4. Theory and Simulation

Fully understanding the comprehensive relationships between materials, structures, and properties remains a big challenge with the current theory of 4D printing. Theories regarding the mechanisms and physics involved in the responses of materials to specific stimuli, such as the underlying kinetics and the associated energy transfer processes, need to be explored extensively in the future. Theories about the printing process have seldom been investigated. Fluid dynamics theories that are widely employed when studying fluids can be applied to analyze the polymerization of extruded inks.

In addition to the theory, simulation tools play a crucial role in understanding the responses to stimuli, allowing the visualization and performance evaluation of 4D-printed structures before conducting experiments, thereby enabling performance optimization and design validation. It is important especially for multi-material and hybrid printing as it helps to avoid collisions between different printed components during the assembly process.

The reported simulation methods usually simplify the boundary conditions and materials model. For example, the thermal expansion method is often employed, where the heat stimulus is used as a substitute for other stimuli. Developing accurate and efficient simulation tools that can capture the intricate behavior of 4D-printed structures is still a challenge. For shape change prediction, a lot of factors need to be considered, such as elasticity, viscoelasticity, and anisotropy. Accounting for the responses of materials to different stimuli and their interaction with the printing process adds more complexity to the simulation. Additionally, the prediction of functionalities is much harder than predicting shape changes.

In the meantime, simulation can be computationally intensive, especially for complex structures or large-scale models. Managing the computational complexity while maintaining acceptable simulation efficiency is a challenge. Developing efficient algorithms, parallel computing tools, and optimization strategies is essential for making simulations practical and accessible.

In the future, ML for 4D printing design may focus on developing advanced algorithms, including deep learning, reinforcement learning, and generative models, to further enhance prediction accuracy.[330] For more complex target shape change, there is an increasing need to upgrade ML models to deal with more complex spatial dependencies. Once an efficient forward ML model is established, various optimization strategies can be explored to further refine the design process. Given the typically vast design space, employing data dimensionality reduction methods such

as principal component analysis, discrete cosine transform, and autoencoder for pre-compression can enhance the learning efficiency and overall performance.[331] Moreover, while ML is primarily used to guide the inverse shape design, future interest may also focus on achieving extraordinary properties and functionalities.

6.5. Measurement

Measurement in 4D printing involves quantifying and characterizing various aspects of 4D-printed structures, including dimensional accuracy, mechanical properties, and shape and functionality changes in response to stimuli. Many measurement methods have been employed, such as 3D scanning to obtain accurate topography, digital image correlation and tracking, infrared camera recording to obtain the temperature distribution, and electrical resistance recording during shape change.

However, unlike the standards suitable for traditional static parts, normalizing a set of standards for 4D printing is hard because of the dynamic shape or functionality changes. Thus, it poses a challenge for the specialized measurement to accurately characterize and compare these properties with each other. Nondestructive in situ and real-time monitoring is considered a future trend of 4D printing to not compromise properties while obtaining reliable experimental data. For example, digital holographic microscopy is a promising solution for characterization of the printing process, especially for capturing changes within a short time interval.[332] In the future, multiscale structures are highly desired, which poses challenges for measuring and quantifying shape changes at different scales within a single structure.

6.6. Applications

As summarized, multifunctional 4D-printed structures have demonstrated great potential in biomedical engineering, electronics, robotics, photonics, aerospace, etc. However, many of these potential applications are still in the early stages of demonstration and validation, and there is still a long journey before achieving true commercialization. The specific applications where 4D printing exhibits superior advantages over traditional fabrication and 3D printing need to be carefully evaluated. It is a sophisticated task to assess the technical feasibility, economic viability, and market value of 4D-printed products in various applications. Scaling up from laboratory research to mass production poses a big challenge as well.

Other challenges in 4D printing include improving the lifetime and cycle capability of products, economic effectiveness, production efficiency, and regulation. Overcoming these challenges requires collaborative efforts among researchers, industry stakeholders, and policymakers. Addressing the technical, economic, and regulatory aspects of 4D printing will contribute to the successful integration and commercialization of this technology in various industries.

In summary, the 4D printing technology has witnessed rapid development and attracted significant attention in the past decade. An increasing number of printing methods, materials, and stimuli are being explored and expanded for 4D printing. This technology presents remarkable advantages in controlling both geometric and functional reconfigurations, thereby demonstrating vast potential across a range of fields. Based on the advancements and significant innovations brought by 4D printing recently, it is believed this technology with more comprehensive studies will bring more opportunities in novel structural and functional devices for commercialization in industries.

Acknowledgements

This study was supported by the National Research Foundation, Prime Minister's Office, Singapore under its Medium-Sized Center funding scheme through the Marine and Offshore Program.

Conflict of Interest

The authors declare no conflict of interest.

Keywords

4D printing, functionality, multi-material, stimuli-responsive materials

Received: November 16, 2023
Revised: March 1, 2024
Published online:

[1] L. J. Tan, W. Zhu, K. Zhou, *Adv. Funct. Mater.* **2020**, *30*, 2003062.
[2] S. Tibbits, The emergence of "4D printing", http://www.ted.com/talks/skylar_tibbits_the_emergence_of_4d_printing (accessed: February 2013).
[3] S. Tibbits, *Architect. Design* **2014**, *84*, 116.
[4] Q. Ge, H. J. Qi, M. L. Dunn, *Appl. Phys. Lett.* **2013**, *103*, 131901.
[5] W. Zhang, H. Wang, H. Wang, J. Y. E. Chan, H. Liu, B. Zhang, Y. F. Zhang, K. Agarwal, X. Yang, A. S. Ranganath, H. Y. Low, Q. Ge, J. K. W. Yang, *Nat. Commun.* **2021**, *12*, 112.
[6] X. Lu, C. P. Ambulo, S. Wang, L. K. Rivera-Tarazona, H. Kim, K. Searles, T. H. Ware, *Angew. Chem., Int. Ed.* **2021**, *60*, 5536.
[7] H. Wei, X. Cauchy, I. O. Navas, Y. Abderrafai, K. Chizari, U. Sundararaj, Y. Liu, J. Leng, D. Therriault, *ACS Appl. Mat. Interfaces* **2019**, *11*, 24523.
[8] Y. Kim, H. Yuk, R. K. Zhao, S. A. Chester, X. H. Zhao, *Nature* **2018**, *558*, 274.
[9] A. S. Gladman, E. A. Matsumoto, R. G. Nuzzo, L. Mahadevan, J. A. Lewis, *Nat. Mater.* **2016**, *15*, 413.
[10] Y. W. Lee, H. Ceylan, I. C. Yasa, U. Kilic, M. Sitti, *ACS Appl. Mat. Interfaces* **2021**, *13*, 12759.
[11] M. Fang, T. Liu, Y. Xu, B. Jin, N. Zheng, Y. Zhang, Q. Zhao, Z. Jia, T. Xie, *Adv. Mater.* **2021**, *33*, 2105597.
[12] Z. Ding, O. Weeger, H. J. Qi, M. L. Dunn, *Mater. Des.* **2018**, *137*, 256.
[13] McKinsey, The top trends in tech, https://www.mckinsey.com/capabilities/mckinsey-digital/our-insights/the-top-trends-in-tech-2021#/ (accessed: March 2024).
[14] Y. Xia, Y. He, F. Zhang, Y. Liu, J. Leng, *Adv. Mater.* **2021**, *33*, 2000713.
[15] J. Delaey, P. Dubruel, S. Van Vlierberghe, *Adv. Funct. Mater.* **2020**, *30*, 1909047.
[16] A. Lendlein, O. E. C. Gould, *Nat. Rev. Mater.* **2019**, *4*, 116.
[17] Q. Zhao, H. J. Qi, T. Xie, *Prog. Polym. Sci.* **2015**, *49*, 79.
[18] K. M. Herbert, H. E. Fowler, J. M. McCracken, K. R. Schlafmann, J. A. Koch, T. J. White, *Nat. Rev. Mater.* **2022**, *7*, 23.

[19] Y. Wang, J. Liu, S. Yang, *Appl. Phys. Rev.* **2022**, *9*, 011301.
[20] M. O. Saed, A. Gablier, E. M. Terentjev, *Chem. Rev.* **2022**, *122*, 4927.
[21] M. Camacho-Lopez, H. Finkelmann, P. Palffy-Muhoray, M. Shelley, *Nat. Mater.* **2004**, *3*, 307.
[22] S. W. Ula, N. A. Traugutt, R. H. Volpe, R. R. Patel, K. Yu, C. M. Yakacki, *Liq. Cryst. Rev.* **2018**, *6*, 78.
[23] D. L. Thomsen, P. Keller, J. Naciri, R. Pink, H. Jeon, D. Shenoy, B. R. Ratna, *Macromolecules* **2001**, *34*, 5868.
[24] M. Brehmer, R. Zentel, G. Wagenblast, K. Siemensmeyer, *Macromol. Chem. Phys.* **1994**, *195*, 1891.
[25] J. Li, C. Wu, P. K. Chu, M. Gelinsky, *Mater. Sci. Engin.: R: Rep.* **2020**, *140*, 100543.
[26] C. Zhang, B. Wu, Y. Zhou, F. Zhou, W. Liu, Z. Wang, *Chem. Soc. Rev.* **2020**, *49*, 3605.
[27] L. Li, J. M. Scheiger, P. A. Levkin, *Adv. Mater.* **2019**, *31*, 1807333.
[28] J. Zhang, Z. Yin, L. Ren, Q. Liu, L. Ren, X. Yang, X. Zhou, *Adv. Mater. Technol.* **2022**, *7*, 2101568.
[29] M. Chen, M. Gao, L. Bai, H. Zheng, H. J. Qi, K. Zhou, *Adv. Mater.* **2023**, *35*, 2209566.
[30] M. del Pozo, J. A. H. P. Sol, A. P. H. J. Schenning, M. G. Debije, *Adv. Mater.* **2022**, *34*, 2104390.
[31] M. Champeau, D. A. Heinze, T. N. Viana, E. R. de Souza, A. C. Chinellato, S. Titotto, *Adv. Funct. Mater.* **2020**, *30*, 1910606.
[32] Y. Dong, S. Wang, Y. Ke, L. Ding, X. Zeng, S. Magdassi, Y. Long, *Adv. Mater. Technol.* **2020**, *5*, 2000034.
[33] M. Rafiee, R. D. Farahani, D. Therriault, *Adv. Sci.* **2020**, *7*, 1902307.
[34] C. de Kergariou, F. Demoly, A. Perriman, A. Le Duigou, F. Scarpa, *Adv. Funct. Mater.* **2023**, *33*, 2210353.
[35] A. Andreu, P. C. Su, J. H. Kim, C. S. Ng, S. Kim, I. Kim, J. Lee, J. Noh, A. S. Subramanian, Y. J. Yoon, *Addit. Manuf.* **2021**, *44*, 102024.
[36] X. Wan, L. Luo, Y. Liu, J. Leng, *Adv. Sci.* **2020**, *7*, 2001000.
[37] A. Sharma, A. Rai, *Mater Today Proc* **2022**, *62*, 367.
[38] C. A. Spiegel, M. Hippler, A. Münchinger, M. Bastmeyer, C. Barner-Kowollik, M. Wegener, E. Blasco, *Adv. Funct. Mater.* **2020**, *30*, 1907615.
[39] W. Zhao, C. Yue, L. Liu, Y. Liu, J. Leng, *Adv. Healthcare Mater.* **2023**, *12*, 2201975.
[40] S. Miao, N. Castro, M. Nowicki, L. Xia, H. Cui, X. Zhou, W. Zhu, S. Lee, K. Sarkar, G. Vozzi, Y. Tabata, J. Fisher, L. G. Zhang, *Mater. Today* **2017**, *20*, 577.
[41] C. M. Gonzalez-Henriquez, M. A. Sarabia-Vallejos, J. Rodriguez-Hernandez, *Prog. Polym. Sci.* **2019**, *94*, 57.
[42] X. Chen, S. Han, W. Wu, Z. Wu, Y. Yuan, J. Wu, C. Liu, *Small* **2022**, *18*, 2106824.
[43] M. Y. Khalid, Z. U. Arif, W. Ahmed, R. Umer, A. Zolfagharian, M. Bodaghi, *Sens. Actuators, A* **2022**, *343*, 113670.
[44] M. C. Biswas, S. Chakraborty, A. Bhattacharjee, Z. Mohammed, *Adv. Funct. Mater.* **2021**, *31*, 2100257.
[45] F. Momeni, S. M. Mehdi Hassani N, X. Liu, J. Ni, *Mater. Des.* **2017**, *122*, 42.
[46] X. Kuang, D. J. Roach, J. T. Wu, C. M. Hamel, Z. Ding, T. J. Wang, M. L. Dunn, H. J. Qi, *Adv. Funct. Mater.* **2019**, *29*, 1805290.
[47] J. Choi, O. C. Kwon, W. Jo, H. J. Lee, M. W. Moon, *3D Print. Addit. Manuf.* **2015**, *2*, 159.
[48] S. Joshi, K. Rawat, Karunakaran C, V. Rajamohan, A. T. Mathew, K. Koziol, V. Kumar Thakur, Balan A S S, *Appl. Mater. Today* **2020**, *18*, 100490.
[49] C. Yang, J. Luo, M. Polunas, N. Bosnjak, S. T. D. Chueng, M. Chadwick, H. E. Sabaawy, S. A. Chester, K. B. Lee, H. Lee, *Adv. Mater.* **2020**, *32*, 2004285.
[50] D. Wang, L. Dong, G. Gu, *Adv. Funct. Mater.* **2023**, *33*, 2208849.
[51] X. Peng, S. Wu, X. Sun, L. Yue, S. M. Montgomery, F. Demoly, K. Zhou, R. R. Zhao, H. J. Qi, *Adv. Mater.* **2022**, *34*, 2204890.
[52] B. Zhang, H. Li, J. Cheng, H. Ye, A. H. Sakhaei, C. Yuan, P. Rao, Y. F. Zhang, Z. Chen, R. Wang, X. He, J. Liu, R. Xiao, S. Qu, Q. Ge, *Adv. Mater.* **2021**, *33*, 2101298.
[53] M. Chen, Y. Hou, R. An, H. J. Qi, K. Zhou, *Adv. Mater.* **2023**, 2303969.
[54] S. Christina, M. K. Deepak, *Stereolithography, IntechOpen, Rijeka* **2018**, https://orcid.org/10.5772/intechopen.78147.
[55] Z. X. Low, Y. T. Chua, B. M. Ray, D. Mattia, I. S. Metcalfe, D. A. Patterson, *J. Membr. Sci.* **2017**, *523*, 596.
[56] I. Bernardeschi, M. Ilyas, L. Beccai, *Advanced Intelligent Systems* **2021**, *3*, 2100051.
[57] A. Camposeo, L. Persano, M. Farsari, D. Pisignano, *Adv. Opt. Mater.* **2019**, *7*, 1800419.
[58] A. Muzaffar, M. B. Ahamed, K. Deshmukh, T. Kovářík, T. Křenek, S. K. K. Pasha, in *3D and 4D Printing of Polymer Nanocomposite Materials*, **2020**.
[59] N. K. Roy, D. Behera, O. G. Dibua, C. S. Foong, M. A. Cullinan, *Microsyst. Nanoeng.* **2019**, *5*, 64.
[60] I. Gibson, D. Rosen, B. Stucker, *Directed Energy Deposition Processes. in Additive Manufacturing Technologies*, Springer, New York, NY **2015**.
[61] H. Gao, J. An, C. K. Chua, D. Bourell, C. N. Kuo, D. T. H. Tan, *Mater. Today* **2023**.
[62] M. Pagac, J. Hajnys, Q. P. Ma, L. Jancar, J. Jansa, P. Stefek, J. Mesicek, *Polymers* **2021**, *13*, 598.
[63] L. Y. Zhou, J. Fu, Y. He, *Adv. Funct. Mater.* **2020**, *30*, 2000187.
[64] F. Zhang, L. Zhu, Z. Li, S. Wang, J. Shi, W. Tang, N. Li, J. Yang, *Addit. Manuf.* **2021**, *48*, 102423.
[65] C. A. Spiegel, M. Hackner, V. P. Bothe, J. P. Spatz, E. Blasco, *Adv. Funct. Mater.* **2022**, *32*, 2110580.
[66] J. Meurer, R. H. Kampes, T. Bätz, J. Hniopek, O. Müschke, J. Kimmig, S. Zechel, M. Schmitt, J. Popp, M. D. Hager, U. S. Schubert, *Adv. Funct. Mater.* **2022**, *32*, 2207313.
[67] S. Liu, X. Dong, Y. Wang, J. Xiong, R. Guo, J. Xiao, C. Sun, F. Zhai, X. Wang, *Adv. Mater. Technol.* **2023**, *8*, 2202004.
[68] Z. Wang, M. Heck, W. Yang, M. Wilhelm, P. A. Levkin, *Adv. Funct. Mater.* **2023**, 2300947.
[69] X. Kuang, J. Wu, K. Chen, Z. Zhao, Z. Ding, F. Hu, D. Fang, H. J. Qi, *Sci. Adv.* **2019**, *5*, eaav5790.
[70] L. Yue, S. Macrae Montgomery, X. Sun, L. Yu, Y. Song, T. Nomura, M. Tanaka, H. Jerry Qi, *Nat. Commun.* **2023**, *14*, 1251.
[71] Q. Zhang, X. Kuang, S. Weng, L. Yue, D. J. Roach, D. Fang, H. J. Qi, *Adv. Funct. Mater.* **2021**, *31*, 2010872.
[72] L. Yue, X. Sun, L. Yu, M. Li, S. M. Montgomery, Y. Song, T. Nomura, M. Tanaka, H. J. Qi, *Nat. Commun.* **2023**, *14*, 5519.
[73] Y. Shi, G. Fang, Z. Cao, F. Shi, Q. Zhao, Z. Fang, T. Xie, *Chem. Eng. J.* **2021**, *426*, 131306.
[74] K. K. Westbrook, V. Parakh, T. Chung, P. T. Mather, L. C. Wan, M. L. Dunn, H. J. Qi, *J Eng Mater Technol* **2010**, *132*, 041010.
[75] Y. Jiang, Q. Y. Leng, Y. Yan, E. L. L. Ng, H. L. Chee, F. Wang, S. Y. Chan, X. J. Loh, J. Wang, B. Q. Y. Chan, *ACS Appl. Polym. Mater.* **2022**, *4*, 8574.
[76] R. Qu, D. Zhou, T. Guo, W. He, C. Cui, Y. Zhou, Y. Zhang, Z. Tang, X. Zhang, Q. Wang, T. Wang, Y. Zhang, *Mater. Des.* **2023**, *225*, 111556.
[77] A. C. Weems, M. C. Arno, W. Yu, R. T. R. Huckstepp, A. P. Dove, *Nat. Commun.* **2021**, *12*, 3771.
[78] L. Wang, F. Zhang, Y. Liu, S. Du, J. Leng, *ACS Appl. Mat. Interfaces* **2021**, *13*, 18110.
[79] Y. Y. C. Choong, S. Maleksaeedi, H. Eng, S. Yu, J. Wei, P. C. Su, *Appl. Mater. Today* **2020**, *18*, 100515.
[80] Q. Shi, K. Yu, X. Kuang, X. M. Mu, C. K. Dunn, M. L. Dunn, T. J. Wang, H. J. Qi, *Mater. Horiz.* **2017**, *4*, 598.
[81] Z. Chen, M. Yang, M. Ji, X. Kuang, H. J. Qi, T. Wang, *Mater. Des.* **2021**, *197*, 109189.
[82] C. Cui, L. An, Z. Zhang, M. Ji, K. Chen, Y. Yang, Q. Su, F. Wang, Y. Cheng, Y. Zhang, *Adv. Funct. Mater.* **2022**, *32*, 2203720.

[83] W. Peng, G. Zhang, Q. Zhao, T. Xie, *Adv. Mater.* **2021**, *33*, 2102473.
[84] X. Xu, Z. Fang, B. Jin, H. Mu, Y. Shi, Y. Xu, G. Chen, Q. Zhao, N. Zheng, T. Xie, *Adv. Mater.* **2023**, *35*, 2209824.
[85] N. A. Traugutt, D. Mistry, C. Luo, K. Yu, Q. Ge, C. M. Yakacki, *Adv. Mater.* **2020**, *32*, 2000797.
[86] C. Luo, C. Chung, N. A. Traugutt, C. M. Yakacki, K. N. Long, K. Yu, *ACS Appl. Mat. Interfaces* **2021**, *13*, 12698.
[87] M. Tabrizi, T. H. Ware, M. R. Shankar, *ACS Appl. Mat. Interfaces* **2019**, *11*, 28236.
[88] T. Tang, S. Alfarhan, K. Jin, X. Li, *Adv. Funct. Mater.* **2023**, *33*, 2211602.
[89] S. Li, H. Bai, Z. Liu, X. Zhang, C. Huang, L. W. Wiesner, M. Silberstein, R. F. Shepherd, *Sci. Adv.* **2021**, *7*, eabg3677.
[90] G. Chen, B. Jin, Y. Shi, Q. Zhao, Y. Shen, T. Xie, *Adv. Mater.* **2022**, *34*, 2201679.
[91] B. Jin, J. Liu, Y. Shi, G. Chen, Q. Zhao, S. Yang, *Adv. Mater.* **2022**, *34*, 2107855.
[92] L. Hiendlmeier, F. Zurita, J. Vogel, F. Del Duca, G. Al Boustani, H. Peng, I. Kopic, M. Nikić, T. F. Teshima, B. Wolfrum, *Adv. Mater.* **2023**, *35*, 2210206.
[93] X. Liu, B. Li, Z. Gu, K. Zhou, *Small* **2023**, *19*, 2207640.
[94] Q. Zhang, X. Kuang, S. Weng, Z. Zhao, H. Chen, D. Fang, H. J. Qi, *ACS Appl. Mat. Interfaces* **2020**, *12*, 17979.
[95] D. Han, R. S. Morde, S. Mariani, A. A. La Mattina, E. Vignali, C. Yang, G. Barillaro, H. Lee, *Adv. Funct. Mater.* **2020**, *30*, 1909197.
[96] Q. Ge, Z. Chen, J. Cheng, B. Zhang, Y. F. Zhang, H. Li, X. He, C. Yuan, J. Liu, S. Magdassi, S. Qu, *Sci. Adv.* **2021**, *7*, eaba4261.
[97] J. Cheng, R. Wang, Z. Sun, Q. Liu, X. He, H. Li, H. Ye, X. Yang, X. Wei, Z. Li, B. Jian, W. Deng, Q. Ge, *Nat. Commun.* **2022**, *13*, 7931.
[98] Y. Shan, A. Krishnakumar, Z. Qin, H. Mao, *Addit. Manuf.* **2022**, *52*, 102653.
[99] X. Xin, L. Liu, Y. Liu, J. Leng, *Adv. Funct. Mater.* **2020**, *30*, 2004226.
[100] X. Xin, L. Liu, Y. Liu, J. Leng, *Adv. Funct. Mater.* **2022**, *32*, 2107795.
[101] B. C. Kholkhoev, K. N. Bardakova, E. O. Epifanov, Z. A. Matveev, T. A. Shalygina, E. B. Atutov, S. Y. Voronina, P. S. Timashev, V. F. Burdukovskii, *Chem. Eng. J.* **2023**, *454*, 140423.
[102] Y. G. Park, H. S. An, J. Y. Kim, J. U. Park, *Sci. Adv.* **2019**, *5*, eaaw2844.
[103] Y. G. Park, I. Yun, W. G. Chung, W. Park, D. H. Lee, J. U. Park, *Adv. Sci.* **2022**, *9*, 2104623.
[104] L. Zhang, X. Huang, T. Cole, H. Lu, J. Hang, W. Li, S. Y. Tang, C. Boyer, T. P. Davis, R. Qiao, *Nat. Commun.* **2023**, *14*, 7815.
[105] Y. Zhang, L. Huang, H. Song, C. Ni, J. Wu, Q. Zhao, T. Xie, *ACS Appl. Mat. Interfaces* **2019**, *11*, 32408.
[106] L. Huang, R. Jiang, J. Wu, J. Song, H. Bai, B. Li, Q. Zhao, T. Xie, *Adv. Mater.* **2017**, *29*, 1605390.
[107] S. Coelho, J. Baek, J. Walsh, J. J Gooding, K. Gaus, *Nat. Commun.* **2022**, *13*, 647.
[108] Z. Wang, C. Hansen, Q. Ge, S. H. Maruf, D. U. Ahn, H. J. Qi, Y. Ding, *Adv. Mater.* **2011**, *23*, 3669.
[109] M. del Pozo, C. Delaney, M. Pilz da Cunha, M. G. Debije, L. Florea, A. P. H. J. Schenning, *Small Struct.* **2022**, *3*, 2100158.
[110] L. Y. Hsu, P. Mainik, A. Münchinger, S. Lindenthal, T. Spratte, A. Welle, J. Zaumseil, C. Selhuber-Unkel, M. Wegener, E. Blasco, *Adv. Mater. Technol.* **2023**, *8*, 2200801.
[111] A. Münchinger, V. Hahn, D. Beutel, S. Woska, J. Monti, C. Rockstuhl, E. Blasco, M. Wegener, *Adv. Mater. Technol.* **2022**, *7*, 2100944.
[112] A. Nishiguchi, H. Zhang, S. Schweizerhof, M. F. Schulte, A. Mourran, M. Möller, *ACS Appl. Mat. Interfaces* **2020**, *12*, 12176.
[113] Y. Hu, Z. Wang, D. Jin, C. Zhang, R. Sun, Z. Li, K. Hu, J. Ni, Z. Cai, D. Pan, X. Wang, W. Zhu, J. Li, D. Wu, L. Zhang, J. Chu, *Adv. Funct. Mater.* **2020**, *30*, 1907377.
[114] F. Rajabasadi, S. Moreno, K. Fichna, A. Aziz, D. Appelhans, O. G. Schmidt, M. Medina-Sánchez, *Adv. Mater.* **2022**, *34*, 2204257.
[115] X. Liu, M. Wei, Q. Wang, Y. Tian, J. Han, H. Gu, H. Ding, Q. Chen, K. Zhou, Z. Gu, *Adv. Mater.* **2021**, *33*, 2100332.
[116] J. W. Boley, W. M. van Rees, C. Lissandrello, M. N. Horenstein, R. L. Truby, A. Kotikian, J. A. Lewis, L. Mahadevan, *Proc. Natl. Acad. Sci. USA* **2019**, *116*, 20856.
[117] K. J. Chen, L. Zhang, X. Kuang, V. Li, M. Lei, G. Z. Kang, Z. L. Wang, H. J. Qi, *Adv. Funct. Mater.* **2019**, *29*, 1903568.
[118] X. Kuang, K. J. Chen, C. K. Dunn, J. T. Wu, V. C. F. Li, H. J. Qi, *ACS Appl. Mat. Interfaces* **2018**, *10*, 7381.
[119] H. Wei, Q. Zhang, Y. Yao, L. Liu, Y. Liu, J. Leng, *ACS Appl. Mater. Interfaces* **2017**, *9*, 876.
[120] Y. Deng, F. Zhang, M. Jiang, Y. Liu, H. Yuan, J. Leng, *ACS Appl. Mat. Interfaces* **2022**, *14*, 42568.
[121] Y. Deng, F. Zhang, Y. Liu, S. Zhang, H. Yuan, J. Leng, *ACS Appl. Polym. Mater.* **2023**, *5*, 1283.
[122] Y. Zhou, Y. Yang, A. Jian, T. Zhou, G. Tao, L. Ren, J. Zang, Z. Zhang, *Compos. Sci. Technol.* **2022**, *227*, 109603.
[123] X. Wan, Y. He, Y. Liu, J. Leng, *Addit. Manuf.* **2022**, *53*, 102689.
[124] D. Ravichandran, M. Kakarla, W. Xu, S. Jambhulkar, Y. Zhu, M. Bawareth, N. Fonseca, D. Patil, K. Song, *Composites, Part B* **2022**, *247*, 110352.
[125] D. Ravichandran, R. J. Ahmed, R. Banerjee, M. Ilami, H. Marvi, G. Miquelard-Garnier, Y. Golan, K. Song, *J. Mater. Chem. C* **2022**, *10*, 13762.
[126] J. N. Rodriguez, C. Zhu, E. B. Duoss, T. S. Wilson, C. M. Spadaccini, J. P. Lewicki, *Sci. Rep.* **2016**, *6*, 27933.
[127] Y. Zhang, X. Y. Yin, M. Y. Zheng, C. Moorlag, J. Yang, Z. L. Wang, *J. Mater. Chem. A* **2019**, *7*, 6972.
[128] W. He, D. Zhou, H. Gu, R. Qu, C. Cui, Y. Zhou, Y. Wang, X. Zhang, Q. Wang, T. Wang, Y. Zhang, *Macromol. Rapid Commun.* **2023**, *44*, 2200553.
[129] S. Chen, J. Li, H. Shi, X. Chen, G. Liu, S. Meng, J. Lu, *Chem. Eng. J.* **2023**, *455*, 140655.
[130] C. Zhang, D. Cai, P. Liao, J. W. Su, H. Deng, B. Vardhanabhuti, B. D. Ulery, S. Y. Chen, J. Lin, *Acta Biomater.* **2021**, *122*, 101.
[131] S. Puthanveetil, W. C. Liu, K. S. Riley, A. F. Arrieta, H. Le Ferrand, *Compos. Sci. Technol.* **2022**, *217*, 109097.
[132] H. Chi, Z. Lin, Y. Chen, R. Zheng, H. Qiu, X. Hu, H. Bai, *ACS Appl. Mat. Interfaces* **2022**, *14*, 13758.
[133] S. Weng, X. Kuang, Q. Zhang, C. M. Hamel, D. J. Roach, N. Hu, H. J Qi, *ACS Appl. Mat. Interfaces* **2021**, *13*, 12797.
[134] P. Zhu, W. Yang, R. Wang, S. Gao, B. Li, Q. Li, *ACS Appl. Mat. Interfaces* **2018**, *10*, 36435.
[135] S. Wu, Q. Ze, R. Zhang, N. Hu, Y. Cheng, F. Yang, R. Zhao, *ACS Appl. Mat. Interfaces* **2019**, *11*, 41649.
[136] Q. Ze, X. Kuang, S. Wu, J. Wong, S. M. Montgomery, R. Zhang, J. M. Kovitz, F. Yang, H. J. Qi, R. Zhao, *Adv. Mater.* **2020**, *32*, 1906657.
[137] C. Ma, S. Wu, Q. Ze, X. Kuang, R. Zhang, H. J. Qi, R. Zhao, *ACS Appl. Mat. Interfaces* **2021**, *13*, 12639.
[138] L. Cera, G. M. Gonzalez, Q. Liu, S. Choi, C. O. Chantre, J. Lee, R. Gabardi, M. C. Choi, K. Shin, K. K. Parker, *Nat. Mater.* **2021**, *20*, 242.
[139] C. P. Ambulo, J. J. Burroughs, J. M. Boothby, H. Kim, M. R. Shankar, T. H. Ware, *ACS Appl. Mat. Interfaces* **2017**, *9*, 37332.
[140] A. Kotikian, R. L. Truby, J. W. Boley, T. J. White, J. A. Lewis, *Adv. Mater.* **2018**, *30*, 1706164.
[141] M. Lopez-Valdeolivas, D. Q. Liu, D. J. Broer, C. Sanchez-Somolinos, *Macromol. Rapid Commun.* **2018**, *39*, 1700710.
[142] D. J. Roach, X. Kuang, C. Yuan, K. J. Chen, H. J. Qi, *Smart Mater. Struct.* **2018**, *27*, 125011.
[143] D. J. Roach, C. Yuan, X. Kuang, V. C. F. Li, P. Blake, M. L. Romero, I. Hammel, K. Yu, H. J. Qi, *ACS Appl. Mat. Interfaces* **2019**, *11*, 19514.
[144] A. Kotikian, C. McMahan, E. C. Davidson, J. M. Muhammad, R. D. Weeks, C. Daraio, J. A. Lewis, *Sci Robot* **2019**, *4*, eaax7044.
[145] W. F. Fei Zhai, *Yingyong Huaxue* **2021**, *38*, 1389.
[146] F. Zhai, Y. Feng, Z. Li, Y. Xie, J. Ge, H. Wang, W. Qiu, W. Feng, *Matter* **2021**, *4*, 3313.

[147] M. O. Saed, C. P. Ambulo, H. Kim, R. De, V. Raval, K. Searles, D. A. Siddiqui, J. M. O. Cue, M. C. Stefan, M. R. Shankar, T. H. Ware, *Adv. Funct. Mater.* **2019**, *29*, 1806412.
[148] C. Zhang, X. L. Lu, G. X. Fei, Z. H. Wang, H. S. Xia, Y. Zhao, *ACS Appl. Mat. Interfaces* **2019**, *11*, 44774.
[149] C. M. Yakacki, M. Saed, D. P. Nair, T. Gong, S. M. Reed, C. N. Bowman, *RSC Adv.* **2015**, *5*, 18997.
[150] W. Liao, Z. Yang, *Mater. Horiz.* **2023**, *10*, 576.
[151] A. Kotikian, J. M. Morales, A. Lu, J. Mueller, Z. S. Davidson, J. W. Boley, J. A. Lewis, *Adv. Mater.* **2021**, *33*, 2101814.
[152] C. P. Ambulo, M. J. Ford, K. Searles, C. Majidi, T. H. Ware, *ACS Appl. Mater. Interfaces* **2021**, *13*, 12805.
[153] M. Barnes, S. M. Sajadi, S. Parekh, M. M. Rahman, P. M. Ajayan, R. Verduzco, *ACS Appl. Mat. Interfaces* **2020**, *12*, 28692.
[154] Z. Wang, Z. Wang, Y. Zheng, Q. He, Y. Wang, S. Cai, *Sci. Adv.* **2020**, *6*, eabc0034.
[155] Y. Wang, R. Yin, L. Jin, M. Liu, Y. Gao, J. Raney, S. Yang, *Adv. Funct. Mater.* **2023**, *33*, 2210614.
[156] Z. Wang, N. Boechler, S. Cai, *Addit. Manuf.* **2022**, *52*, 102678.
[157] L. Ren, B. Li, Y. He, Z. Song, X. Zhou, Q. Liu, L. Ren, *ACS Appl. Mat. Interfaces* **2020**, *12*, 15562.
[158] L. Ren, Y. He, L. Ren, Z. Wang, X. Zhou, Q. Wu, K. Wang, B. Li, Q. Liu, *Addit. Manuf.* **2023**, *61*, 103376.
[159] X. Yang, C. Valenzuela, X. Zhang, Y. Chen, Y. Yang, L. Wang, W. Feng, *Matter* **2023**, *6*, 1278.
[160] Q. Wang, X. Tian, D. Zhang, Y. Zhou, W. Yan, D. Li, *Nat. Commun.* **2023**, *14*, 3869.
[161] H. Finkelmann, S. T. Kim, A. Muñoz, P. Palffy-Muhoray, B. Taheri, *Adv. Mater.* **2001**, *13*, 1069.
[162] J. A. H. P. Sol, L. G. Smits, A. P. H. J. Schenning, M. G. Debije, *Adv. Funct. Mater.* **2022**, *32*, 2201766.
[163] J. A. H. P. Sol, R. F. Douma, A. P. H. J. Schenning, M. G. Debije, *Adv. Mater. Technol.* **2023**, *8*, 2200970.
[164] E. C. Davidson, A. Kotikian, S. Li, J. Aizenberg, J. A. Lewis, *Adv. Mater.* **2020**, *32*, 1905682.
[165] S. J. D. Lugger, R. M. C. Verbroekken, D. J. Mulder, A. P. H. J. Schenning, *ACS Macro Lett.* **2022**, *11*, 935.
[166] S. J. D. Lugger, L. Ceamanos, D. J. Mulder, C. Sánchez-Somolinos, A. P. H. J. Schenning, *Adv. Mater. Technol.* **2023**, *8*, 2201472.
[167] L. K. Rivera-Tarazona, T. Shukla, K. A. Singh, A. K. Gaharwar, Z. T. Campbell, T. H. Ware, *Adv. Funct. Mater.* **2022**, *32*, 2106843.
[168] K. Li, J. Zhao, A. Zhussupbekova, C. E. Shuck, L. Hughes, Y. Dong, S. Barwich, S. Vaesen, I. V. Shvets, M. Möbius, W. Schmitt, Y. Gogotsi, V. Nicolosi, *Nat. Commun.* **2022**, *13*, 6884.
[169] P. J. Díaz-Payno, M. Kalogeropoulou, I. Muntz, E. Kingma, N. Kops, M. D'Este, G. H. Koenderink, L. E. Fratila-Apachitei, G. J. V. M. van Osch, A. A. Zadpoor, *Adv. Healthcare Mater.* **2023**, *12*, 2201891.
[170] J. Simińska-Stanny, M. Nizioł, P. Szymczyk-Ziółkowska, M. Brożyna, A. Junka, A. Shavandi, D. Podstawczyk, *Addit. Manuf.* **2022**, *49*, 102506.
[171] H. Zhao, Y. Huang, F. Lv, L. Liu, Q. Gu, S. Wang, *Adv. Funct. Mater.* **2021**, *31*, 2105544.
[172] B. Narupai, P. T. Smith, A. Nelson, *Adv. Funct. Mater.* **2021**, *31*, 2011012.
[173] X. Hu, Z. Ge, X. Wang, N. Jiao, S. Tung, L. Liu, *Composites, Part B* **2022**, *228*, 109451.
[174] W. Hu, G. Z. Lum, M. Mastrangeli, M. Sitti, *Nature* **2018**, *554*, 81.
[175] S. Wu, C. M. Hamel, Q. Ze, F. Yang, H. J. Qi, R. Zhao, *Advanced Intelligent Systems* **2020**, *2*, 2000060.
[176] C. Ma, Y. Chang, S. Wu, R. R. Zhao, *ACS Appl. Mat. Interfaces* **2022**, *14*, 33892.
[177] L. Zhou, J. Ye, J.. Fu, Q. Gao, Y. He, *ACS Appl. Mat. Interfaces* **2020**, *12*, 12068.
[178] Y. Shao, F. Long, Z. Zhao, M. Fang, H. Jing, J. Guo, X. Shi, A. Sun, G. Xu, Y. Cheng, *Chem. Eng. J.* **2023**, *454*, 140271.
[179] R. Xing, J. Yang, D. Zhang, W. Gong, T. V. Neumann, M. Wang, R. Huang, J. Kong, W. Qi, M. D. Dickey, *Matter* **2023**, *6*, 2248.
[180] X. Chen, X. Liu, M. Ouyang, J. Chen, O. Taiwo, Y. Xia, P. R. N. Childs, N. P. Brandon, B. Wu, *Sci. Rep.* **2019**, *9*, 3973.
[181] G. Liu, Y. Zhao, G. Wu, J. Lu, *Sci. Adv.*, *4*, eaat0641.
[182] T. Li, Q. Liu, H. Qi, W. Zhai, *Small* **2022**, *18*, 2204032.
[183] F. Wang, C. Liu, H. Yang, H. Wang, H. Zhang, X. Zeng, C. Wang, W. Zhang, W. Lv, P. Zhu, B. Li, *Addit. Manuf.* **2023**, *63*, 103411.
[184] T. Liu, L. Liu, C. Zeng, Y. Liu, J. Leng, *Compos. Sci. Technol.* **2020**, *186*, 107935.
[185] B. Goo, C. H. Hong, K. Park, *Mater. Des.* **2020**, *188*, 108485.
[186] D. Chen, Q. Liu, Z. Han, J. Zhang, H. Song, K. Wang, Z. Song, S. Wen, Y. Zhou, C. Yan, Y. Shi, *Adv. Sci.* **2020**, *7*, 2000584.
[187] K. McLellan, T. Li, Y. C. Sun, M. B. Jakubinek, H. E. Naguib, *ACS Appl. Polym. Mater.* **2022**, *4*, 8774.
[188] C. Zeng, L. Liu, W. Bian, Y. Liu, J. Leng, *Composites, Part B* **2020**, *194*, 108034.
[189] C. Zeng, L. Liu, W. Bian, J. Leng, Y. Liu, *Compos. Struct.* **2022**, *280*, 114952.
[190] K. Dong, H. Ke, M. Panahi-Sarmad, T. Yang, X. Huang, X. Xiao, *Mater. Des.* **2021**, *198*, 109303.
[191] W. Peng, J. Yin, X. Zhang, Y. Shi, G. Che, Q. Zhao, J. Liu, *Adv. Funct. Mater.* **2023**, *33*, 2214505.
[192] C. Lin, Z. Huang, Q. Wang, Z. Zou, W. Wang, L. Liu, Y. Liu, J. Leng, *Adv. Healthcare Mater.* **2023**, *12*, 2201999.
[193] T. van Manen, S. Janbaz, K. M. B. Jansen, A. A. Zadpoor, *Communications Materials* **2021**, *2*, 56.
[194] N. Li, W. Zhao, F. Li, L. Liu, Y. Liu, J. Leng, *Matter* **2023**, *6*, 940.
[195] F. Wang, F. Luo, Y. Huang, X. Cao, C. Yuan, *Adv. Mater. Technol.* **2023**, *8*, 2201383.
[196] J. N. Chapuis, K. Shea, *Mater. Des.* **2023**, *232*, 112163.
[197] Y. Wang, X. Li, *Composites, Part B* **2021**, *219*, 108918.
[198] X. Yang, W. Chen, H. Liu, B. Yang, Y. Xie, Y. Wang, Y. Lei, L. Xue, *Adv. Mater. Technol.* **2022**, *7*, 2200266.
[199] B. Peng, Y. Yang, T. Ju, K. A. Cavicchi, *ACS Appl. Mat. Interfaces* **2021**, *13*, 12777.
[200] Q. Chen, L. Han, J. Ren, L. Rong, P. Cao, R. C. Advincula, *ACS Appl. Mat. Interfaces* **2020**, *12*, 50052.
[201] J. Joe, J. Shin, Y. S. Choi, J. H. Hwang, S. H. Kim, J. Han, B. Park, W. Lee, S. Park, Y. S. Kim, D. G. Kim, *Adv. Sci.* **2021**, *8*, 2103682.
[202] L. Cecchini, S. Mariani, M. Ronzan, A. Mondini, N. M. Pugno, B. Mazzolai, *Adv. Sci.* **2023**, *10*, 2205146.
[203] M. A. Wagner, J. L. Ocana-Pujol, A. Hadian, F. Clemens, R. Spolenak, *Mater. Des.* **2023**, *225*, 111418.
[204] Y. Deng, B. Yang, F. Zhang, Y. Liu, J. Sun, S. Zhang, Y. Zhao, H. Yuan, J. Leng, *Biomaterials* **2022**, *291*, 121886.
[205] M. del Pozo, L. Liu, M. Pilz da Cunha, D. J. Broer, A. P. H. J. Schenning, *Adv. Funct. Mater.* **2020**, *30*, 2005560.
[206] L. Ceamanos, Z. Kahveci, M. López-Valdeolivas, D. Liu, D. J. Broer, C. Sánchez-Somolinos, *ACS Appl. Mat. Interfaces* **2020**, *12*, 44195.
[207] L. Dai, L. Wang, B. Chen, Z. Xu, Z. Wang, R. Xiao, *Soft Science* **2023**, *3*, 5.
[208] V. Maurin, Y. Chang, Q. Ze, S. Leanza, J. Wang, R. R. Zhao, *Adv. Mater.* **2023**, 2302765.
[209] Y. Zhang, Q. Wang, S. Yi, Z. Lin, C. Wang, Z. Chen, L. Jiang, *ACS Appl. Mat. Interfaces* **2021**, *13*, 4174.
[210] L. Ren, Z. Wang, L. Ren, Q. Liu, W. Li, Z. Song, B. Li, Q. Wu, X. Zhou, *Mater. Tod. Chem.* **2023**, *29*, 101470.
[211] X. Dong, F. Zhang, L. Wang, Y. Liu, J. Leng, *Composites, Part A* **2022**, *157*, 106925.
[212] W. Zhao, Z. Huang, L. Liu, W. Wang, J. Leng, Y. Liu, *Compos. Sci. Technol.* **2021**, *203*, 108563.

[213] C. A. Chatham, T. E. Long, C. B. Williams, *Prog. Polym. Sci.* **2019**, *93*, 68.
[214] S. Yuan, F. Shen, C. K. Chua, K. Zhou, *Prog. Polym. Sci.* **2019**, *91*, 141.
[215] H. Wu, O. Wang, Y. Tian, M. Wang, B. Su, C. Yan, K. Zhou, Y. Shi, *ACS Appl. Mat. Interfaces* **2021**, *13*, 12679.
[216] H. Ouyang, X. Li, X. Lu, H. Xia, *ACS Appl. Polym. Mater.* **2022**, *4*, 4035.
[217] S. Mei, J. Wang, Z. Li, B. Ding, S. Li, X. Chen, W. Zhao, Y. Zhang, X. Zhang, Z. Cui, P. Fu, X. Pang, M. Liu, *J. Manuf. Processes* **2023**, *92*, 157.
[218] S. Li, Z. Li, S. Mei, X. Chen, B. Ding, Y. Zhang, W. Zhao, X. Zhang, Z. Cui, P. Fu, X. Pang, M. Liu, *Adv. Mater. Technol.* **2023**, *8*, 2202066.
[219] C. Y. Yap, C. K. Chua, Z. L. Dong, Z. H. Liu, D. Q. Zhang, L. E. Loh, S. L. Sing, *Appl. Phys. Rev.* **2015**, *2*, 041101.
[220] J. Ma, B. Franco, G. Tapia, K. Karayagiz, L. Johnson, J. Liu, R. Arroyave, I. Karaman, A. Elwany, *Sci. Rep.* **2017**, *7*, 46707.
[221] W. J. Lee, B. Weber, G. Feltrin, C. Czaderski, M. Motavalli, C. Leinenbach, *Mater. Sci. Eng., A* **2013**, *581*, 1.
[222] D. Kim, I. Ferretto, C. Leinenbach, W. Lee, *Adv. Mater. Interfaces* **2022**, *9*, 2200171.
[223] D. Abolhasani, S. W. Han, C. J. VanTyne, N. Kang, Y. H. Moon, *J. Alloys Compd.* **2022**, *922*, 166228.
[224] W. Wu, Y. Zhou, Q. Liu, L. Ren, F. Chen, J. Y. H. Fuh, A. Zheng, X. Li, J. Zhao, G. Li, *Adv. Sci.* **2023**, *10*, 2206486.
[225] M. Ziaee, N. B. Crane, *Addit. Manuf.* **2019**, *28*, 781.
[226] M. P. Caputo, A. E. Berkowitz, A. Armstrong, P. Müllner, C. V. Solomon, *Addit. Manuf.* **2018**, *21*, 579.
[227] C. Zheng, A. Mostafaei, P. R. de Vecchis, I. Nettleship, M. Chmielus, *Addit. Manuf.* **2021**, *47*, 102276.
[228] D. Raviv, W. Zhao, C. McKnelly, A. Papadopoulou, A. Kadambi, B. Shi, S. Hirsch, D. Dikovsky, M. Zyracki, C. Olguin, R. Raskar, S. Tibbits, *Sci. Rep.* **2014**, *4*, 7422.
[229] Q. Ge, C. K. Dunn, H. J. Qi, M. L. Dunn, *Smart Mater. Struct.* **2014**, *23*, 094007.
[230] X. Mu, N. Sowan, J. A. Tumbic, C. N. Bowman, P. T. Mather, H. J. Qi, *Soft Matter* **2015**, *11*, 2673.
[231] Y. Mao, Z. Ding, C. Yuan, S. Ai, M. Isakov, J. Wu, T. Wang, M. L. Dunn, H. J. Qi, *Sci. Rep.* **2016**, *6*, 24761.
[232] J. Wu, C. Yuan, Z. Ding, M. Isakov, Y. Mao, T. Wang, M. L. Dunn, H. J. Qi, *Sci. Rep.* **2016**, *6*, 24224.
[233] Z. Ding, C. Yuan, X. R. Peng, T. J. Wang, H. J. Qi, M. L. Dunn, *Sci. Adv.* **2017**, *3*, 1602890.
[234] J. A. Fan, W. H. Yeo, Y. Su, Y. Hattori, W. Lee, S. Y. Jung, Y. Zhang, Z. Liu, H. Cheng, L. Falgout, M. Bajema, T. Coleman, D. Gregoire, R. J. Larsen, Y. Huang, J. A. Rogers, *Nat. Commun.* **2014**, *5*, 3266.
[235] G. X. Gu, M. Takaffoli, M. J. Buehler, *Adv. Mater.* **2017**, *29*, 1700060.
[236] G. X. Gu, C. T. Chen, D. J. Richmond, M. J. Buehler, *Mater. Horiz.* **2018**, *5*, 939.
[237] J. Li, V. Slesarenko, S. Rudykh, *Soft Matter* **2018**, *14*, 6171.
[238] D. Wang, H. Xu, J. Wang, C. Jiang, X. Zhu, Q. Ge, G. Gu, *ACS Appl. Mat. Interfaces* **2020**, *12*, 22146.
[239] Y. F. Zhang, Z. Li, H. Li, H. Li, Y. Xiong, X. Zhu, H. Lan, Q. Ge, *ACS Appl. Mat. Interfaces* **2021**, *13*, 41414.
[240] B. E. Carroll, T. A. Palmer, A. M. Beese, *Acta Mater.* **2015**, *87*, 309.
[241] C. Tan, Q. Li, X. Yao, L. Chen, J. Su, F. L. Ng, Y. Liu, T. Yang, Y. Chew, C. T. Liu, T. DebRoy, *Adv. Sci.* **2023**, *10*, 2206607.
[242] G. Chen, Y. Ma, X. Teng, J. Liu, B. Zhang, J. Cao, Y. Huang, *Appl. Mater. Today* **2023**, *31*, 101749.
[243] X. Peng, X. Kuang, D. J. Roach, Y. Wang, C. M. Hamel, C. Lu, H. J. Qi, *Addit. Manuf.* **2021**, *40*, 101911.
[244] D. J. Roach, X. Sun, X. Peng, F. Demoly, K. Zhou, H. J. Qi, *Adv. Funct. Mater.* **2022**, *32*, 2203236.
[245] H. Wu, X. Zhang, Z. Ma, C. Zhang, J. Ai, P. Chen, C. Yan, B. Su, Y. Shi, *Adv. Sci.* **2020**, *7*, 1903208.
[246] K. Benyahia, H. Seriket, R. Prod'hon, S. Gomes, J. C. André, H. J. Qi, F. Demoly, *Addit. Manuf.* **2022**, *58*, 102993.
[247] K. Benyahia, H. Seriket, R. Prod'hon, S. Gomes, J. C. André, H. J. Qi, F. Demoly, *Proc. CIRP* **2023**, *119*, 396.
[248] Q. Zhang, D. Yan, K. Zhang, G. Hu, *Sci. Rep.* **2015**, *5*, 8936.
[249] J. Liao, C. Ye, J. Guo, C. E. Garciamendez-Mijares, P. Agrawal, X. Kuang, J. O. Japo, Z. Wang, X. Mu, W. Li, T. Ching, L. S. Mille, C. Zhu, X. Zhang, Z. Gu, Y. S. Zhang, *Mater. Today* **2022**, *56*, 29.
[250] L. Ceamanos, D. J. Mulder, Z. Kahveci, M. López-Valdeolivas, A. P. H. J. Schenning, C. Sánchez-Somolinos, *J. Mater. Chem. B* **2023**, *11*, 4083.
[251] Y. Wang, H. Cui, Y. Wang, C. Xu, T. J. Esworthy, S. Y. Hann, M. Boehm, Y. L. Shen, D. Mei, L. G. Zhang, *ACS Appl. Mat. Interfaces* **2021**, *13*, 12746.
[252] C. Deng, Y. Liu, X. Fan, B. Jiao, Z. Zhang, M. Zhang, F. Chen, H. Gao, L. Deng, W. Xiong, *Adv. Funct. Mater.* **2023**, *33*, 2211473.
[253] A. Cortés, A. Cosola, M. Sangermano, M. Campo, S. González Prolongo, C. F. Pirri, A. Jiménez-Suárez, A. Chiappone, *Adv. Funct. Mater.* **2021**, *31*, 2106774.
[254] D. Chen, Q. Liu, P. Geng, S. Tang, J. Zhang, S. Wen, Y. Zhou, C. Yan, Z. Han, Y. Shi, *Compos. Sci. Technol.* **2021**, *208*, 108746.
[255] L. H. Shao, B. Zhao, Q. Zhang, Y. Xing, K. Zhang, *Extreme Mech Lett* **2020**, *39*, 100793.
[256] F. Zhang, N. Wen, L. Wang, Y. Bai, J. Leng, *International Journal of Smart and Nano Materials* **2021**, *12*, 375.
[257] H. Liu, F. Wang, W. Wu, X. Dong, L. Sang, *Composites, Part B* **2023**, *248*, 110382.
[258] P. G. Saiz, A. Reizabal, S. Luposchainsky, J. L. Vilas-Vilela, S. Lanceros-Mendez, P. D. Dalton, *Adv. Mater. Technol.* **2023**, *8*, 2202063.
[259] T. Kuhnt, S. Camarero-Espinosa, M. Takhsha Ghahfarokhi, M. Arreguín, R. Cabassi, F. Albertini, D. Nieto, M. B. Baker, L. Moroni, *Adv. Funct. Mater.* **2022**, *32*, 2202539.
[260] D. Podstawczyk, M. Nizioł, P. Szymczyk, P. Wiśniewski, A. Guiseppi-Elie, *Addit. Manuf.* **2020**, *34*, 101275.
[261] X. Cao, S. Xuan, S. Sun, Z. Xu, J. Li, X. Gong, *ACS Appl. Mat. Interfaces* **2021**, *13*, 30127.
[262] H. Zhu, Y. He, Y. Wang, Y. Zhao, C. Jiang, *Advanced Intelligent Systems* **2022**, *4*, 2100137.
[263] X. Kuang, S. Wu, Q. Ze, L. Yue, Y. Jin, S. M. Montgomery, F. Yang, H. J. Qi, R. Zhao, *Adv. Mater.* **2021**, *33*, 2102113.
[264] J. Sim, S. Wu, J. Dai, R. R. Zhao, *Adv. Mater.* **2023**, *35*, 2303541.
[265] M. Lalegani Dezaki, M. Bodaghi, *Sens. Actuators, A* **2023**, *349*, 114063.
[266] L. Ren, Z. Li, Q. Liu, L. Ren, Q. Wu, B. Li, G. Li, Z. Song, X. Zhou, *Adv. Mater. Technol.* **2021**, *6*, 2001289.
[267] F. G. Bonifacich, O. A. Lambri, V. Recarte, V. Sánchez-Alarcos, J. I. Pérez-Landazábal, *Compos. Sci. Technol.* **2021**, *201*, 108538.
[268] S. Parimita, A. Kumar, H. Krishnaswamy, P. Ghosh, *J. Manuf. Processes* **2023**, *85*, 875.
[269] Z. Mao, K. Zhu, L. Pan, G. Liu, T. Tang, Y. He, J. Huang, J. Hu, K. W. Y. Chan, J. Lu, *Adv. Mater. Technol.* **2020**, *5*, 1900974.
[270] Y. Zhang, A. Raza, Y. Q. Xue, G. Yang, U. Hayat, J. Yu, C. Liu, H. J. Wang, J. Y. Wang, *Bioact Mater* **2023**, *23*, 343.
[271] K. Kim, Y. Guo, J. Bae, S. Choi, H. Y. Song, S. Park, K. Hyun, S. K. Ahn, *Small* **2021**, *17*, 2100910.
[272] D. Correa, S. Poppinga, M. D. Mylo, A. S. Westermeier, B. Bruchmann, A. Menges, T. Speck, *Philos. Trans. R. Soc., A* **2020**, *378*, 20190445.
[273] T. Cheng, M. Thielen, S. Poppinga, Y. Tahouni, D. Wood, T. Steinberg, A. Menges, T. Speck, *Adv. Sci.* **2021**, *8*, 2100411.
[274] A. Le Duigou, T. Fruleux, R. Matsuzaki, G. Chabaud, M. Ueda, M. Castro, *Mater. Des.* **2021**, *211*, 110158.

[275] C. Zarna, S. Rodríguez-Fabià, A. T. Echtermeyer, G. Chinga-Carrasco, *Addit. Manuf.* **2022**, *59*, 103166.
[276] C. Y. Wu, J. R. Chen, C. K. Su, *Anal. Chim. Acta* **2022**, *1204*, 339733.
[277] A. Ding, O. Jeon, D. Cleveland, K. L. Gasvoda, D. Wells, S. J. Lee, E. Alsberg, *Adv. Mater.* **2022**, *34*, 2109394.
[278] B. Liu, B. Dong, C. Xin, C. Chen, L. Zhang, D. Wang, Y. Hu, J. Li, L. Zhang, D. Wu, J. Chu, *Small* **2023**, *19*, 2204630.
[279] C. Chen, M. Zhang, C. Guo, H. Chen, *Innovative Food Sci. Emerging Technol.* **2021**, *68*, 102605.
[280] T. Y. Koh, A. Sutradhar, *Addit. Manuf.* **2022**, *56*, 102866.
[281] B. Ma, Y. Zhang, J. Li, D. Chen, R. Liang, S. Fu, D. Li, *Chem. Eng. J.* **2023**, *466*, 143420.
[282] A. Ding, S. J. Lee, S. Ayyagari, R. Tang, C. T. Huynh, E. Alsberg, *Bioact Mater* **2022**, *7*, 324.
[283] S. Jang, S. Park, *Sens. Actuators, B* **2023**, *384*, 133654.
[284] I. Gibson, D. Rosen, B. Stucker, M. Khorasani, in *Additive Manufacturing Technologies*, Springer, Cham **2021**.
[285] C. Yuan, T. Lu, T. J. Wang, *Forces Mech* **2022**, *7*, 100081.
[286] L. C. Wang, Q. Zhang, Z. Zhao, W. L. Song, D. Fang, *Nanosens. Smart Manuf.* **2022**, *01*, 2230001.
[287] F. Demoly, M. L. Dunn, K. L. Wood, H. J. Qi, J. C. André, *Mater. Des.* **2021**, *212*, 110193.
[288] S. Vatanparast, A. Boschetto, L. Bottini, P. Gaudenzi, *Appl. Sci.*, https://doi.org/10.3390/app13137744.
[289] O. Sigmund, K. Maute, *Struct Multidiscipl Optim* **2013**, *48*, 1031.
[290] K. Maute, A. Tkachuk, J. Wu, H. J Qi, Z. Ding, M. L. Dunn, *Int. J. Mech. Mater. Des.* **2015**, *137*, 111402.
[291] M. J. Geiss, N. Boddeti, O. Weeger, K. Maute, M. L. Dunn, *Int. J. Mech. Mater. Des.* **2019**, *141*, 051405.
[292] M. Tanaka, S. M. Montgomery, L. Yue, Y. Wei, Y. Song, T. Nomura, H. J. Qi, *Sci. Adv.*, *9*, eade4381.
[293] W. Li, Y. Jia, F. Wang, O. Sigmund, X. S. Zhang, *Int J Eng Sci* **2023**, *191*, 103881.
[294] C. Yuhn, Y. Sato, H. Kobayashi, A. Kawamoto, T. Nomura, *Comput Methods Appl Mech Eng* **2023**, *414*, 116187.
[295] T. S. Lumpe, K. Shea, *J. Mater. Res.* **2021**, *36*, 3642.
[296] T. S. Lumpe, M. Tao, K. Shea, D. I. W. Levin, *Smart Mater. Struct.* **2023**, *32*, 015008.
[297] O. Weeger, *Struct Multidiscipl Optim* **2022**, *65*, 43.
[298] O. Weeger, B. Narayanan, M. L. Dunn, *Comput Methods Appl Mech Eng* **2019**, *345*, 26.
[299] R. Solomonoff, *Matematika* **1958**, *2*, 139.
[300] A. Zolfagharian, A. Kaynak, A. Kouzani, *Mater. Des.* **2020**, *188*, 108411.
[301] C. M. Hamel, D. J. Roach, K. N. Long, F. Demoly, M. L. Dunn, H. J. Qi, *Smart Mater. Struct.* **2019**, *28*, 065005.
[302] D. Athinarayanarao, R. Prod'hon, D. Chamoret, H. J. Qi, M. Bodaghi, J. C. André, F. Demoly, *npj Comput. Mater.* **2023**, *9*, 1.
[303] X. Sun, L. Yue, L. Yu, H. Shao, X. Peng, K. Zhou, F. Demoly, R. Zhao, H. J. Qi, *Adv. Funct. Mater.* **2022**, *32*, 2109805.
[304] X. Sun, L. Yu, L. Yue, K. Zhou, F. Demoly, R. R. Zhao, H. J. Qi, *J Mech Phys Solids* **2024**, *186*, 105561.
[305] A. Zolfagharian, L. Durran, S. Gharaie, B. Rolfe, A. Kaynak, M. Bodaghi, *Sens. Actuators, A* **2021**, *328*, 112774.
[306] J. W. Su, D. Li, Y. Xie, T. Zhou, W. Gao, H. Deng, M. Xin, J. Lin, *Smart Mater. Struct.* **2021**, *30*, 015028.
[307] P. Suryavanshi, J. Wang, I. Duggal, M. Maniruzzaman, S. Banerjee, *Pharmaceutics* **2023**, *15*, 1266.
[308] Y. Yu, K. Qian, H. Yang, L. Yao, Y. J. Zhang, *J. Mater. Process. Technol.* **2022**, *302*, 117497.
[309] S. Dimassi, F. Demoly, C. Cruz, H. J. Qi, K. Y. Kim, J. C. André, S. Gomes, *Comput Ind* **2021**, *126*, 103374.
[310] S. Dimassi, F. Demoly, H. Belkebir, C. Cruz, K. Y. Kim, S. Gomes, H. J. Qi, J. C. André, *Comput Ind* **2023**, *145*, 103824.
[311] G. Liu, X. Zhang, X. Chen, Y. He, L. Cheng, M. Huo, J. Yin, F. Hao, S. Chen, P. Wang, S. Yi, L. Wan, Z. Mao, Z. Chen, X. Wang, Z. Cao, J. Lu, *Mater. Sci. Engin.: R: Rep.* **2021**, *145*, 100596.
[312] S. H. Kim, Y. B. Seo, Y. K. Yeon, Y. J. Lee, H. S. Park, M. T. Sultan, J. M. Lee, J. S. Lee, O. J. Lee, H. Hong, H. Lee, O. Ajiteru, Y. J. Suh, S. H. Song, K. H. Lee, C. H. Park, *Biomaterials* **2020**, *260*, 120281.
[313] A. Ding, S. J. Lee, R. Tang, K. L. Gasvoda, F. He, E. Alsberg, *Small* **2022**, *18*, 2202196.
[314] H. Wei, M. Lei, P. Zhang, J. Leng, Z. Zheng, Y. Yu, *Nat. Commun.* **2021**, *12*, 2082.
[315] Y. He, R. Yu, X. Li, M. Zhang, Y. Zhang, X. Yang, X. Zhao, W. Huang, *ACS Appl. Mat. Interfaces* **2021**, *13*, 36286.
[316] L. B. Huang, J. C. Han, S. Chen, Z. Sun, X. Dai, P. Ge, C. H. Zhao, Q. Q. Zheng, F. C. Sun, J. Hao, *Nano Energy* **2021**, *84*, 105873.
[317] D. Wang, B. Zhao, X. Li, L. Dong, M. Zhang, J. Zou, G. Gu, *Nat. Commun.* **2023**, *14*, 5067.
[318] M. Pathan, R. Devaramani, S. M. Adinarayanappa, *Mater. Today* **2023**.
[319] M. Ali, F. Alam, Y. F. Fah, O. Shiryayev, N. Vahdati, H. Butt, *Composites, Part B* **2022**, *230*, 109514.
[320] C. Y. Wu, J. R. Chen, C. K. Su, *Anal. Chem.* **2021**, *93*, 11497.
[321] H. Huang, C. Liao, M. Zou, D. Liu, S. Liu, Y. Wang, Z. Bai, D. Liu, B. Li, J. Huang, F. Wang, J. Zhou, C. Zhao, X. Weng, L. Liu, J. Qu, Y. Wang, *ACS Photonics* **2023**, *10*, 1916.
[322] J. Chen, X. Liu, Y. Tian, W. Zhu, C. Yan, Y. Shi, L. B. Kong, H. J. Qi, K. Zhou, *Adv. Mater.* **2022**, *34*, 2102877.
[323] W. G. Chung, E. Kim, Y. W. Kwon, J. Lee, S. Lee, I. Jeong, J. U. Park, *Adv. Funct. Mater.* **2023**, 307990.
[324] S. Kim, Y. G. Park, J. Y. Kim, E. Kim, D. H. Lee, J. H. Lee, J. Cheon, J. U. Park, *ACS Appl. Mat. Interfaces* **2023**, *15*, 28954.
[325] Z. Wang, Y. Wu, D. Wu, D. Sun, L. Lin, *Composites, Part B* **2022**, *231*, 109596.
[326] J. R. Tumbleston, D. Shirvanyants, N. Ermoshkin, R. Janusziewicz, A. R. Johnson, D. Kelly, K. Chen, R. Pinschmidt, J. P. Rolland, A. Ermoshkin, E. T. Samulski, J. M. DeSimone, *Science* **2015**, *347*, 1349.
[327] M. Lei, W. Hong, Z. Zhao, C. Hamel, M. Chen, H. Lu, H. J. Qi, *ACS Appl. Mat. Interfaces* **2019**, *11*, 22768.
[328] S. Leanza, S. Wu, X. Sun, H. J. Qi, R. R. Zhao, *Adv. Mater.* **2023**, *36*, 2302066.
[329] L. S. Novelino, Q. Ze, S. Wu, G. H. Paulino, R. Zhao, *Proc. Natl. Acad. Sci. USA* **2020**, *117*, 24096.
[330] W. Choi, R. C. Advincula, H. F. Wu, Y. Jiang, *MRS Commun.* **2023**, *13*, 714.
[331] X. Sun, K. Zhou, F. Demoly, R. R. Zhao, H. J. Qi, *J Appl Mech* **2023**, *91*, 030801.
[332] Y. Emery, T. Colomb, E. Cuche, *J. Phys. Photonics* **2021**, *3*, 034016.

Xue Wan is a Research Fellow under the supervision of Professor Kun Zhou at the Singapore Centre for 3D Printing, School of Mechanical and Aerospace Engineering, Nanyang Technological University, Singapore. She received her Ph.D. in Materials Science from Harbin Institute of Technology, China in 2022. Her research interests include stimuli-responsive materials, 4D printing, and multifunctional fibers.

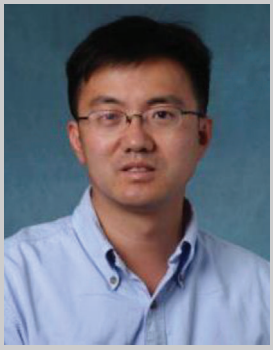

Hang Jerry Qi is a Professor of Mechanical Engineering at Georgia Institute of Technology and is the site director of NSF Industry–University Cooperative Research Center on Science of Heterogeneous Additive Printing of 3D Materials (SHAP3D). His research focuses on developing a fundamental understanding of multi-field properties of soft active materials, including shape memory polymers, light-activated polymers, liquid crystal elastomers, and vitrimers. He was elected Fellow of American Society of Mechanical Engineers.

Kun Zhou is a professor in the School of Mechanical and Aerospace Engineering at Nanyang Technological University, Singapore. His research interests focus on additive manufacturing, mechanics of materials, and modeling and design of sustainable materials. He was elected Fellow of American Physical Society, Institution of Mechanical Engineers, Royal Aeronautical Society, Royal Society of Chemistry, Institute of Physics, and Institute of Materials, Minerals & Mining.